Development and evaluation of a nonlinear regression model for parameter estimation using simulated and patient data

Pro Gradu
University of Turku
Physics
2026
LuK Satu Jasmin Jalo
Examiners:
Prof. Jyrki Piilo
Docent Jarmo Teuho

The originality of this thesis has been checked in accordance with the University of Turku quality assurance system using the Turnitin OriginalityCheck service.

UNIVERSITY OF TURKU
Department of Physics and Astronomy

Jalo, Satu Development and evaluation of a nonlinear regression model for parameter estimation using simulated and patient data

Master's thesis, 61 p. + 56p. appendices.
Data-analytical physics
June 2026

Non-linear regression models are common modelling methods. These are used in medical image processing and in extracting information that could be otherwise hard to extract. In PET-imaging blood flow can be measured with high accuracy when using radiowater as a tracer. Commonly time activity curves (TAC) and Arterial input functions (AIF) are measured. To extract information from this data, it is common practice to use different compartment models.

In this thesis exponential non-linear regression model (NAIST) that PET-Centre had received in collaboration was further developed. This version of the model was also done for one TAC and AIF set, and it was further developed to work dynamically for large data. This model was explored further by developing another model, NASTα, that used the same exponential modelling part but had different parameter optimization decisions. PET-Centre had existing compartmental models built in TPClib that were used to evaluate how well the models eventually ended up working. The model used for measuring myocardial blood flow was called fitmbf, and the other model that measured blood flow in tissue perfusion fit_h2o.

The models were evaluated using Pearson correlation coefficient. The optimized parameters were: blood flow, Va, K1, k2, vd, and α. NAIST had high to moderate correlation in flow from 0.57 to 0.92 in perfusions of 0.5-4 [ml/min/g] compared to fit_h2o. NASTα model had high to moderate correlation for flow from 0.59 to 0.99 in perfusion values of 1-3 [ml/min/g]. Both the NAIST and NASTα models had high correlation over 0.9 or near in normal ranges of perfusion for Va. With NASTα α had high correlation in perfusion of 0.5-3 [ml/min/g] and lower correlation with higher perfusion. For vd in NAIST the correlation was over or near 0.9 for perfusions in range 0.5 to 6 [ml/min/g]. In NASTα vd had correlation values over 0.8 in low perfusions from 0.5 to 2 [ml/min/g].

Patient outcomes are examined based on whether the model results cluster at the same values across patients. Some of the values did group but the models need more tuning to be able to perform with real patient data.

Keywords: Simulation, non-linear Regression, Model, Automation, PET, AIF, TAC, MBF, Va, Perfusion, Blood flow

UNIVERSITY OF TURKU
Fysiikan ja tähtitieteen laitos

Jalo, Satu Epälineaarisen regressiomallin kehittäminen ja arviointi parametrien estimointiin käyttäen simuloitua ja potilasdataa

Pro Gradu, 61 s. + 56 s. liitteet.
Data-analyyttinen Fysiikka
Kesäkuu 2026

Epälineaariset regressiomallit ovat yleisiä mallinnusmenetelmiä. Näitä käytetään lääketieteellisessä kuvankäsittelyssä ja sellaisen tiedon poimimisessa, jota muuten olisi vaikea saada. PET-kuvantamisessa verenvirtausta voidaan mitata suurella tarkkuudella käyttämällä merkkiaineena radiovettä. Yleensä mitataan aika-aktiivisuuskäyriä (TAC) ja valtimoiden sisääntulofunktioita (AIF). Näistä tiedon poimimiseksi on yleistä käyttää erilaisia lokeromalleja.

Tässä opinnäytetyössä jatko kehitettiin PET-keskuksen yhteistyössä saamaa eksponentiaalista epälineaarista regressiomallia (NAIST). Tämä versio mallista oli tehty yhdelle TAC- ja AIF-joukolle, ja sitä jatko kehitettiin toimimaan dynaamisesti suurten tietomäärien kanssa. Tätä mallia kehitettiin edelleen luomalla toinen malli, NASTα, joka käytti samaa eksponentiaalista mallinnusosaa, mutta jolla oli erilaiset parametrien optimointimenetelmät. PET-keskuksella oli TPClib-lokeromalleja, joita käytettiin arvioimaan, kuinka hyvin uudet mallit lopulta toimivat. Sydänlihaksen verenvirtauksen mittaamiseen käytettyä mallia kutsuttiin fitmbf:ksi ja toista mallia, joka mittasi verenvirtausta kudosperfuusiossa fit_h2o:ksi.

Malleja arvioitiin Pearsonin korrelaatiokertoimella. Optimoidut parametrit olivat: verenvirtaus, Va, K1, k2, vd ja α. NAIST:n virtauskorrelaatio oli korkea tai kohtalainen välillä 0,57–0,92 perfuusioissa 0,5–4 [ml/min/g] verrattuna fit_h2o:hon. NASTα-mallin virtauskorrelaatio oli korkea tai kohtalainen välillä 0,59–0,99 perfuusioarvoilla 1–3 [ml/min/g]. Sekä NAIST- että NASTα-malleilla oli korkea korrelaatio, yli 0,9 tai lähellä, normaalilla perfuusioalueella Va:lle. NASTα:n tapauksessa α:lla oli korkea korrelaatio perfuusiossa 0,5–3 [ml/min/g], ja matalampi korrelaatio korkeamman perfuusion yhteydessä. NAIST:n vd:n korrelaatio oli yli 0,9 tai lähellä sitä, perfuusio väleillä 0,5-6 [ml/min/g]. NASTα-tutkimuksessa vd:n korrelaatioarvot olivat yli 0,8 matalilla perfuusioilla välillä 0,5–2 [ml/min/g].

Potilastuloksia tarkastellaan sen perusteella, onko mallien tulokset ryhmittyneet samoihin arvoihin potilaittain. Jotkin arvot ryhmittyivät, mutta mallit tarvitsevat lisää hienosäätöä, jotta ne voivat toimia oikean potilas datan kanssa.

Avainsanat: Simulointi, epälineaarinen regressio, malli, automaatio, PET, AIF, TAC, MBF, Va, perfuusio, verenkierto

Contents

List of abbreviations

Abbreviation	Meaning
PET	Positron Emission Tomography
CAD	Coronary Artery Disease
MBF	Myocardial Blood Flow
TAC	Time Activity Curve
AIF	Arterial Input Function
ROI	Region of Interest
LOR	Line of Response
SNR	Signal-To-Noise
TOF	Time of Flight
LV	Left Ventricle
LA	Left Atrium
MPI	Myocardial Perfusion Imaging
HF	Heart Failure
ATP	Adenosine Triphosphate
LLM	Large Language Models
AIC	Akaike Information Criterion

Introduction

This thesis goes over the basics of radiation physics with more detailed explanation on positron emission tomography (PET) and how it is used to gather data that can be used in the medical field to study and diagnose multiple different diseases. In this thesis, focus is on coronary artery disease (CAD), the world's leading cause of mortality, and its common cause myocardial ischemia. Before going to the actual thesis explanation some common modeling methods are explained, as they are commonly used in medical fields to study different diseases. In the last section the whole study and its parts are gone over in detail. There were two different models that were compared with two existing models. Before this could be done, the code was obtained from from a collaborator needed to be changed as it did not work in the beginning. So the work started with fixing the first code for the model, creating another model with alpha (α) parameter, simulating data with the already existing program from TPClib, creating the BASH code to run the TPClib programs used in simulation and modeling to create the evaluation methods for all the modeling results. In the end all these models were run again using a small sample of ten patient's to compare how they performed to see how they worked compared. Our study focuses on developing evaluation models for myocardial blood flow and possible other parameters commonly associated explaining normal or abnormal the myocardium behaviour.

1 Theory

This section starts with an overview of fundamental physics concepts relevant to medical imaging. It provides a brief introduction to the cardiovascular system combined with an overview of some common diseases. Finally are the commonly used modeling methods before moving to the actual materials and methods in the next section.

1.1 Physics behind imaging

In this starting section the basics of radiation physics are covered. Understanding of the underlying physical principles is essential to this thesis, as PET-imaging is based on radiation physics. To understand how the patient data is collected in the PET-imaging, basic theory of radiation physics is in place.

Radiation can be particle-like and electromagnetic radiation. During the 17th Century, Isaac Newton believed that photons, which are electromagnetic radiation, exhibit particle properties. Where Christiaan Huygen believed that photons showed wave-like properties. Both were partially right, as quantum mechanics has proven, photons, which are massless, as well as electrons and other particles that have mass, exhibit both wave and particle properties. First, it was proved for photons by Albert Einstein with his theory of photoelectric effect. In 1924 Louis De Broglie found that normal matter exhibits both wave and particle properties, when the phenomena got a name of wave-particle duality. From these findings quantum mechanics got its beginning by Werner Heisenberg, Erwin Schrödinger and Paul Dirac. Dirac continued the research during 1928 and had a theory, electrons have opposite particles that have a positive charge and same mass. Some years later in 1932 Carl Anderson started calling it positron, when it was observed in cosmic radiation when an electron-positron pair was formed. [1] These findings inspired some of the new discoveries in physics that almost everyone knows. One of these findings was Einstein's

famous Eq. 1 for special relativity.

$$E = mc^2 \tag{1}$$

Here the energy (E) of a particle is defined by the mass (m) of a particle and the speed (c) squared. Without these findings PET-imaging wouldn't be possible. In PET, particles are accelerated in the hospital settings to study and diagnose different diseases and their detection is mainly based in physics. [2]

1.1.1 Radiation physics

The actual physics behind radiation is highly connected to chemistry, and these two depend on each other. The atom's properties define how it interacts and behaves in the universe. Atoms are tiny particles that are built from electrons (-), protons (Z) and neutrons (N). The number of Z in the atom defines the atomic number of the atom and $A = Z + N$ defines the atomic mass number. The amount of Z defines what type of element is in question, and this element has the equal number of electrons. The amount of N defines what isotope of a specific element is in question. But only certain combinations can be stable. These atoms can group up together with same or different atoms creating molecules.[2] [3]

There are several types of radiation, and we are taking a closer look at electromagnetic radiation and particulate radiation. Radioactivity is created when an unstable nucleus starts to lose its energy, creating new elements. So, in this decay a new nuclide is produced. When this decay happens it can exist as an electromagnetic wave or as a particulate that has kinetic energy, these two still have both properties, but this is the way they are categorized. What kind of decay happens depends on what particulate is decaying. Electromagnetic radiation is commonly visualized and most easily understood as a spectrum where in the longer wavelength of radiation are things like radio, microwave, infrared and visible light. On the other end of the spectrum the wavelength gets decreasingly smaller. These smaller wavelength

radiations include ultraviolet X-ray and gamma-rays (γ). These different types of radiation have different features that affect the surrounding differently, they have a feature of not ionizing or ionizing. The non-ionizing radiation means that the radiation has low energy, small frequency and large wavelength. This type of radiation is generally harmless because it is unable to produce charged ions. It can excite electrons to a higher state, but this will not alter the atom permanently. However ionizing radiation has high energy, high frequency and small wavelength. This large amount of energy gives the radiation the possibility to remove the outer electrons from atoms, making modifications to them, and in the worst case alter the cell DNA if the dose is too high or there is too frequent exposure, eventually going over a safety limit. From electromagnetic radiation this kind of ionizing radiation is X-rays and γ-rays. Every different type of electromagnetic radiation has different wavelength (λ), frequency (f) and speed (c) and they can be solved when one is known using Eq. 2 as speed of light is a known constant.

$$c = \lambda f \tag{2}$$

As radiation has energy, the amount of energy defines how long the matter can move and whether it can ionize matter or not. There are differently charged particles that are also radiating, but there are also neutral particles. These kinds of particles are the ones mentioned previously γ, X-ray as well as neutrons that are inside the atom, meaning these are not charged. Neutrons are capable of creating charged particles through interaction with matter. These particles are then called secondary charged particles. These charged particles are normal electrons and protons that continue to interact with the medium.[2]

In particular, radiation belongs to charged particles such as α and β particles. In addition to having ionizing and non-ionizing radiation categories, the effects can be further divided into deterministic and stochastic. Deterministic means detection

of cellular death. In this case a threshold has been crossed and damage occurred. Stochastic means that there is a change in the mutations of the genes increasing the change in cancer. Stochastic doesn't have a strict threshold and is more connected to cumulative dosages. [4] The reason these high energy, short wavelength radiations can go through different materials is due to the properties of wave particle duality. What this means is that an electron can pass certain points of space as a particle and certain points as a wave. If it could exhibit only one type, i.e. being only a particle, the electron would not be able to pass through certain areas. [5] There are two ways radiation can be created, artificially and by natural isotopes. Artificially created radiation uses machines like the X-ray machine and accelerators, where the energy is received from voltage. Isotopes, on the other hand, get their energy from their original property, nuclear decay. However, these isotopes can also be artificially made using nuclear reactors or accelerators. Radioactive substances have an activity that can change in time and can be calculated using the Eq. 3.

$$A(t) = |\frac{dN}{dt}| = \lambda N(t). \tag{3}$$

where N is the number of neutrons. With the following Eq. 4, the activity in a certain time for the mother nucleus can be calculated.

$$A_p = A_p(0)e^{-\lambda_p t}. \tag{4}$$

Here $A_p(0)$ is the activity that the nucleus has in the beginning and λ_p is the decay constant. When the isotope decays, it decays to the stable daughter nucleus D. From this we can see that as time goes by the amount of radiation decreases. When it comes to radioactivity it is connected to a term half-life that, as the name indicates, measures how long it will take for the number of radioactive nuclei to be half from the original it presented in the beginning. This can be represented by Eq. 5.

$$t_{\frac{1}{2}} = \frac{ln(2)}{\lambda}. \tag{5}$$

In theory, it never reaches zero, but eventually it reaches such a small value that it can be considered as such. [2] [6]

1.1.2 Radiation interaction with matter

In the earlier subsection, the different types of radiation were explained. These different types of radiation have different abilities and energies. Because of this they also interact with matter differently, which is depending on the type of medium it is interacting with. They can interact with excitation where the electron in the orbital shells rises to a higher orbital shell in the atom. This is not permanent and the electron will go back to its original shell in time and happens when non-ionizing radiation interacts with matter. But with ionization there is more energy and, when the energy is high enough, it can remove the electron from the atom's orbit completely. After the electron is removed, it can go further and ionize or excite electrons from other atoms if they are still carrying enough energy. When all the energy is used, the electron will come to rest. Energy is affecting how far the particles move but also their mass, charge and kinetic energy affect this. On top of these the medium they move in affects the distance, as the medium can have different features, i.e. the density of the matter defines how many collisions are possible. In air there are less atoms to collide with, and in denser matter there are more. Meaning the possibility for collisions are higher and the distance it can move is shorter. So the particles possible maximum moving distance depends on the properties of the matter as well as the particles.[7] [2]

Linear energy transfer (LET) is used to describe the amount of energy which will be absorbed when the particle is moving in the medium. The radiation propagates in a straight trajectory until it undergoes interactions with atoms. As mentioned earlier there are multiple different kinds of ionizing radiation. These are α, β that are particulate radiation and γ and X-ray that are electromagnetic radiation. With

each of these radiations they have different types of features. Particulate radiation α has a high mass and it is known to be a densely ionizing. The α particle is like helium nuclei having the mass of 4 and positive charge of 2. As the mass of α particle is large the ionization is higher than the smaller particles or electromagnetic radiations. The good thing is that regardless of the high ionization energy all of it will be used in a short distance, in just a couple of centimetres in the air or faced with a thin layer of paper. The other particulate radiation β has a way smaller mass then α particle and they need thicker medium to lose their energy. The ionizing electromagnetic radiation, X-ray and γ rays also known as photons, are not as easily absorbed in the medium. The γ-ray have a small wavelength, while having the highest energy in the electromagnetic wave spectrum.

They interact with matter by three different mechanisms called photoelectric absorption, Compton scattering and pair production. The interaction type depends on the amount of energy these photons have. Most commonly in nuclear medicine photoelectric effect and Compton scattering are used to detect the photons. In the photoelectric effect when these photons interact with the medium it collides with the electron, giving all its energy, making the electron leave from the atom's shells. In this case ionization happens. In Compton scattering some of the energy from the photon will be transferred to the electron it interacts with, that is in the outer shell. These electrons have less energy than the inner shell electrons so they will be easier to eject from the atom. After the collision the photon scatters having lower energy, different direction and different wavelength. When the scattering happens the photons energy changes, as follows in the Eq. 6.

$$E_s = \frac{E}{1 + \frac{E}{m_0 c^2}(1 - cos\theta)}. \tag{6}$$

Here the E is energy of incident photon, m_0 rest mass energy of the electron, c speed of light and θ the scattering angle. It is possible that due to the scattering the photon

loses its energy before reaching the detector. One of the problems with scattering is that it can cost the contrast of the images. Compton scattering increases the number of detections and can cause errors and biases. This may cause photons to reach the detector at a different angle than was predicted. It is also possible that both photons will undergo scattering, as well that many photons simultaneously scatter. When this happens, the detected photons might be considered as random events. In the pair production, the energy carried by the photon can create a positron electron pair. For pair production to happen a minimum amount of energy of 1.02 MeV is needed but the energies can get higher than this. [4] [8] [9]

1.2 Positron emission tomography (PET) imaging

In this section the basic working principles of PET-imaging are covered. As in the earlier section, radiations and their interaction with matter are discussed. Next will be explained how radiation is used in PET-imaging and how the information can be used in the medical field. To start the imaging process a radio tracer is given to the patient. The tracers used are selected so that they annihilate almost immediately when they collide with electrons in the body [10]. What tracers are commonly used and what kind of features they have, will be discussed in more detail in later sections.

A positron is the antiparticle of an electron, meaning it has the same mass but opposite charge, an electron having a negative charge and positron positive charge. When a positron collides with an electron a positronium is created. This is a short-lived particle that will be annihilated. This annihilation releases a standard amount of energy of 511 keV and two photons that are emitted on opposite sides from each other. This is called the line of response (LOR). This simultaneous emission is used in detecting and localizing where the emission has taken place and it is called a true coincidence. When simultaneous detection happens also small change of 4-12 ns is accepted for the coincidence to be considered simultaneous. This is a

simplified version of what happens, in reality multiple similar events happen around the area of imaging. So, localizing the correct pairs of emission is its own challenge. To add to this there can also be false detections, randoms. This happens when simultaneously with photon detection another photon is detected but not on the opposing side, but rather off from the LOR. This is an important part of detecting what detections are from the same locations as these need to be filtered away to have better image quality. Also scattering can happen. Here the annihilated photons are scattered from the original LOR and reach the detector off from the LOR. [11] [12] To detect all these photons the PET scanner is designed so that a ring of detectors are aligned next to each other. In each detector are scintillation crystals that are aligned in an array having little to no space between each crystal. This is done to ensure good contrast for the images. Then these detector rings are stacked next to each other to ensure a wider area to collect photons and ensure wider coverage. These crystals are critical, as they absorb these emitted photons, which create a flash from the energy, and this flash is then absorbed by photo sensors. These are behind the crystal, and turn the detections into an electronic signal. As mentioned earlier with the real detections, randoms and scatters, there are ways of fixing these, but they do cost the image resolution. In the modern 3D and 4D time of flight (TOF) PET-imaging a high sensitivity image with good resolution can be achieved, meaning the signal-to-noise-ratio (SNR) is better. The version of 4D-PET includes the three spatial dimensions (3D), width, depth and height plus the dimension of time. In TOF the measurement from the annihilation to the detector is measured. It also uses probabilities that detect the most probable possible location for where the annihilation has happened. Older methods used non-TOF which has the same probability all around the LOR and is not as accurate as finding the origin of the annihilation event. [13] [14] [12] [10] [15]

1.2.1 Image and data acquiring

Now that the basics of how the actual physics behind the detection is covered, it is possible to focus on how the collected data is processed to acquire static or dynamic images (during a longer time period where many images are taken, producing a video also known as 4D). From dynamic imaging more parameters can be detected such as blood flow that in our case will be one of the parameters of interest. To be able to create images, the raw data must be processed and eventually reconstructed. There are two types used to create the parametric images. First one uses sinograms or list mode data. The list mode data is fitted to time frames. From these sinogram is extracted. It is also possible to record the data straight as sinograms. Sinogram is connected to LOR as when multiple LOR lines are connected one sinogram is created. For one sinogram the parallel LORs are presented. Sinogram is half of a sine wave that is presented sideways. The more there is LOR lines the more there is sine waves that are in the same sinogram. The advantage of the sinograms is that it takes less space when the data is stored this way. Sinograms can also be done for 2D and 3D images. To reduce even more space, michelogram can be used, which merges multiple sinograms together. In the images it is quite common to have a high noise that is caused by the limited counting statistics. The sensitivity on the other hand has been increasing in the newer machines. [14] [11]

1.2.2 Time activity curves and Region of interests

This subsection provides a more detailed explanation of how images and data are processed following acquisition in order to enable their subsequent use. Time activity curves (TAC) and Region of Interests (ROI's) are an important part of the actual study part of this thesis. So, understanding the way they work and what kind of information they can give is needed. TAC's are commonly measured for specific ROI, commonly left ventricle (LV) or left atrium. To get TAC's this curve can be

obtained from dynamic PET-imaging. As explained earlier, noise and statistical changes can affect the curve when having real patient data. It is also possible that the curve can get affected by spillover, which means the radioactivity leaks to another ROI affecting the overall radioactivity level detected in that specific ROI. From the TAC's it is possible to create dynamic compartment models. Also, arterial input function (AIF) is used to measure the activity in blood. This is done during imaging. The subject of compartment models is explained in more detail in section 3.1.1. TAC's can be used to extract information from the measures. Commonly different parameters can be extracted like blood flow, tissue fraction and arterial blood volume, that can give indication on whether the patient might need medical help to prevent severe diseases that can lead to severe consequences. [16][17] [18]

1.2.3 Tracers

In PET-imaging a radio tracer is used in studying a specific disease. For this common way is to use radioactive radionuclides that interact with matter. These tracers are called radiopharmaceuticals. The radionuclides used are produced by using a cyclotron system. Cyclotron bombards targets using charged particles where the nuclei will be neutron deficient. Common subjects for using radionuclides are cancers, myocardial ischemia and CAD. [19] [2] The most widely used tracers for perfusion studies are [2-^{18}F]FDG (^{18}F-flurpiridaz), $H_2{}^{15}O$ (radiowater), ^{15}O (carbon monoxide), ^{13}N-ammonia and ^{82}Rb (Rubidium-82). [12] In this study radiowater is the tracer of interest as it is used in the models in PET-centre. There are many other tracers in addition to these tracers. Many new tracers are constantly being tested and produced, so the field is constantly developing also in the radiopharmaceuticals side as well as the other equipment's. Next taking a closer look at radiowater how it behaves and why it is a good tracer. [19]

1.2.4 The radioactive water $H_2{}^{15}O$ as a tracer

To better understand why the radiowater is the tracer of interest, some of the features of it outshines the other tracers. In myocardial tissue radiowater has the extraction fraction of 1. This makes it possible to measure the perfusion directly. But when it comes to the Rubidium-82 and ^{13}N-ammonia they are also dependable on their own metabolism as well as perfusion, and they have more limited extraction fraction then what radiowater has. Different tracers have different half-life as well as maximum positron energies. They can also differ with the ways they are produced as well as how they are absorbed in the body. In example ^{13}N-ammonia and radiowater $H_2{}^{15}O$ are produced using a cyclotron whereas ^{82}Rb is produced using a generator. [20] [19] Radiowater is a tracer commonly used in non-invasive PET-imaging studies and clinically. Its half life is 2.2 minutes which is relatively short as only Rb-82 has a lower half life with 1.25 minutes. The average positron energy of a O-15 radionuclide is 0.72 MeV; maximum energy is 1.74 MeV and the maximum range in tissue is 8.4mm. O-15 radionuclide has one of the highest average positron energies released. [12] [19]

To be able to study diseases like CAD and myocardial ischemia commonly myocardial perfusion imaging is used. With high contrast it can be possible to detect the disease earlier and therefore, to treat the problems before it gets irreversible. If the functioning of LV is disturbed it can affect the other functions radically as LV is responsible for moving the oxidised blood everywhere in the body. [21]

1.3 Cardiovascular system, diseases and diagnosis via PET imaging

The highest mortality causes in modern times are linked to the diseases of the myocardium and the coronary artery. When small problematic changes build up, they can have devastating effects all around the body. Myocardium and the vascular system create the oxygen cycling system. The blood vascular system is a closed system, which creates a certain range of pressure in a rest state. But when the body needs more oxygen, i.e. in a stress state, heart rate gets elevated and pressure in the vascular system increases. In a healthy individual, this pressure shift is normal phenomena, but with a patient that has a blockage in the arteries, the pressure is inevitably higher and can lead to dangerously high pressures that can have devastating outcomes. [22] [23] The following sections will go over the critical information to understand the basics of the myocardial functions, blood flow and their importance for heart health. Also, the disease explanation of CAD and myocardial ischemia are explained, as these are the most common causes for problems in circulatory systems in the myocardium.

1.3.1 Cardiovascular systems functions

Oxygen is essential for normal physiological function. In its absence, the brain and other vital organs sustain damage, and prolonged oxygen deprivation ultimately results in death. Our heart has an important job, for delivering oxygen rich blood to all around our body, so that our muscles and cells can function. Oxygen demands change in time depending on what the body currently needs. The myocardial muscle is more easily prone to damage then the other parts of the body, as it contains very limited glycogen stocks and its metabolism is mostly aerobic. Meaning that the energy function needs to be constantly on going to ensure there is no damage caused to the heart. [23] [24]

1.3.2 Myocardial blood flow (MBF)

PET is the leading imaging method used in myocardial blood flow measuring. Myocardial perfusion imaging (MPI) using PET has outstanding accuracy in diagnostics compared to other methods. Myocardial segments with myocardial blood flow of $\approx$ 2.3 mL/min/g or less during stress measurements can indicate abnormal flow values. Myocardial blood flow is an important measurement on defining certain diseases like CAD and myocardial ischemia. Disturbances in the blood flow can mean there is a problem in the coronary artery. If there is an abnormal blockage in the coronary arteries, this will cause narrowing, which causes the blood flow to be disturbed causing higher pressures and stress for the arteries. Aortic pressure is also known as parietal stress (PS), and according to Laplace, it is directly proportional to the pressure (P) in the cavitaries and the radius (r) and inversely related to parietal thickness (2h). This can be reviewed from Eq. 7.

$$PS = \frac{P \cdot r}{2h}. \tag{7}$$

From this one can see how the change in the radius caused by plaque build up can increase the pressure and obstruct the blood flow. [23] [24] [25]

To study the myocardial blood flow, it is common to use imaging for rest and stress perfusion. Depending on the tracer, different methods are used. In the case of radiowater and its short decay time, a pharmacological stress test is used, where a substance is used to increase the blood flow. A common substance to increase the heart rate that causes increase in the blood flow is adenosine triphosphate (ATP). This is done as it can be hard to detect the reduction of blood flow only measuring the rest state as the range of what is considered normal can vary greatly depending on the patient's sex and age. A key aspect is that estrogen has been found having protective effects on the micro vascular system in the coronary arteries. This also influences the stress perfusion values. When the stress is chemically induced it is easier for the physicians to notice whether the myocardium has a reduced blood flow

or not. Commonly in the stress state a value under 2.3 [ml/min/g] is considered reduced blood flow. To sufficiently deliver oxygen in a stress state the blood flow should be higher. Reduced blood flow value shows there is an obstruction in the vessels. [26] [27] [28]

1.4 Heart failure and its most common causes

The most common causes for HF are CAD and myocardial ischemia. HF causes most of the hospitalizations worldwide, while it is daily also affecting approximately 30 million people. HF happens when there are structural and/or functional abnormalities in the myocardium. These abnormalities can lead to defects of the myocardium which can further cause problems in the filling and ejection of the myocardium chambers. One of the most common causes of HF is the reduced ventricular myocardium function, which causes insufficient blood supply. There can be different kinds of HF types, i.e. HF with preserved and reduced ejection fractions. Changes in pathogenic mechanisms associated with HF can be caused by increased hemodynamic overload, meaning there is a high possibility of acute HF and injury in the myocardial muscle. If the disease has developed to acute HF it is severely life-threatening. HF can be caused also by more severe causes like myocardial ischemia because it can lead to necrosis in the myocytes. This will lead to lower coronary perfusion which can result in severe global ischemic myocardial injury. [29] [30] [24]

Over half of the cases of the hospitalized patients with HF are diagnosed with underlying CAD and in North America and Europe finding of myocardial ischemia has the same diagnosing frequency. If the case of CAD has developed to myocardial ischemia and if the ischemia hasn't caused any necrosis, it might be possible to treat it to avoid occurrence of the HF or necrosis to develop. [24] [31]

1.4.1 Atherosclerosis

Atherosclerosis will be next explained, as it provides essential background for understanding CAD and myocardial ischemia. Atherosclerotic disease causes most of the strokes and myocardial infarctions in developed countries. As a disease atherosclerosis is not a new one, it has been met over 4000 years ago. Some of the youngest patients noticed to have lesions are infants, making it partly related to genetics. It is not quite sure whether these lesions from a young age mean they will be affecting the individual in adulthood. But the number of cases has increased that do affect patients. Whereas these are mainly a result of living habits of a modern human and developed countries where habits have gotten more sedentary, following a worsened diet, having higher rates of type two diabetes as well as higher rates of smoking and drinking combined with high stress environments.

Arteriolosclerosis is a type of atherosclerosis where the walls of small arteries stiffen and get narrowed. This can happen in the elastic arteries, specifically in the aorta and in coronary arteries. It is quite common that when the disease appears in the patient's arteries, it is not spread out evenly. Rather it affects certain areas that are more prone to stress and other factors. It is also quite common to find lesions that are in different stages. In a case where the blockage is chronic or worsening, when the myocardium is contracting the blood flow is increasingly reduced.[28] [32]

1.4.2 Coronary artery disease (CAD)

CAD is caused by the atherosclerosis that has caused narrowing in the coronary arteries [33]. There are two types of CAD, obstructive and non-obstructive. The differences with these two are that non-obstructive is mainly caused by different chronic syndromes affecting the blood flow or myocardium and not obstruction from lipids and inflammation. Non-obstructive CAD won't lead to fatalities with the same rates as obstructive CAD. Here we are focusing more on the latter. [34]

CAD is one of the leading causes for stenosis in the arteries. If CAD goes unnoticed, it can cause problems in the oxygen extraction. And as mentioned earlier in the worst-case scenario it can cause myocardial ischemia which can cause necrosis from the lack of oxygen. It is especially deadly for patients over 35. CAD is also associated with chronic inflammation and if CAD is not treated it is highly possible the problems in the micro vascular system will get worse as well as the atherosclerosis will become more advanced, leading to increasingly decreasing MBF values. [28] [26] [27]

1.4.3 Myocardial ischemia

As mentioned earlier the myocardium is highly dependable from high oxygen delivery through blood flow. If the oxygen delivery is unbalanced, it can lead to severe complications like necrosis of the muscle. The problem with ischemia is that most of the time the disease has advanced so far that the damage is irreversible as dysfunction in cardiac functions has occurred. [30] [35]

The narrowed arteries cause the increase in the LV filling pressure as explained in the earlier sections. Also, when the walls of LV are thickened there is an even higher chance of ischemia and is commonly combined with increased pressure. This increased pressure causes myocytes to stretch which will cause even more problems in the arteries. Eventually when this will result in an ischemic heart, troponin will be released. When the muscular layer is exposed to the higher level of myocardial pressure, the possibility of necrosis caused by ischemia is even more elevated. In the case of HF, which will lead to ischemic injury, the pressure in the ventricular has risen so high that myocardium's capability to keep the cardiac output normal is compromised resulting in a reduced output. [24] The problem with myocardial ischemia is that it is a self-propagating process, making the prognosis poor. Also, if myocardial ischemia is found there is a possibility of finding necrosis. [24] [31]

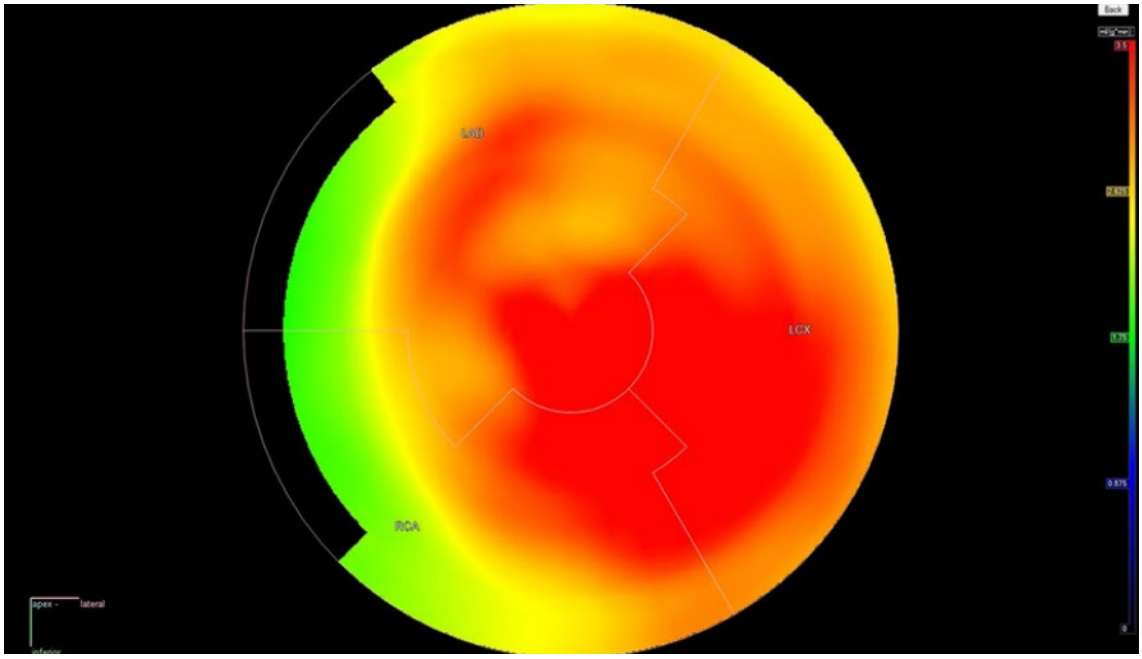

Figure 1. Polar map made with CARIMAS software used in PET-imaging studies and diagnosing methods. This polar map is divided using 3-segments. [39]

1.4.4 How Ischemia and CAD are diagnosed using PET

It is common to use PET-imaging combined with radiowater $H_2^{15}O$ to diagnose ischemia and CAD. It is a non-invasive way of assessing the myocardial blood flow values. Like discussed earlier other tracers can be used, but radiowater has some advantages. In the PET imaging of myocardium, the flow is measured in the whole coronary artery network, meaning the larger and smaller vessels are both included. To diagnose CAD 17-segment polar maps can be analysed scoring each segment from 0-4. Where 0 means normal perfusion and 4 absent perfusion. Then the sum of all the segments is used to see whether results are normal or severely abnormal. In normal cases the sum stays under 4 and the other abnormal ranges are 4-8,9-13 and lastly the severely abnormal where the sum is higher than 13. [36] [37] [38]

PET imaging can quantify the MBF and myocardial flow reserve. As these values can be retrieved separately it can help diagnosing CAD with higher accuracy. As the cut off values are not strict it is important to follow the MBF values during

rest and stress and see how they are changing. Pharmacological enhanced stress has similar sensitivity and specificity as exercise tests. When the images are analysed, a 17-segment model of the LV is created. From this image myocardial ischemia can be detected by comparing the rest and stress images, in the different segments. Polar map shows using different colors what is the perfusion value in a specific area. If the value is lower than it should, this can indicate myocardial ischemia finding. Ischemia is defined by perfusion of at least 2 adjacent myocardial segments with blood flow of 2.3 [ml/min/g] or less. This cutoff is not strict, and signs of ischemia can appear in higher MBF levels as well. In Figure 1 we can see a polar map divided into 3-segments. [39] The detection of CAD is primarily related to the measured values of blood flow. Values for MBF without significant CAD in rest are 1.00 $\pm$ 0.25 [ml/min/g] and for stress 3.26 $\pm$1.04 [ml/min/g], these values are from radiowater PET [40]. In ischemia the stress value is under 2.3 [ml/min/g]. [25] [26] [28] [41]

1.5 Use of models as tools for analysis of PET studies

Using models is a common practice to study and test hypotheses before possible implementations. In medical fields it is common to model different scenarios, as not every patient's data can be used in studies, not enough data is available or other parameters need to be extracted that otherwise would not be possible. Being able to retrieve more information using just a small amount of data or to generate more of it can be beneficial to better understand different scenarios. In the coming sections dynamic modelling is explained. For compartment modelling commonly a dynamic model is used. To optimize parameters with the models different methods can be used. [42] [43] In the following sections a quick look on the basics behind different modeling methods and where they are derived from is explained, as some of these methods are used in the study.

1.5.1 Modelling of the MBF

Kinetic models are used to determine rate constants which describe the biological function of the measured PET signal from the TACs. The radioactivity in the tissue depends on the tissues metabolism as well as from AIF which is the concentration of radioactivity in the arterial blood over time. The model tries to explain the functionality of the tissue determined by the parameters. The model's purpose is to describe the kinetics. To define the model parameters, a simulated TAC can be fitted to the actual data and the parameters predicted. When creating a model it needs to be validated in some ways as well as defining when the model is good enough and when it is in need of further development. Making a model having perfect accuracy is not something that is necessary and commonly using a simpler model will do just fine. [44]

1.5.2 Compartmental modeling

For every compartment model the prediction of the rate constants (k_n) is one of the main goals. There are different sizes of compartment models. They normally are notated as (C_1,C_2,...,C_n). The model works by following the change in the movements of the tracer molecules. For PET the larger compartment models are not needed. Depending on the size of the compartment model a different amount of rate constants are produced. For the smaller ones commonly one to six constants are used and they are marked as K_1,k_2,...,k_6. Once the rate constant is determined, it can be used to determine physiological parameters. Obtaining these parameters is usually the goal of modelling methods using tissue radioactivity measurements. I.e. The constant of blood flow is the one depicting the transfer from arterial blood to the tissue compartment. [44]

1.6 Model fitting methods

In modelling different models are used, depending on what kind of problem is in question. Simpler models can be used for simple problems as more complex models could over fit. It is good to note that using a complex model for a simple task might work well for the given data but causes problems when trying to generalize to different data. Some of these models that are used belong to the type of regression models. There are multiple different kinds of regression models, such as linear, exponential, logistic, polynomial, ridge and lasso regressions. [42] Linear regression is an example of a simple regression model. There are also different ways to execute it. The simplest example of linear regression model is such where the function of the model includes a single regressor x and this has a relation to a y creating a straight line. This straight line is the result from the linearity of the function. This simple linear regression can be more easily understood from the Eq. 8.

$$\mu = \beta_0 + \beta_1 x + \epsilon. \tag{8}$$

Where the β_0 is intercept and β_1 slope and they are unknown constants that are commonly called as regression coefficients. There can be multiple slope constants in the function. Whereas the ϵ is a random error component. There are also other linear regression models like multiple linear regression models as well as weighted linear regression models. In the weighted model prior weights are used w_i. Commonly matrix presentation is used to simplify the math. Due this the X in Eq. 9, becomes model matrix $\mathbf{X} = [\mathbf{x_0},\mathbf{x_1},...,\mathbf{x_n}]$ including the other regressor.

$$\mu = \beta X. \tag{9}$$

And the $\mu = E[\mathbf{y}]$ leading to Eq. 10:

$$\text{var}[\mathbf{y}] = W^{-1}\sigma^2. \tag{10}$$

Where the W^-1 is prior weights that are represented as the n x n identity matrix I_n where the n represents the size of the matrix. The linearity of the model comes from when the quantitative explanatory is linear. [43] [45] Next closer look is taken in the non-linear regression model where polynomial, logistic and exponential regression belong. A closer look of the exponential regression model is taken as that is the type used in the study itself.

1.6.1 Non-linear Regression models

The solutions used in compartmental modelling are commonly non-linear as the number of parameters is larger and the connections between the system are defined by non-linear functions. The regression model tries to find the most optimal parameters that minimizes the loss function and will help to achieve more accurate modelling. Non-linear regression models are also considered as a machine learning algorithm. This is due to the fact they are made to make predictions from complex relationships that the variables represent, and these predictions are depending non-linearly from the unknown parameters. Common non-linear regression functions

are exponential decay, growth function and the rational function. The exponential function is represented in Eq. 11.

$$f(x,\theta) = \theta_1 exp(-\theta_2 x). \tag{11}$$

Here θ is the parameter vector and x is the predicted variable. This function should also satisfy the first order differential equation. It can also be that the exponential function is a higher-order function when the differential equation as well will be in higher-order.[44] [46] [47]

1.6.2 Optimizers used for parameter optimization

During the parameter optimization the goal is to find the best fit. This is done by minimizing the optimization function that is used. For the optimization function to work initial guesses, input values are needed, and these can affect how well the model works. These guesses are used and furthermore modified during each step. This modification makes the algorithm iterative, and in each epoch the parameters are updated. While this goes on the optimizer function gets a smaller value. Eventually the optimization will converge, resulting in the changes being minimal to non-existing. When the loss function is small enough the optimized parameters are then furthermore saved as output values and returned to be used. The loss function basically compares the created function between the original and reports the difference between the original data and generated data. So, the optimizers point is trying to minimize the loss function to find the optimal parameters, by finding the global minimum. Different optimizers and different loss functions can be used in different problems. The optimization of loss functions is one of the key concepts in machine learning.

For the sake of the study a quick look is taken on the optimizing algorithm adaptive moment estimation also known as ADAM. ADAM is from 2015 and was created by D. Kingma and J. Ba and it uses adaptive learning rates for each pa-

rameter. This is different from the standard stochastic gradient descent (SGD) that only uses one learning rate for all samples. In the stochastic gradient descent, the weights are updated by each sample instead of the whole data which the standard gradient descent does.[44] [46]

1.7 Simulations and models in diagnosing CAD and ischemia

In PET studies it is common to use compartmental modelling to fit tissue curves as well as to analyse dynamic PET data. For this the input function in plasma is used. The simplest compartment model used in PET studies is the 1 tissue compartment model. In this model there are two rate constants K1 and k2. The tissue TAC is used to model tracer concentration (C_T(t)) as a function in time. Also, the function for the arterial blood (a(t)) or commonly known as AIF, is needed. It can be measured from the image or by blood sampling. Here in Eq. 12 is the tracer concentration.

$$C_T(t) = K_1 a(t) \otimes exp(-k_2 t). \tag{12}$$

and that can be further more used for the TAC and ROI modeling using Eq. 13.

$$R(t) = C_T(t) + V_a a(t). \tag{13}$$

or with the tissue fraction α in the Eq. 14.

$$R(t) = \alpha C_T(t) + V_a a(t). \tag{14}$$

Here the K1 represents the estimate for blood flow whereas sometimes the k2 can be multiplied using the water partition coefficient (p) to estimate the blood flow. When it comes to diagnosing a disease, these parameters can provide important information. [48] [18]

2 Materials and methods

In this part of the thesis the study and its phases are explained. The study focuses on developing and comparing different models.

2.1 The goal of the study

We aimed to compare the results from fit_h2o and fitmbf, that are part of TPClib, to new models. These models are the NAIST model and NASTα model, which was developed from the base of NAIST. Simulations from b2t_h2o, were used to create simulated time-radioactivity concentration TAC curves. These were used as a base to run all the other models and to be able to compare the TAC functions with a true value. A wide range of simulated data was selected because the robustness of the models wanted to be tested. Making the models data handling dynamic was one of the key details. Also a small real patient data set was used to compare the models and how they worked with real data. The main goal was to develop the NAIST model further and make another model that has some differences for the NAIST. Lastly, the models are evaluated and the performances compared.

2.1.1 Pipeline

The pipeline of the study is visualized in the Figure 2. This chart represents the core structure of the overall process. While smaller parts are also critical, they are omitted from the figure for simplicity. These steps included code fixing and debugging errors. TPClib software was downloaded using MINGW64, which is a BASH shell environment made for Windows-based operating systems for downloading systems that are meant to be downloaded using Linux operating system.

When the TPClib worked the debugging started to identify why the NAIST model failed. These phases are explained in the later subsection of compiling a working jupyter notebook. When the notebook was fixed, it was developed further

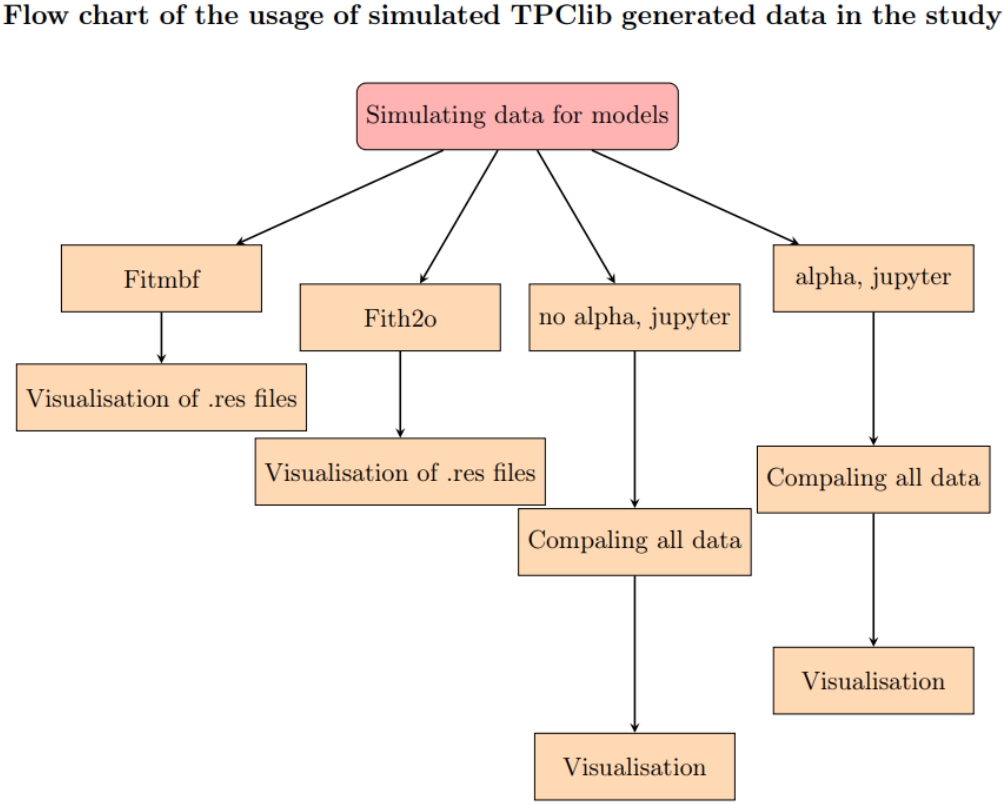

Figure 2. Flow chart of the study. The first phase is where the data is simulated using b2t_h2o. Next this data is used for all the models and from this all the box-plots and functions are done. Each model had either weighted sum of squares or R^2 and Akaike Information Criterion (AIC) used as a measure of goodness of fit.

by adding other key details like data organization, dynamic running, and parameter saving. To have a wide range of simulated TAC data, different parameters were used in the TPClib's b2t_h2o. This simulation was combined with another TPClib model fit_h2o.

After fixing the NAIST model the development of NASTα started. Both NAIST and NASTα models are run using the simulated TAC-data from the TPClib's b2t_h2o simulation. Both of these models employ an optimizer to estimate the global values of the parameters used for the optimization and use these to model its own TAC's and ROIS's. For the NAIST model one starting guess is used while for the NASTα model, multiple starting guesses depending on the sum of the b2t_h2o simulation TACs. Later, fitmbf was run using the same b2t_h2o data. When all the models were finished the results were then visualized and evaluated. The amount of data generated and modeled was large so making the visualizations of the parameters as well as the models dynamic was important. For the visualizations box plots were used as a trend for the parameters created could be noticed from these. While parameters as a function of perfusions were made to see how the models work, and whether there are some points that the code malfunctions. These methods were compared with the Akaike information criteria (AIC) measure as well as the R^2. In the end the Pearson correlation coefficient between the models is performed from NAIST with fit_h2o and fitmbf and NASTα with fit_h2o and fitmbf.

2.2 TPCLIB

TPClib is command-line based software that is used for processing and analysing data mainly created by Vesa Oikkonen and a group of other contributors after creation. It is coded using C and C# coding languages, and it is operated using BASH code. The software includes different functions. In this case interest is focused towards b2t_h2o, fitmbf and fit_h2o models, as these are crucial for creating the

Table I.
Variables used in the math explanation as well as the parameters used in the TPClib code [49]

Variable	Explanation	Unit
$C_i(t)$	Myocardial tissue radioactivity concentration at time t	[kBq ml^{-1}]
$a(t)$	True input function	[kBq ml^{-1}]
$ROI(t)$	TAC of radioactivity of ROI in LV myocardial region	[kBqml^{-1}]
$LV(t)$	TAC of radioactivity of ROI in the area of LV cavity	[kBqml^{-1}]
f	Blood flow of pefusable tissue	[ml min^{-1}ml^{-1}]
p	Partition coefficient of water	[ml ml^{-1}]
α	Tissue fraction volume of perfusable tissue in ROI	[ml ml^{-1}]
V_a	Arterial blood volume	[ml ml^{-1}]
β	Recovery coeffisient of left-ventricular ROI	[-]
$K1/k2 = vd$	partition coefficient	[-]
$K1$	Rate constants	$[\frac{g}{ml}]$
$k2$	Rate constants	$[\frac{1}{min}]$

simulated data and running these two models on that simulated data to have results that the NAIST and NASTα models can be compared to. In the last case also a small patch of patient data is run through these models.

In Table I are represented the variables used in the upcoming mathematical explanation, mathematical functions of the models. Some of these same variables are also presented in the model parameters that are either needed to feed to the modeling function or are the parameters the model will give out, i.e., the V_a, K_1 and k_2. These same parameters will also be used in the NAIST and NASTα models which are explained in later sections. In the fit_h2o model the perfusion that is talked about is tissue perfusion. In fitmbf perfusion is myocardial perfusion where

the blood flows through the heart muscle.

The fitmbf model from TPClib is explained in a report [49]. "The model estimates the parameters f, α and V_a. In this method those parameters together with larger ROI and LV cavity the arterial blood curve is calculated, and this is then used to estimate the parameters for the smaller ROIs." All the functions in this subsection come from the report. [49]

The equations that are used in these models are more complex then in the following NAIST application. The perfusion is calculated based on these three main equations Eq. 15, 16 and 17.

$$C_i(T) = f\int_0^T a(t)dt - \frac{f}{p}\int_0^T C_i(t)dt, \tag{15}$$

$$ROI(T) = \alpha C_i(T) + V_a a(T), \tag{16}$$

$$LV(T) = \beta a(T) + (1-\beta)C_i(T). \tag{17}$$

To be able to calculate the C_i(T) Eq. 15 and the ROI(T) Eq. 16 for the whole myocardial, the a(T) is first calculated from LV(T) Eq. 17 followed by adding that to the ROI(T) Eq. 16 and calculating the C_i(T) Eq. 15 from there. This calculation can be seen in the appendix A as this was solved more from an understanding point. Eventually the Eq. 18 is in the shape that it is used in the TPClib models.

$$ROI(T) = K1\int_0^T LV(T)dt - k2\int_0^T ROI(T)dt + V_{fit}LV(T). \tag{18}$$

For the smaller ROI's the C_i(T) Eq. 19 is defined from the ROI(T) Eq. 16, and that equation and its integral is then placed to the $C_i(T)$ Eq. 15. This solving is kept here as the α was also used in the NASTα version and this solving actually helped to understand the function in the code creation.

$$C_i(T) = \frac{ROI(T) - V_a a(T)}{\alpha} \tag{19}$$

And to be able to place it to the Eq. 15, the integral is taken.

$$\int_0^T C_i(t) = \frac{\int_0^T ROI(T) - V_a \int_0^T a(T)}{\alpha}. \tag{20}$$

And when Eq. 19 and 20 are added to Eq. 15, we get Eq. 21.

$$\frac{ROI(T) - V_a a(T)}{\alpha} = f \int_0^T a(t)dt - \frac{f}{p\alpha}(\int_0^T ROI(T) - V_a \int_0^T a(T)). \tag{21}$$

From where the values are grouped to get an end result seen in Eq. 22.

$$\frac{ROI(T) - V_a a(T)}{\alpha} = f(1 + \frac{V_a}{p\alpha}) \int_0^T a(t)dt - \frac{f}{p\alpha} \int_0^T ROI(T)dt|| \cdot \alpha. \tag{22}$$

To which $V_a a(T)$ is added in Eq. 23.

$$ROI(T) - V_a a(T) = f(\alpha + \frac{V_a}{p}) \int_0^T a(t)dt - \frac{f}{p} \int_0^T ROI(T)dt|| + V_a a(T). \tag{23}$$

$$ROI(T) = f(\alpha + \frac{V_a}{p}) \int_0^T a(t)dt - \frac{f}{p} \int_0^T ROI(T)dt + V_a a(T). \tag{24}$$

Now the model uses coefficients Eq. 25 and the Eq. 24 is in the two compartmental model shape.

$$\begin{cases} V_{fit} & = V_a, \\ K_1 & = f(\alpha + \frac{V_a}{p}), \\ k_2 & = \frac{f}{p}. \end{cases} \tag{25}$$

After substituting the parameters with coefficients from Eq. 25, the result eventually is Eq. 26.

$$ROI(T) = K_1 \int_0^T a(t)dt - k_2 \int_0^T ROI(T)dt + V_{fit} a(T). \tag{26}$$

2.2.1 BASH code for the TPClib's simulation and models

The BASH script is used to simulate the data and for the modeling. The parameters the data used for the data simulation with b2t_h2o were perfusion (f), vascular volume(Vb) and arterial fraction (fA). The BASH script was run on a remote computer using the Linux system. The time to run the first model that was combined

with the fit_h2o model, was approximately nine days and for the fitmbf around two days. The reason for the shorter running time was that the fitmbf used the already simulated data that was produced in the same BASH loop with the fit_h2o model. The amount of data simulated was 13860 function files with the noises. This simulated data was used for all the models used in this study. The first simulation BASH code for the fit_h2o can be viewed in appendix B and the fitmbf in appendix C.

The fitmbf produces the following parameters: myocardial blood flow in perfusable tissue (f), perfusable tissue fraction (PTF), arterial blood volume and spillover (Va). Whereas the fit_h2o is a one-tissue compartmental water model and produces the parameters of blood flow from tissue perfusion (f), partition coefficient (K_1/k_2), arterial blood volume (V_a) and time delay (ΔT). TAC-data from b2t_h2o was used as input data. A separate python code in jupyter-notebook was made to be able to analyse the parameters.

2.2.2 Parameters used in the TPCLIB-codes

In the b2t_h2o simulation the parameters that were used are in Table II. The amount of noise added was from 0 to 0.42 [kBq/ml] in steps of 0.042, so with 10 different noise amounts. For cv the range goes from zero to ten [0,...,10] in steps of two (,2). Vb had three values and perfusion went from 50 to 100 and from there to 1000 with steps of 100.

Range for the perfusion was selected to test the models robustness. Selecting values in the range 0.5 to 4 [ml/min/g] (or 50-400 [ml min-1 ml-1]), would have been sufficient, but for testing how the models perform in higher perfusion the resulting range 5-10 [ml/min/g] was added to the selection. Sometimes high values are reached in real life but rarely over 6 [ml/min/g]. Using radiowater the values of around 6 [ml/min/g] are sometimes received [50]. Arterial fraction percentage is not

Table II. Parameters used in TPClib simualtion b2t_h2o for generating the data to be used in the fitmbf, fit_h2o, NAIST and NASTα models.

Parameters	Explanation	Range
cv	Percentage of noise	([0,...,10],2)
j	Different noise value	([0001,...,0010],0001)
value	Perfusion	([50,100,...,1000],100)
Vb	Vascular volume	[10,12,14]
fA	Arterial fraction in percentages	([0,...,30],5)

represented for the heart but for the whole body it is 20-30% and in cerebral blood volume it is approximately 30%. Therefore a wide range was chosen to be used here as there is no proper recorded range [51]. For Vb the range of 10-14 was chosen as for CAD patient 12.9% was recorded and a value of 14% for total Vb [52] [53].

2.3 NAIST - Non-linear model for modeling MBF

The model didn't perform as intended, as there was a class and a function with the same name. When the function was invoked, execution never reached the intended target function; instead, it consistently resolved to the first matching function encountered, namely the one defined within the class. The original code only had the TAC-modelling, code was changed to be able to simulate ROI's as well. It was made to be dynamic to work for large amounts of data as well as saving all the parameters, functions and values in the same folder while named consistently.

2.3.1 Compiling a working jupyter notebook

To be able to tune the model jupyter notebook was used. It was compiled by collecting all the functions in the model and calling the needed imports. The code had some key points that needed to be tuned, so the parameters it would generate

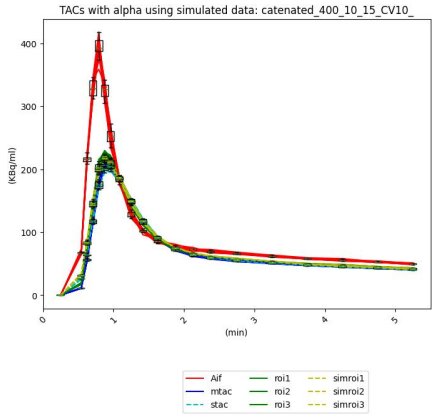

R2 tac_0001: 0.9948	R2 tac_0002: 0.9951	R2 tac_0003: 0.9950	R2 tac_0004: 0.9948	R2 tac_0005: 0.9946
R2 roi1_0001: 0.9964	R2 roi1_0002: 0.9967	R2 roi1_0003: 0.9966	R2 roi1_0004: 0.9965	R2 roi1_0005: 0.9963
R2 roi2_0001: 0.9964	R2 roi2_0002: 0.9966	R2 roi2_0003: 0.9965	R2 roi2_0004: 0.9964	R2 roi2_0005: 0.9962
R2 roi3_0001: 0.9964	R2 roi3_0002: 0.9966	R2 roi3_0003: 0.9965	R2 roi3_0004: 0.9964	R2 roi3_0005: 0.9962
AIC tac_0001: 78.4038	AIC tac_0002: 78.0973	AIC tac_0003: 78.3550	AIC tac_0004: 78.6937	AIC tac_0005: 80.0858
AIC roi1_0001: 73.4490	AIC roi1_0002: 73.0947	AIC roi1_0003: 73.5816	AIC roi1_0004: 73.7211	AIC roi1_0005: 75.0524
AIC roi2_0001: 73.2990	AIC roi2_0002: 73.0241	AIC roi2_0003: 73.4498	AIC roi2_0004: 73.5613	AIC roi2_0005: 75.0151
AIC roi3_0001: 73.3077	AIC roi3_0002: 72.9920	AIC roi3_0003: 73.4540	AIC roi3_0004: 73.5571	AIC roi3_0005: 75.0035
R2 tac_0006: 0.9943	R2 tac_0007: 0.9942	R2 tac_0008: 0.9945	R2 tac_0009: 0.9949	R2 tac_0010: 0.9942
R2 roi1_0006: 0.9961	R2 roi1_0007: 0.9960	R2 roi1_0008: 0.9962	R2 roi1_0009: 0.9966	R2 roi1_0010: 0.9960
R2 roi2_0006: 0.9960	R2 roi2_0007: 0.9960	R2 roi2_0008: 0.9961	R2 roi2_0009: 0.9965	R2 roi2_0010: 0.9960
R2 roi3_0006: 0.9960	R2 roi3_0007: 0.9960	R2 roi3_0008: 0.9961	R2 roi3_0009: 0.9965	R2 roi3_0010: 0.9960
AIC tac_0006: 79.6828	AIC tac_0007: 79.3141	AIC tac_0008: 80.3010	AIC tac_0009: 78.1513	AIC tac_0010: 79.9447
AIC roi1_0006: 74.7318	AIC roi1_0007: 74.3483	AIC roi1_0008: 75.3876	AIC roi1_0009: 73.1308	AIC roi1_0010: 74.9882
AIC roi2_0006: 74.6091	AIC roi2_0007: 74.2549	AIC roi2_0008: 75.2533	AIC roi2_0009: 72.9848	AIC roi2_0010: 74.8758
AIC roi3_0006: 74.7127	AIC roi3_0007: 74.2636	AIC roi3_0008: 75.2527	AIC roi3_0009: 72.9906	AIC roi3_0010: 74.8357

Figure 3. Example image to show how the radioactivity value was modeled and fitted. Result produces the TAC and ROI functions. In the images the noise amount is shown as a box-plots. For each simulated function a AIC and R2 value is calculated to see how good the fit is. This image has the functions that are produced using the AIF-information using perfusion value of 400 [ml min-1 ml-1] as input. The simulated b2t_h2o functions (mtac,roi1-roi3) and the NASTα modeled functions (stac,simroi1-simroi3) are both plotted in the image. In this one, the modeled functions are approximately the same. Which can also be seen from the R2 and AIC values, as well from the fact the functions have almost identical functions.

wouldn't produce unrealistic values. ROI simulations were added to the model. The model creates the TACs and ROIs using the AIF-input function. The notebook was made dynamic and organized combined with data saving methods that avoid overwriting. In this NAIST model the beginning guesses for the parameters can be seen in the Table III. They were based on selecting values that would be near literature values, mentioned earlier. For end result perfusion was calculated using the optimized parameters. For NAIST Eq. 27 was used. Here the calculated perfusion uses the optimized Va and K1 values. This is the same perfusion that is used in the fit_h2o model.

$$F = (1 - Va) \cdot K1 \tag{27}$$

The NAIST model took around five days to run.

Parameter name	Value
K1	3.3
k2	4.03
Va	0.3
k_min	0
k_max	5.0
k_initial_max	0.5
learn_rate	2e-2
iter_single_component	750

Table III. Parameters used for the non-linear regression models starting guesses for the optimizing in the NAIST model.

2.4 NASTα model build from the base of NAIST

When developing the NASTα model the parameter α was added. Multiple approaches in the model development were investigated, but the original function proved to work with this model as well. The modification needed the adding of the α in the get_tac_from_aif function. This function ended up being the one presented in Eq. 16. Working with the NASTα model took a lot of debugging to get it to work properly.

In NASTα model difference came from having multiple different guesses in the beginning. For each perfusion from 0.5 to 4 [ml/min/g] unique guesses were used and for the rest 5-10 [ml/min/g] same guesses. To define how to select what parameter guesses need to be used, the sum of original TAC data was used. This worked well when using the simulated data, but in the patient data, it ended up not working. This is probably due to the real data being noisier than the slightly noisy data used for the model development. For the NASTα model, the parameters changing during guesses can be viewed in the table IV and the parameters that stay the same can be viewed in table V. Additionally the perfusion was calculated from the optimized

Perfusion [ml min-1 ml-1]	50	100	200	300	400	500-1000
Parameters	Values					
K1	0.6	0.9	1.9	3.2	3.7	4.7
k2	1.2	1.6	2.3	3.5	4.4	5.0
Va	0.8	0.6	0.4	0.3	0.2	0.25
α	0.7	0.7	0.6	0.5	0.3	0.25

Table IV. The parameter guesses used in the NASTα model to optimize the non-linear regression models parameter optimization in larger range of perfusions.

parameters The NASTα model used the k2 parameter to calculate the perfusion using a partition coefficient value of p=0.9464 that was used also in [49]. This model did take around ten days to run.

2.5 Evaluation methods used for NAIST and NASTα

The NAIST and NASTα models and data simulated using the b2t_h2o are compared using the goodness of fit parameters of R^2 and AIC. The R^2 and AIC value are saved and presented i.e. Figure 3. To see how much the noise affects the modeled functions a box plots are plotted in the images that gives the range of how much noise is generated.

The values for R^2 are calculated using skicit from python that are defined in Eq. 28. Also using the Eq. 29 and 30. Using only R^2 is not sufficient, and that's why Akaike Information Criterion (AIC) is also used Eq. 31. In the AIC_c Eq. 32 n is the amount of data points, the number of times the measurement is taken, meaning the time data. In the data the used n is 20. Whereas k is the approximated number of parameters of current model+2. In the NAIST model the k is 5 and NASTα k is 6. Because the amount of time data points is under 40 the Eq. 32 must be used in the calculations of the change in AIC. To calculate the change Eq. 33 is used where AIC_A is the minimum AIC that the others are compared and AIC_B is the current

Parameters	Values
k_min	0
k_max	6
k_initial_max	0.5
learn_rate	2e-3
iter_single_component	1500

Table V. The parameter guesses used in the NASTα model that staid the same with different perfusion values to optimize the non-linear regression models parameter search.

AIC. The smaller the AIC value the better the fit is. [54] The delta AIC values are represented in the box plots of the NAIST-and NASTα-models that are shown later in the results.

$$R^2(y,\hat{y}) = 1 - \frac{\sum_{i=1}^{n}(y_i - \hat{y}_i)^2}{\sum_{i=1}^{n}(y_i - \mathbf{y})^{\mathbf{2}}}, \tag{28}$$

$$\mathbf{y} = \frac{1}{n}\sum_{i=1}^{n} y_i, \tag{29}$$

$$\sum_{i=1}^{n}(y_i - \hat{y}_i)^2 = \sum_{i=1}^{n}\epsilon_i^2, \tag{30}$$

$$AIC = n \cdot ln(\frac{SS}{n}) + 2 \cdot k = n \cdot ln(SS) - n \cdot ln(n) + 2 \cdot k, \tag{31}$$

$$AIC_c = AIC + \frac{2 \cdot k \cdot (k+1)}{n - k - 1}, \tag{32}$$

$$\Delta AIC = AIC_B - AIC_A = n \cdot ln(\frac{SS_B}{SS_A}) + 2 \cdot (k_B - k_A). \tag{33}$$

2.6 Pseudocode

In this section the phases of creating the actual code are presented. To avoid leaking to any Large Language Models (LLM) the code is done as a pseudocode. Therefore

Table VI. Explanation for the math variables used in the code.

Parameters	Explanation
c_0	current AIF-point
c_1	next AIF-point
t_0	current time
t_1	future time

all the NAIST and NASTα codes debugging, and code creation is done without the usage of LLM's. The finalized pseudocodes that are used to run over the models can be seen in D appendix for NAIST and F appendix for NASTα.

Both models use the same exponential Eq. 34 in the code that calculates the desired modeled TAC and ROI functions from the input. In the NASTα model the Eq. 16 was used in the class to optimize the parameters as well as in the get_roi_from_aif function to get the actual TAC's. In the original NAIST model a Eq. 39 was used. In the table VI the parameters used to get the variables a,b,d and T from the Eq. 35, 36, 37 and 38 are explained. These are derived from the AIF-function. It iterates over the time finding the correct points for the functions.

$$ccc = k1 \cdot \frac{a}{k2 \cdot T + d} + (ccc - k1 \cdot d) \otimes \exp -k2 \cdot T, \tag{34}$$

$$a = \frac{c_1 - c_0}{t_1 - t_0}, \tag{35}$$

$$b = c_0, \tag{36}$$

$$d = \frac{b}{k_2} - \frac{a}{k_2^2}, \tag{37}$$

$$T = t_1 - t_0, \tag{38}$$

$$ROI(T) = C_i(T) + V_a a(T). \tag{39}$$

2.7 Usage of patient's data

Lastly the models were tested using small set of patient data. This included data from 10 patient. They only had TAC and AIF data recorded. For running the patient data in the TPClib modified BASH-code was used shown here:

```
#! /usr/bin/bash
export PATH=/directory/where/the/software/is:$PATH
path_to_save_data="/path/where/the/data/is/saved/"
for dir in /home/data/directory/name/here/
do
 echo "dir=$dir"
 for file in $dir/*
 do
  if [ -f $file ]; then
   echo "file= $file"
   file=${file##*/}
   fit_h2o -ml -fpt -k2 -Delay=0
            -fit="${path_to_save_data}1__All.dft"
            "${path_to_save_data}2__All.dft" "${dir}/${file}"
            360 "${path_to_save_data}/${file%*.dft}_h2o.res"
  fi
 done
done
```

And the same code was used for the fitmbf with the exception of changing fit_h2o line to:

```
    fitmbf -beta=0.95 "${path_to_save_data}manual_TACs.dft" "2" "1"
    "${path_to_save_data}/${file%*.dft}_mbf.res"
```

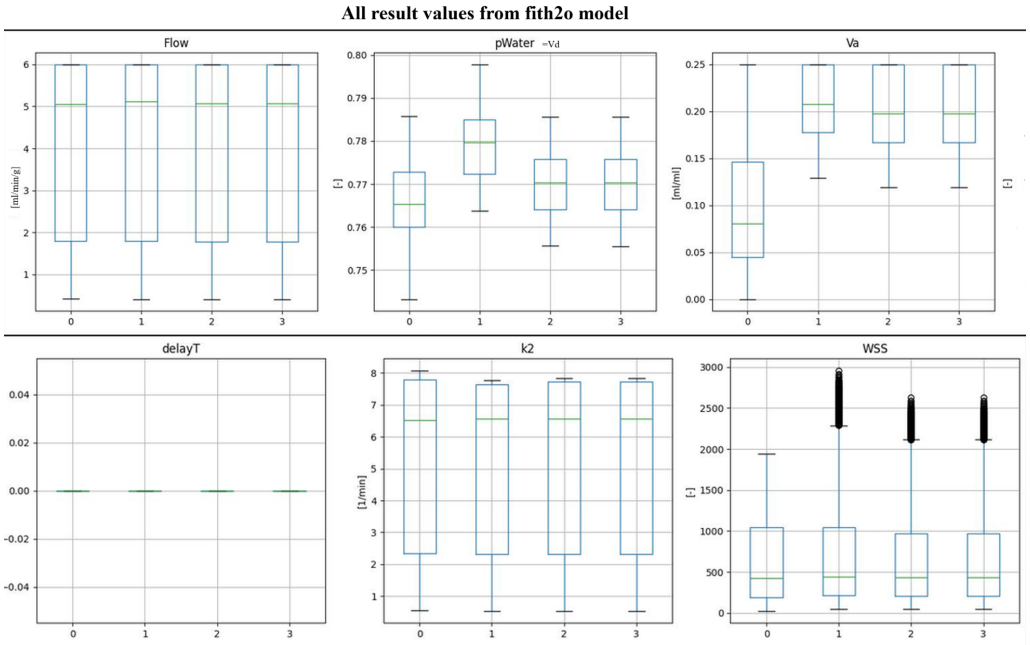

Figure 4. In this figure are represented all the optimized parameters that were produced using the fit_h2o model. The perfusion peaks at 6 [ml/min/g] , where the input used to optimize the values went all the way till 10 [ml/min/g]. The ranges here are wide, as the amount of different perfusions and the corresponding other parameters are represented. Delay T is zero, as there was no delay added to the original data. In the x-axis are plotted 0=TAC and the 1-3 are the ROIS 1-3.

For running the code using NAIST and NASTα some changes were made, but those mainly included data formatting and data reading whereas the base of the models stayed untouched. The Figure for a flow chart for the patient data running is represented in K appendix in Figure K.1.

3 Results

In this section the overall results are explained. Starting from comparison with the generated parameters that ended up being approximately 1.2 billion not including the TACs modeled. The decision for the large dataset was due to the tuning need of the models but also due to the robustness testing. The results were plotted for each perfusion for each model and for each model one with all the produced parameters from all different perfusions. Only some of the figures are shown but all the other perfusion parameters and functions are in the appendix section. The appendix sections are specified in the place the results are given.

One modeling result was shown as an example from the generated figures where the simulated TAC and ROIs are shown in Figure 3. There were 1360 of these figure. Also the AIC and R^2 values for each function was plotted in the image. For the different models an example from all the perfusion values where the parameters are in one box plot and parameters with perfusion value of 2 [ml/min/g] are shown. Some examples of the parameters as a function of perfusion are shown. In the end a correlation test performed using Pearson's r-value test is shown.

3.1 Comparisons between TPClib and NAIST-models.

Values for patients with prior history of myocardial infarction the mean values collected in rest are for perfusion 1.16 [ml/min/g], for α 0.79 [g/ml] and for Va 0.18 [ml/ml]. And the ranges for over all normal rest ranges are shown in the table VII [55].

3.1.1 fit_h2o

In Figure 4 are all the values generated with fit_h2o model. Flow is blood flow perfusion tissue, pWater is K_1/k_2 (vd) and the WSS weighted sum of squares. The model will not produce perfusion values larger than 6 [ml/min/g]. In the Figure 5

Table VII. Mean parameter values measured in rest from healthy individuals.[55]

Parameter	Ranges
Perfusion LAT	0.85±0.13 [ml/min/g]
Perfusion ANT	0.79 ±0.14 [ml/min/g]
α LAT	0.71±0.05 [g/ml]
α ANT	0.72±0.09 [g/ml]
Va LAT	0.22±0.10 [ml/ml]
Va ANT	0.23±0.10 [ml/ml]

is an example from the perfusion value of 2 [ml/min/g]. The flow is near to 2, the WSS is relatively small, and the Va is near of the reference values. In the x axis in both figures 0=TAC and 1-3 are the different ROIs. The rest of the perfusions can be seen in the F.1 appendix for the box plots and F.2 for the functions and mean values with standard deviation in F.3. The parameter data per perfusion values of 0.5,1,3-6 [ml/min/g] are in figures F.1, F.2, F.3, F.4, F.5, F.6 respectively from the fit_h2o model. In the function plots are all the parameters plotted as a function of perfusion for perfusion in Figure F.7, k2 in Figure F.8 ,pWater (vd) in Figure F.9 and for va in F.10. The mean with standard deviation values can be viewed in F.11.

3.1.2 fitmbf

In the Figure 6 are shown all the generated values from the fitmbf model. The difference here compared to the other models can be seen in the perfusion box plot, it goes till 10 [ml/min/g]. Correctly modeled parameters peaked at perfusion of 5 [ml/min/g], where the WSS got significantly higher. The fitmbf model produces parameters perfusion, Va, WSS, PTF (α) and rMBF (mean myocardial blood flow). In the Figure 7 are shown the results from perfusion value of 2 [ml/min/g] for the fitmbf. Here the optimized flow was 2 [ml/min/g], α is in range as is the Va. The

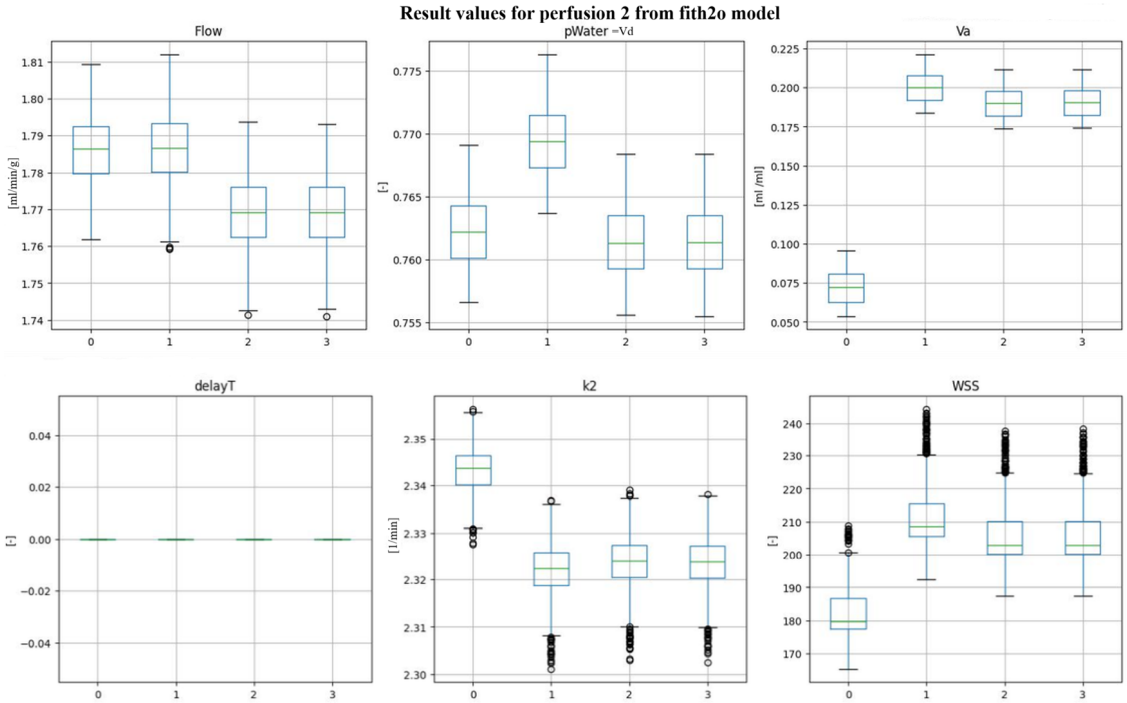

Figure 5. Optimized parameters from the fit_h2o model. In this figure are presented the values that were obtained using the simulated data of perfusion value of 2 [ml/min/g]. Here can be seen how the values are more limited compared to the plot whit all the values. These have a better fit as can be seen from the WSS boxes. Delay T is zero, as there was no delay added to the original data. In the x-axis are plotted 0=TAC and the 1-3 are the ROIS 1-3.

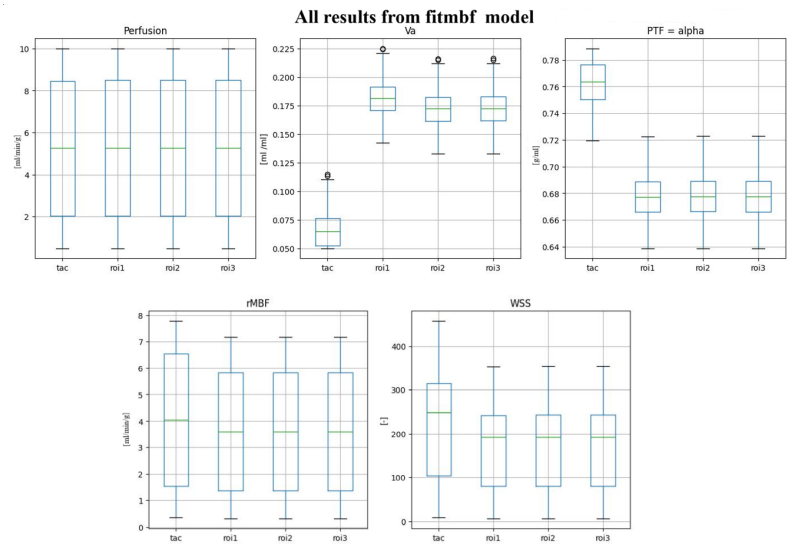

Figure 6. In this figure are represented all the optimized parameter values from all different perfusions from the fitmbf model. The perfusion goes all the way to 10 [ml/min/g], like the input data. So this model doesn't peak the same way as the fit_h2o. The Optimized parameters seem to be limited still as they won't look too far from the reference values. The ranges here are wide for the rMBF (mean myocardial blood flow), perfusion and WSS (weighted sum of squares) as it includes all of the values.

function against which the model was compared yielded small WSS values for all the functions. Rest of the perfusion plots can be seen in the G.1 appendix for the boxplots and G.2 for the functions and G.3 for mean values from the parameter values with standard deviation in Figure G.10. The parameter data as box-plots per perfusion values of 0.5,1,3-5 [ml/min/g] are in figures G.1, G.2, G.3, G.4 and G.5 respectively from the fitmbf model. In the function plots are all the parameters plotted as a function of perfusion for perfusion in Figure G.6, α in Figure G.7, rMBF in Figure G.8 and for va in G.9.

3.1.3 NAIST

In the Figure 8 are all the parameter values from all the perfusion values generated using the NAIST model. Here the k2 has also reached its peak approximately around perfusion of 5-6 [ml/min/g]. Values for Va are high as it includes all the data. The

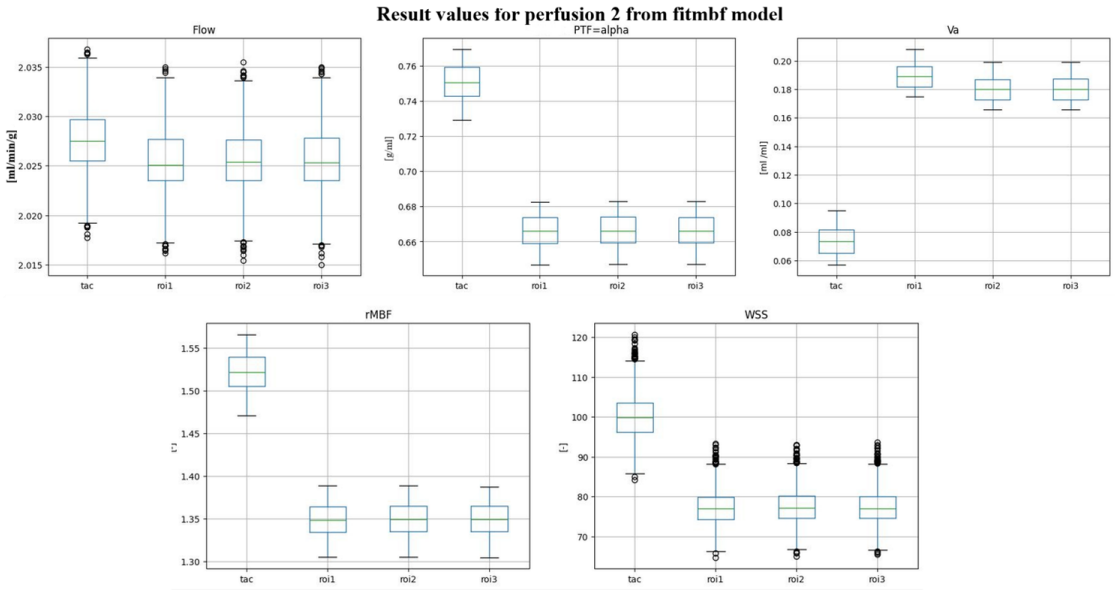

Figure 7. Optimized parameters from the fitmbf model. In this figure are presented the values that were produced using the simulated data of perfusion value of 2 [ml/min/g]. The values have small amount of fluctuating, and the values correspond well with the reference values mentioned earlier.

function comparison has produced small ΔAIC values for all the TACs. In the Figure 9 represent the values generated using perfusion of 2 [ml/min/g]. Here the k2 is in range. For the Va the values are almost identical with the other models. Values for Vd are under one like they should and ΔAIC have produced small values. Rest of the results for the NAIST model can be viewed in the H.1 appendix for the box plots, H.2 the function plots and H.3 for all the mean values with the standard deviations in Figure H.15. The parameter data per perfusion values of 0.5,1,3-10 [ml/min/g] are in Figures H.1, H.2, H.3, H.4, H.5, H.6, H.7, H.8, H.9 and H.10 respectively from the NAIST model. In the function plots are all the parameters plotted as a function of perfusion for K1 in Figure H.11, k2 in Figure H.12 , Va in Figure H.13 and for vd in H.14.

3.1.4 NASTα

In the Figure 10 are all the parameters represented that were retrieved from the NASTα model. As this one is slightly more complex model and the parameter guessing significantly affects the end results, it can be seen that some of the values are too high, Vd is over 1, when it should stay under and the α is much higher then approximately 0.7 [g/ml], which is a common value for α. In the Figure 11 are separate perfusion parameters represented for the perfusion value of 2 [ml/min/g]. Here we can also see that the model works better in the small perfusions when using the simulated data. The Va is almost identical with the other models, and the α is near what fitmbf had. Here again small ΔAIC values are received. The rest of the other perfusion values can be viewed in the appendix I.1 for the box plots, I.2 for the functions and I.3 for all the mean data with standard deviation from the parameters in Figure I.15. The perfusion value was not generated but it was calculated using the k2 and p and it is included in the comparison but not in the box plots. The parameter data per perfusion values of 0.5,1,3-10 [ml/min/g] are in Figures I.1, I.2, I.3, I.4, I.5, I.6, I.7, I.8, I.9 and I.10 respectively from the NASTα model. In the function plots are all the optimized parameters plotted as a function of perfusion for k2 in Figure I.11, flow in Figure I.12, va in Figure I.13 and for vd in I.14. For easier comparison between parameters mean and standard deviation values all the values were also plotted to a table. This can be viewed in the J appendix J.1.

3.1.5 Behavior during modeling

To understand how the model works, plots as a function of perfusions are explained. In the Figures 12 and 13 outliers are a result from the NASTα models parameter guessing failing. Resulting the use of a wrong set of guesses in the beginning. In the Figure 12 the function keeps on going down around the perfusion of 5 [ml/min/g]. This indicates that the model will not work in the high perfusion values. In the

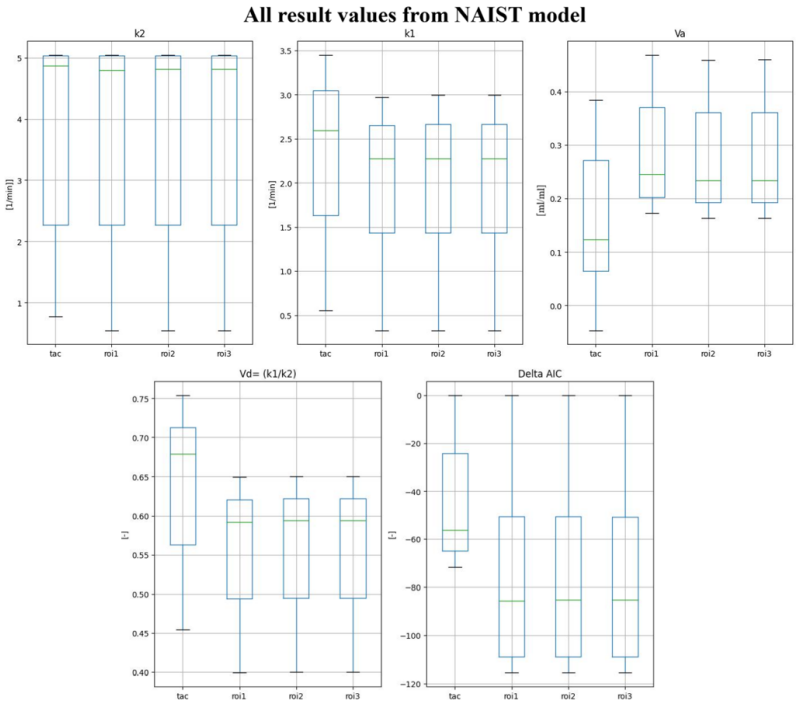

Figure 8. In this figure are represented all the optimized parameter values from all different perfusions from the NAIST model. Here we can see the k2 peaking at 5. This indicates that the model fails to operate reliably under conditions of high perfusion values. Due to this, high Va values for TAC is measured. Regardless the ΔAIC value stays relatively small. And Vd under 1.

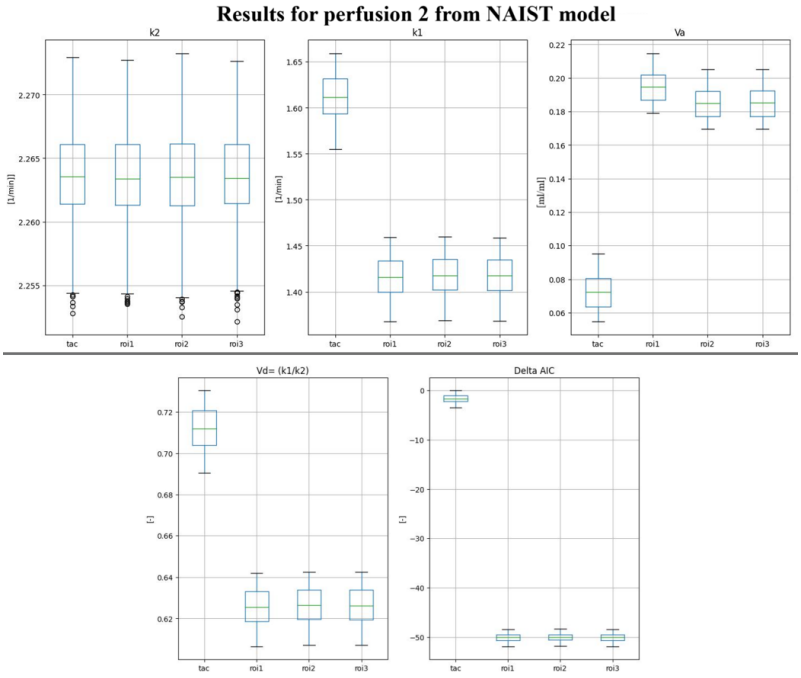

Figure 9. Optimized parameters from the NAIST's model. In this figure are presented the values that were obtained using the simulated data of perfusion value of 2 [ml/min/g]. Here the Va is around what it should be and the other values also stay under the limits. Here the measures ΔAIC value have been really small meaning a near identical fit for the TAC functions.

Figure 13 around perfusion of 5 [ml/min/g] is a point where the model has produced near similar value for the rest of the data which indicates it has peaked.

In the Figures 14 and 15 the perfusion they are plotted against is generated to understand what happens after reaching the point where the NAIST model peaked. This model also peaked in the perfusion of 5 [ml/min/g] that can be seen from the box plot 8 for the k2 value that is approximately the same as perfusion. From the Figures 14 and 15 it is also easy to see how the parameter generation changes depending on the used simulated b2t_h2o TAC's, causing zigzag to form in the plots. More of these functions are in the appendixes mentioned earlier. When comparing the models through the Figures 13 and 14 we can see that a similar outlier situation doesn't happen in the NAIST model that happened with the NASTα. In the functions all the values are grouped and no clear outliers appear. When comparing the

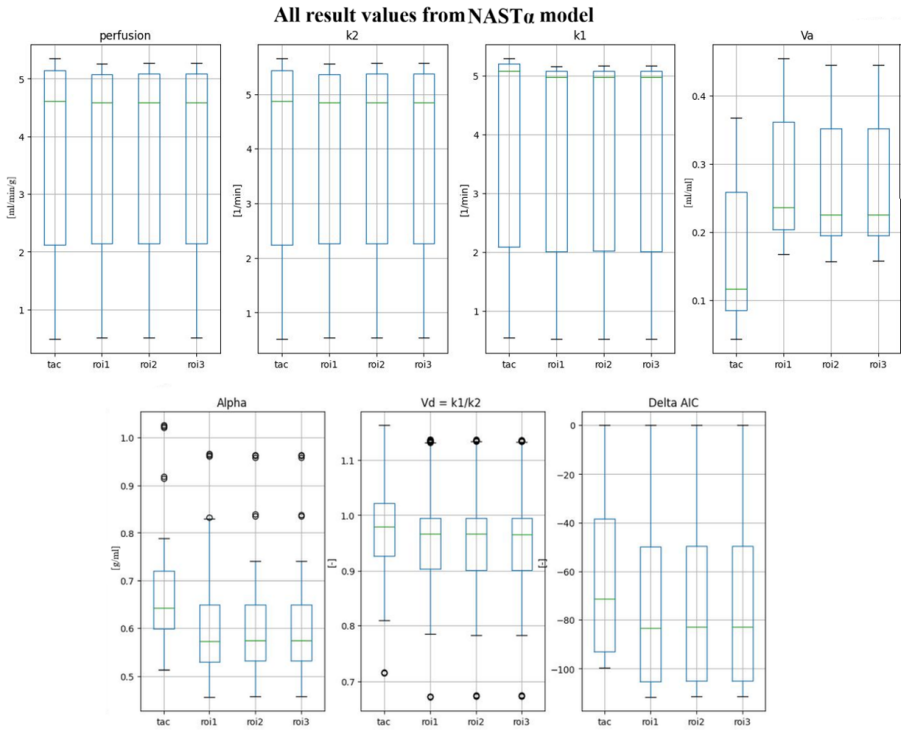

Figure 10. In this figure are represented all the optimized parameter values from all different perfusions from the NASTα model. Here again a perfusion peak can be seen, in around 5 [ml/min/g]. In α and Vd outliers can be seen. These differences are most likely attributable to the manner in which the parameter settings were selected. Is those cases the set of parameters used for the beginning guess was determined wrong and the outcome is correlating the model failing to be successful with those parameters.

box plot values all the models have similar results in the small perfusions. Except that the NAIST model failed to produce positive Va value for the TAC in small perfusions. NASTα model on the other hand performed well on all perfusions from 0.5 till 5 [ml/min/g].

3.1.6 Model correlations

Lastly, comparison between the NAIST with fitmbf and fit_h2o and NASTα with fitmbf and fit_h2o was done. For this the Pearson correlation coefficient r was calculated for TACs and ROI1s. In Figure 17 are first the r values between fit_h2o and NAIST. Here the correlation for Va with all perfusion is over 0.9 except for Va

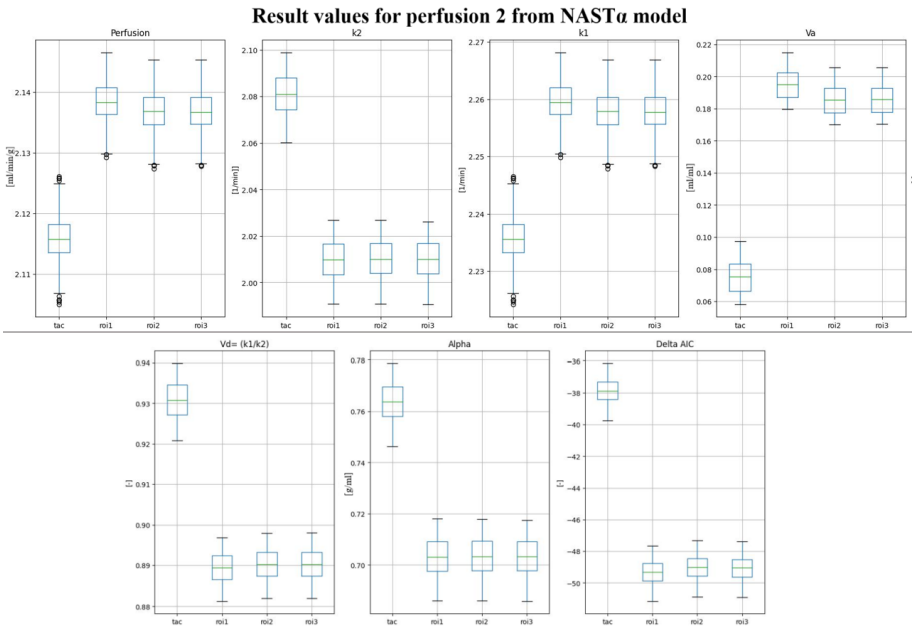

Figure 11. Optimized parameters from the NASTα model. In this figure are presented the values that were obtained using the simulated data of perfusion value of 2 [ml/min/g]. Here the values again are located in a ranges that could be expected from similar real values.

from perfusion 1 [ml/min/g] where it is 0.73. Value for k2 is not correlated whereas vd is near 0.9 for all perfusion. The perfusion correlation for ROIs flow is high 0.90 or near, in low perfusion and lowering after perfusion 4 [ml/min/g]. In the low 0.5 and 1 [ml/min/g] perfusion the TAC flow is not correlating. But in the flow values after this till 4 [ml/min/g] have from high to moderate correlation ranging from 0.629-0.889. The statistical test for p_value was mainly 0. In Figure 18 Va and flow are compared. The values are near to 1 or 1 for Va till perfusion of 5 [ml/min/g] and after not correlated. This also shows how the models peaked. For the flow there is no correlation with fitmbf. Which is understandable as the flow calculation was similar to fit_h2o.

Values for NASTα model compared with fit_h2o are in Figure 19. The flow values compared to fit_h2o have low correlation. This is acceptable as they are calculated differently. For the middle perfusion 2-4 [ml/min/g] there is small cor-

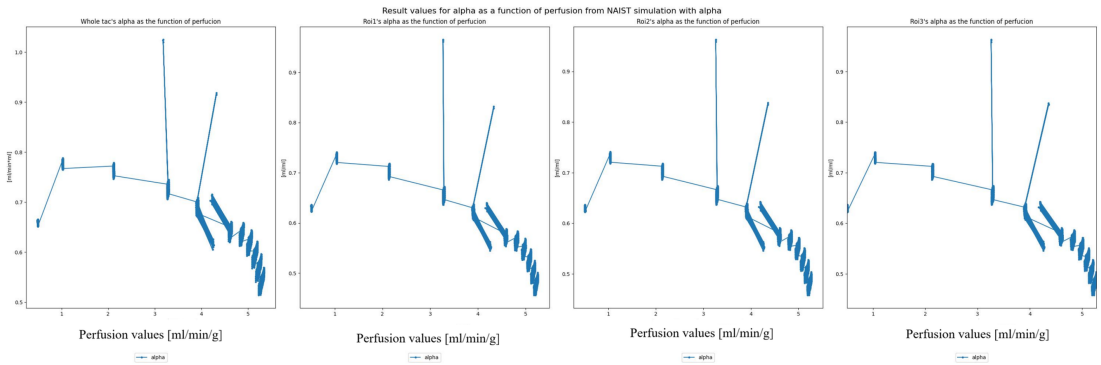

Figure 12. Results for α from the NASTα model as a function of perfusion. Different subplots have the results from tac, roi1,roi2 and roi3. These functions where plotted to get an idea of weather the model have worked in optimizing the parameters and to get an idea of the overall trend. This meaning what can also be seen in this figure, the first slow decline and really similar values in each perfusion and then after 4 [ml/min/g] having more fluctuation and all the rest perfusion being put in between 4-5 [ml/min/g]. In the perfusion 3 [ml/min/g] and 4 [ml/min/g] we can see outliers which have failed properly in the optimizing, making them be way off from the other values. These most likely where the results of parameter decision failing.

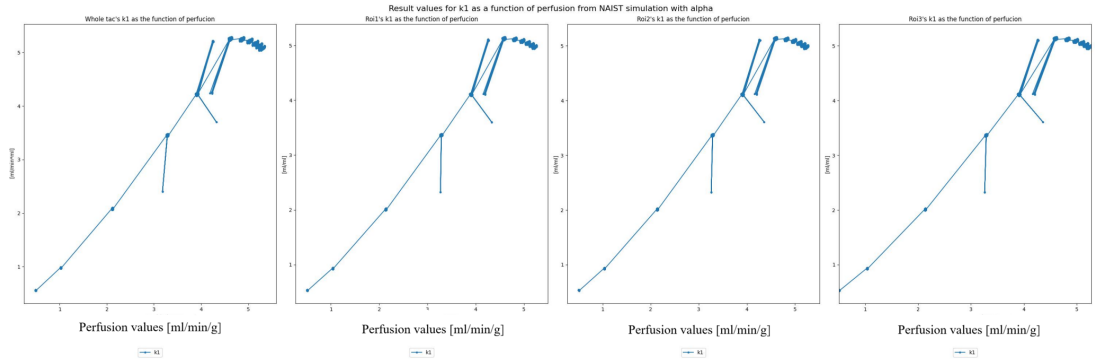

Figure 13. Results for $k1$ from the NASTα model as a function of perfusion. Different subplots have the results from tac, roi1,roi2 and roi3. Here we can see similar outliers and similar other similar behavior, seen in 12. The results that succeeded well seem as a dot in the graph where as the once showing problems have outliers and other noise presented mainly in the 4-5 [ml/min/g] are and some small problems in 3 [ml/min/g].

relation. Here the Va is 1 or 0.998 till perfusion of 300. After it stays high, over 0.85 for all the perfusions. So similar results with NAIST comparing the Va parameter. NASTα has negative k2 values for r in small perfusions (0.5 [ml/min/g]) and in higher than 4 [ml/min/g]. NAIST also has only four negative r values for k2, but they are more random occurring in 0.5, 1 and 6 [ml/min/g] for TAC and 5 [ml/min/g] for ROI1. For NASTα vd has correlation over 0.8 till perfusion of 3 [ml/min/g] and again in perfusion 6 [ml/min/g]. In the last Figure 20 the values for flow, Va and α are show for the NASTα models correlation with fitmbf. The flow has low correlation in perfusion of 0.5 [ml/min/g], and from perfusion 4 [ml/min/g] on wards. But 1-3 [ml/min/g] high to moderate correlation ranging with 0.979-0.589. As the k2 had low correlation in the earlier model and the perfusion is calculated using it. The correlation is high for Va and α parameters except for perfusion 3 [ml/min/g] TAC for α. The peaking of the model can be seen here as well, as after perfusion of 6 [ml/min/g] there is nonexistent to low correlation.

3.2 Patient results

Next going over the results that were obtained using the real patient data for all the models. These results are visualized in Figure 16. In the figure are reported the perfusion, k2, K1, Va, vd and α plotted against perfusion. The fit_h2o is big circle "O", fitmbf small circle "·", NAIST "x" and NASTα is the diamond shape.

In the first sub figure all the values are fitted to the same line. On the sub figure for k2, some patients parameter results received using the different models fit near each other, especially the fit_h2o and NAIST models. Basically the optimal result would be that the same patient's data from fitmbf, NAIST and NASTα would scatter together.

The NASTα version has some patients with similar results as the other models but most of the patients do not align. In the sub figure for k1 with fit_h2o and

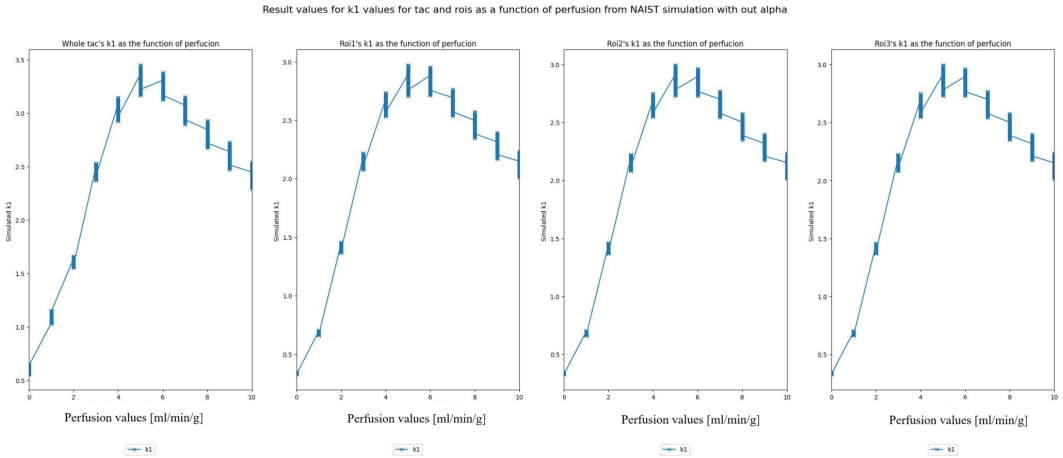

Figure 14. Results for $k1$ from the NAIST model as a function of perfusion. Different subplots have the results from tac, roi1,roi2 and roi3. Here to be able to see better what actually happen, the perfusions were generated to go from 0.5-10 [ml/min/g]. Here we can see the model working in the smaller perfusions under 5 [ml/min/g] and after that starting to decline and again having more fluctuation compared to the smaller perfusions.

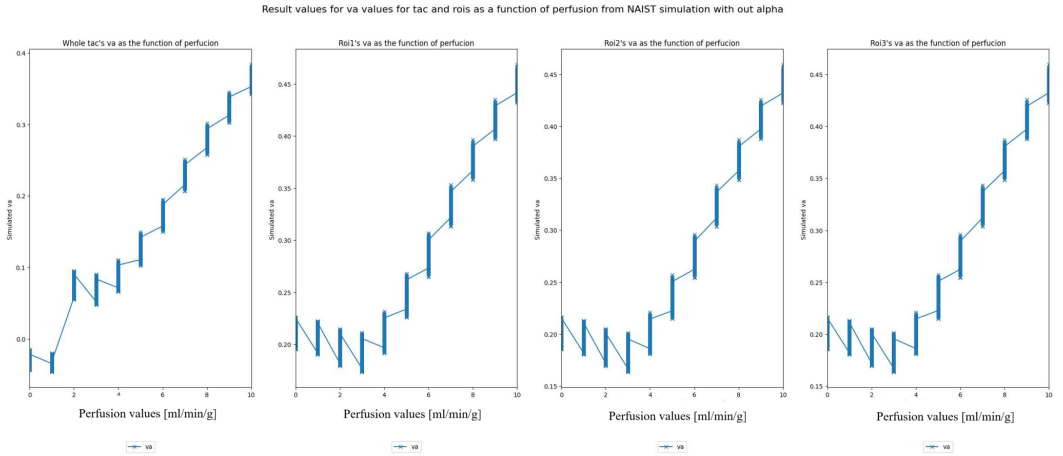

Figure 15. Results for Va from the NAIST model as a function of perfusion. Different subplots have the results from tac, roi1,roi2 and roi3. Here again can see the similar trend as in the 14, model failing after perfusion 5 [ml/min/g]. In this plot the wanted result would have been that the mean of the values would in the ROIs should by f(x)= 0.2 [ml/ml]. But here the values till 5 [ml/min/g] are what to expect and after that the values start to get larger increasing linearly.

NAIST we can see that small perfusion valued patients being near to each others, but in this point the k_max parameter value of 5.0 might be a cause for that the NAIST is limited with the max perfusion of $\approx$ 4.2 and the high perfusion values can't be matched. What comes to the NASTα model, we can see there is something going on with the model as it shouldn't have the same value of five for all but rather a linear function like with the fit_h2o. This is most likely due to the beginning guessing failing. On the sub figure for Va, it is possible to see when the perfusion value is small, the other model's group up excluding the NASTα model. At higher perfusion levels, all models demonstrate greater separation of the data points within the same patients. With the second last sub figure vd the fit_h2o and NAIST model demonstrated generally satisfactory level of performance, however there is still room for further improvement. The wanted value is to stay under one, whereas the NASTα model result won't be surprising as it has shown already that there are some problems with the beginning guess. In the last figure are only two models that used the α parameter. The wanted value is to stay between 0.6-0.9 so it is also possible to see the problems with the NASTα model.

The fit_h2o model measures different perfusion than the other models as mentioned in the earlier sections. Here in these results the hoped end results would have been that the models work with the parameters that fit_h2o model does not work and where the fitmbf does not work.

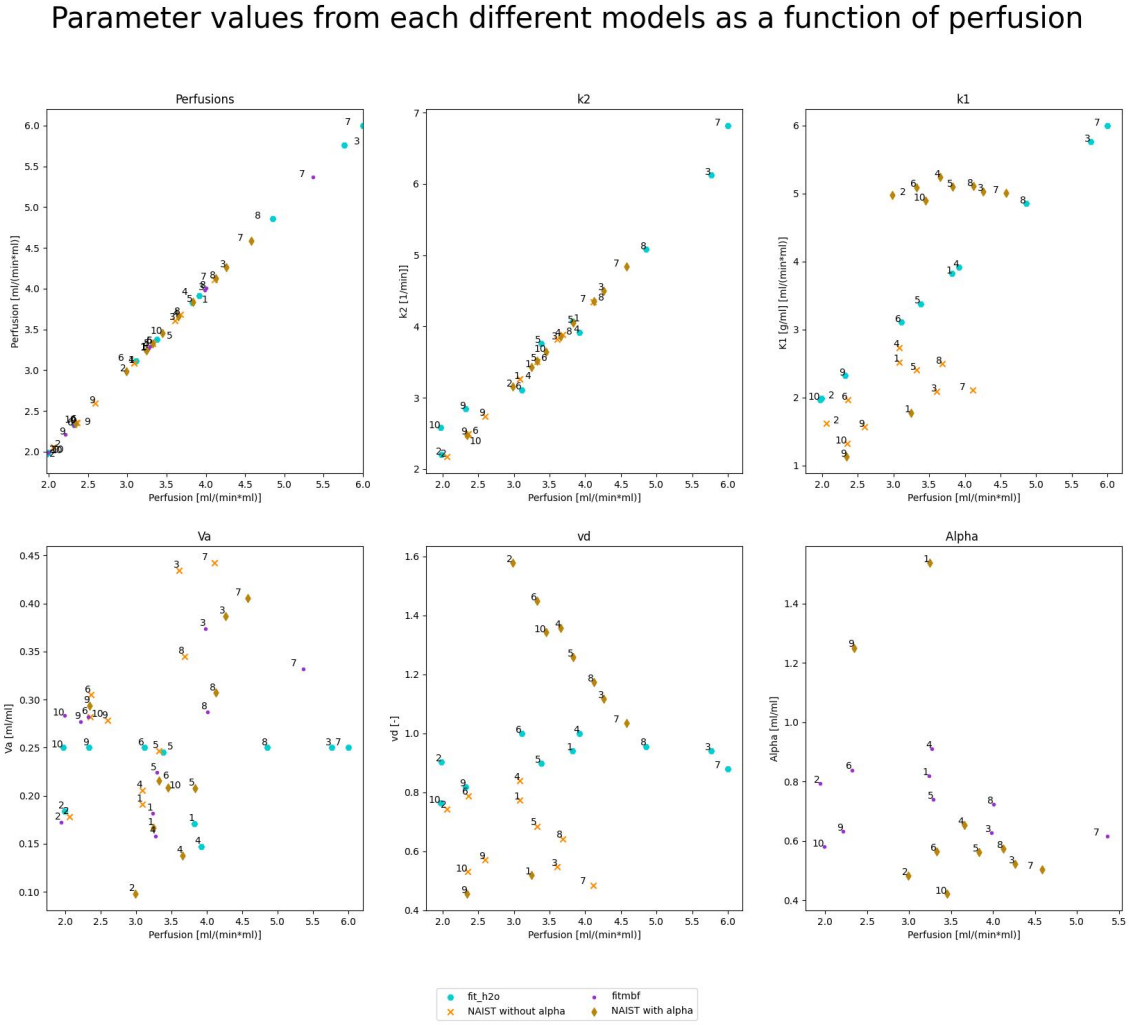

Figure 16. In this figure are represented all the results received from each different model. The data contained a test set of ten patient data that was anonymized. As noted earlier not all models have all the same output parameters. In the legend the shape and color of each model is represented to know what model have produced and which result. The optimal result would have been that the same patients results in different models clamp together, meaning the models would produce similar results, with similar perfusion values. This can be seen with some patients in smaller perfusions, like the number 9, 10, 5 and 2. But here not every model worked for them and not with every parameter. Nastα model especially has problems but these are mainly caused by the decision of what parameters to use for the model running. Here we can see the difference in Fit_h2o model as it models the dynamics of radiowater. In Va when comparing the other models it can be seen that the results are not that far off. For the other parameter results, there is more fluctuation with the results, and for K1, Vd and (α) larger changes in the results can be seen.

Pearson and p_value between fit_h2o and NAIST

Perfusion	Region	Parameter	Model_1	Model_2	r	p_value
50	roi1	Flow	fith2o	NAIST	0.916	0.0
50	roi1	k2	fith2o	NAIST	0.729	0.0
50	roi1	va	fith2o	NAIST	1.0	0.0
50	roi1	vd	fith2o	NAIST	0.885	0.0
50	tac	Flow	fith2o	NAIST	-0.863	0.0
50	tac	k2	fith2o	NAIST	-0.769	0.0
50	tac	va	fith2o	NAIST	0.963	0.0
50	tac	vd	fith2o	NAIST	0.905	0.0
100	roi1	Flow	fith2o	NAIST	0.897	0.0
100	roi1	k2	fith2o	NAIST	0.829	0.0
100	roi1	va	fith2o	NAIST	1.0	0.0
100	roi1	vd	fith2o	NAIST	0.91	0.0
100	tac	Flow	fith2o	NAIST	-0.835	0.0
100	tac	k2	fith2o	NAIST	-0.658	0.0
100	tac	va	fith2o	NAIST	0.703	0.0
100	tac	vd	fith2o	NAIST	0.956	0.0
200	roi1	Flow	fith2o	NAIST	0.877	0.0
200	roi1	k2	fith2o	NAIST	0.897	0.0
200	roi1	va	fith2o	NAIST	1.0	0.0
200	roi1	vd	fith2o	NAIST	0.917	0.0
200	tac	Flow	fith2o	NAIST	0.899	0.0
200	tac	k2	fith2o	NAIST	0.926	0.0
200	tac	va	fith2o	NAIST	1.0	0.0
200	tac	vd	fith2o	NAIST	0.925	0.0
300	roi1	Flow	fith2o	NAIST	0.806	0.0
300	roi1	k2	fith2o	NAIST	0.684	0.0
300	roi1	va	fith2o	NAIST	0.996	0.0
300	roi1	vd	fith2o	NAIST	0.92	0.0
300	tac	Flow	fith2o	NAIST	0.838	0.0
300	tac	k2	fith2o	NAIST	0.787	0.0
300	tac	va	fith2o	NAIST	0.998	0.0
300	tac	vd	fith2o	NAIST	0.928	0.0
400	roi1	Flow	fith2o	NAIST	0.569	0.0
400	roi1	k2	fith2o	NAIST	0.065	0.021
400	roi1	va	fith2o	NAIST	0.97	0.0
400	roi1	vd	fith2o	NAIST	0.912	0.0
400	tac	Flow	fith2o	NAIST	0.629	0.0
400	tac	k2	fith2o	NAIST	0.231	0.0
400	tac	va	fith2o	NAIST	0.98	0.0
400	tac	vd	fith2o	NAIST	0.922	0.0
500	roi1	Flow	fith2o	NAIST	0.284	0.0
500	roi1	k2	fith2o	NAIST	-0.13	0.0
500	roi1	va	fith2o	NAIST	0.907	0.0
500	roi1	vd	fith2o	NAIST	0.877	0.0
500	tac	Flow	fith2o	NAIST	0.357	0.0
500	tac	k2	fith2o	NAIST	0.01	0.725
500	tac	va	fith2o	NAIST	0.93	0.0
500	tac	vd	fith2o	NAIST	0.893	0.0
600	roi1	Flow	fith2o	NAIST	nan	nan
600	roi1	k2	fith2o	NAIST	0.015	0.603
600	roi1	va	fith2o	NAIST	0.937	0.0
600	roi1	vd	fith2o	NAIST	0.844	0.0
600	tac	Flow	fith2o	NAIST	nan	nan
600	tac	k2	fith2o	NAIST	-0.002	0.931
600	tac	va	fith2o	NAIST	0.969	0.0
600	tac	vd	fith2o	NAIST	0.89	0.0

Figure 17. Correlation calculations between the fit_h2o and NAIST model. In the parameter column are all the parameters and on the corresponding row is the used region (TAC/ROI1), perfusion, Pearson value (r) and p_value.

Pearson and p_value between fitmbf and NAIST

Perfusion	Region	Parameter	Model_1	Model_2	r	p_value
50	roi1	Flow	fitmbf	NAIST	0.251	0.0
50	roi1	va	fitmbf	NAIST	1.0	0.0
50	tac	Flow	fitmbf	NAIST	-0.176	0.0
50	tac	va	fitmbf	NAIST	0.962	0.0
100	roi1	Flow	fitmbf	NAIST	0.259	0.0
100	roi1	va	fitmbf	NAIST	1.0	0.0
100	tac	Flow	fitmbf	NAIST	-0.157	0.0
100	tac	va	fitmbf	NAIST	0.702	0.0
200	roi1	Flow	fitmbf	NAIST	0.291	0.0
200	roi1	va	fitmbf	NAIST	1.0	0.0
200	tac	Flow	fitmbf	NAIST	0.287	0.0
200	tac	va	fitmbf	NAIST	1.0	0.0
300	roi1	Flow	fitmbf	NAIST	0.286	0.0
300	roi1	va	fitmbf	NAIST	1.0	0.0
300	tac	Flow	fitmbf	NAIST	0.294	0.0
300	tac	va	fitmbf	NAIST	1.0	0.0
400	roi1	Flow	fitmbf	NAIST	0.167	0.0
400	roi1	va	fitmbf	NAIST	0.989	0.0
400	tac	Flow	fitmbf	NAIST	-0.21	0.0
400	tac	va	fitmbf	NAIST	0.986	0.0
500	roi1	Flow	fitmbf	NAIST	0.041	0.147
500	roi1	va	fitmbf	NAIST	0.955	0.0
500	tac	Flow	fitmbf	NAIST	-0.527	0.0
500	tac	va	fitmbf	NAIST	0.934	0.0
600	roi1	Flow	fitmbf	NAIST	0.005	0.849
600	roi1	va	fitmbf	NAIST	-0.078	0.006
600	tac	Flow	fitmbf	NAIST	0.134	0.0
600	tac	va	fitmbf	NAIST	0.061	0.029
700	roi1	Flow	fitmbf	NAIST	0.003	0.961
700	roi1	va	fitmbf	NAIST	0.193	0.001
700	tac	Flow	fitmbf	NAIST	0.008	0.835
700	tac	va	fitmbf	NAIST	0.25	0.0
800	roi1	Flow	fitmbf	NAIST	-0.256	0.0
800	roi1	va	fitmbf	NAIST	0.217	0.001
800	tac	Flow	fitmbf	NAIST	-0.206	0.0
800	tac	va	fitmbf	NAIST	-0.01	0.851
900	roi1	Flow	fitmbf	NAIST	-0.067	0.11
900	roi1	va	fitmbf	NAIST	0.061	0.145
900	tac	Flow	fitmbf	NAIST	-0.324	0.0
900	tac	va	fitmbf	NAIST	0.207	0.0
1000	roi1	Flow	fitmbf	NAIST	-0.214	0.0
1000	roi1	va	fitmbf	NAIST	0.253	0.0
1000	tac	Flow	fitmbf	NAIST	-0.341	0.0
1000	tac	va	fitmbf	NAIST	0.362	0.0

Figure 18. Correlation calculations from between the fitmbf and NAIST model. In the parameter column are all the parameters and on the corresponding row is the used region (TAC/ROI1), perfusion, Pearson value (r) and p_value.

Pearson and p_value between fit_h2o and NASTα

Perfusion	Region	Parameter	Model_1	Model_2	r	p_value
50	roi1	Flow	fith2o	NASTα	-0.7	0.0
50	roi1	k2	fith2o	NASTα	-0.452	0.0
50	roi1	va	fith2o	NASTα	1.0	0.0
50	roi1	vd	fith2o	NASTα	0.877	0.0
50	tac	Flow	fith2o	NASTα	-0.727	0.0
50	tac	k2	fith2o	NASTα	-0.534	0.0
50	tac	va	fith2o	NASTα	1.0	0.0
50	tac	vd	fith2o	NASTα	0.885	0.0
100	roi1	Flow	fith2o	NASTα	0.016	0.574
100	roi1	k2	fith2o	NASTα	0.376	0.0
100	roi1	va	fith2o	NASTα	1.0	0.0
100	roi1	vd	fith2o	NASTα	0.895	0.0
100	tac	Flow	fith2o	NASTα	-0.27	0.0
100	tac	k2	fith2o	NASTα	0.071	0.011
100	tac	va	fith2o	NASTα	1.0	0.0
100	tac	vd	fith2o	NASTα	0.897	0.0
200	roi1	Flow	fith2o	NASTα	0.48	0.0
200	roi1	k2	fith2o	NASTα	0.811	0.0
200	roi1	va	fith2o	NASTα	0.999	0.0
200	roi1	vd	fith2o	NASTα	0.86	0.0
200	tac	Flow	fith2o	NASTα	0.074	0.009
200	tac	k2	fith2o	NASTα	0.49	0.0
200	tac	va	fith2o	NASTα	1.0	0.0
200	tac	vd	fith2o	NASTα	0.868	0.0
300	roi1	Flow	fith2o	NASTα	0.582	0.0
300	roi1	k2	fith2o	NASTα	0.894	0.0
300	roi1	va	fith2o	NASTα	0.999	0.0
300	roi1	vd	fith2o	NASTα	0.081	0.004
300	tac	Flow	fith2o	NASTα	0.403	0.0
300	tac	k2	fith2o	NASTα	0.695	0.0
300	tac	va	fith2o	NASTα	0.998	0.0
300	tac	vd	fith2o	NASTα	0.127	0.0
400	roi1	Flow	fith2o	NASTα	-0.133	0.0
400	roi1	k2	fith2o	NASTα	-0.031	0.264
400	roi1	va	fith2o	NASTα	0.887	0.0
400	roi1	vd	fith2o	NASTα	0.016	0.57
400	tac	Flow	fith2o	NASTα	-0.072	0.01
400	tac	k2	fith2o	NASTα	0.013	0.637
400	tac	va	fith2o	NASTα	0.904	0.0
400	tac	vd	fith2o	NASTα	0.005	0.87
500	roi1	Flow	fith2o	NASTα	-0.225	0.0
500	roi1	k2	fith2o	NASTα	-0.166	0.0
500	roi1	va	fith2o	NASTα	0.853	0.0
500	roi1	vd	fith2o	NASTα	0.093	0.001
500	tac	Flow	fith2o	NASTα	-0.199	0.0
500	tac	k2	fith2o	NASTα	-0.166	0.0
500	tac	va	fith2o	NASTα	0.868	0.0
500	tac	vd	fith2o	NASTα	0.089	0.002
600	roi1	Flow	fith2o	NASTα	nan	nan
600	roi1	k2	fith2o	NASTα	0.238	0.0
600	roi1	va	fith2o	NASTα	0.958	0.0
600	roi1	vd	fith2o	NASTα	0.803	0.0
600	tac	Flow	fith2o	NASTα	nan	nan
600	tac	k2	fith2o	NASTα	0.053	0.062
600	tac	va	fith2o	NASTα	0.958	0.0
600	tac	vd	fith2o	NASTα	0.769	0.0

Figure 19. Correlation calculations from between the fit_h2o and NASTα model. In the parameter column are all the parameters and on the corresponding row is the used region (TAC/ROI1), perfusion, Pearson value (r) and p_value.

Pearson and p_value between fitmbf and NASTα

Perfusion	Region	Parameter	Model_1	Model_2	r	p_value
50	roi1	Flow	fitmbf	NASTα	0.203	0.0
50	roi1	alpha	fitmbf	NASTα	0.995	0.0
50	roi1	va	fitmbf	NASTα	1.0	0.0
50	tac	Flow	fitmbf	NASTα	0.145	0.0
50	tac	alpha	fitmbf	NASTα	0.992	0.0
50	tac	va	fitmbf	NASTα	1.0	0.0
100	roi1	Flow	fitmbf	NASTα	0.815	0.0
100	roi1	alpha	fitmbf	NASTα	0.995	0.0
100	roi1	va	fitmbf	NASTα	1.0	0.0
100	tac	Flow	fitmbf	NASTα	0.589	0.0
100	tac	alpha	fitmbf	NASTα	0.994	0.0
100	tac	va	fitmbf	NASTα	1.0	0.0
200	roi1	Flow	fitmbf	NASTα	0.979	0.0
200	roi1	alpha	fitmbf	NASTα	0.993	0.0
200	roi1	va	fitmbf	NASTα	1.0	0.0
200	tac	Flow	fitmbf	NASTα	0.794	0.0
200	tac	alpha	fitmbf	NASTα	0.992	0.0
200	tac	va	fitmbf	NASTα	1.0	0.0
300	roi1	Flow	fitmbf	NASTα	0.948	0.0
300	roi1	alpha	fitmbf	NASTα	0.514	0.0
300	roi1	va	fitmbf	NASTα	1.0	0.0
300	tac	Flow	fitmbf	NASTα	0.734	0.0
300	tac	alpha	fitmbf	NASTα	0.543	0.0
300	tac	va	fitmbf	NASTα	0.998	0.0
400	roi1	Flow	fitmbf	NASTα	0.048	0.089
400	roi1	alpha	fitmbf	NASTα	0.578	0.0
400	roi1	va	fitmbf	NASTα	0.907	0.0
400	tac	Flow	fitmbf	NASTα	0.058	0.039
400	tac	alpha	fitmbf	NASTα	0.6	0.0
400	tac	va	fitmbf	NASTα	0.907	0.0
500	roi1	Flow	fitmbf	NASTα	-0.21	0.0
500	roi1	alpha	fitmbf	NASTα	0.726	0.0
500	roi1	va	fitmbf	NASTα	0.889	0.0
500	tac	Flow	fitmbf	NASTα	0.02	0.48
500	tac	alpha	fitmbf	NASTα	0.717	0.0
500	tac	va	fitmbf	NASTα	0.88	0.0
600	roi1	Flow	fitmbf	NASTα	0.012	0.689
600	roi1	alpha	fitmbf	NASTα	-0.017	0.588
600	roi1	va	fitmbf	NASTα	0.052	0.092
600	tac	Flow	fitmbf	NASTα	-0.065	0.033
600	tac	alpha	fitmbf	NASTα	0.192	0.0
600	tac	va	fitmbf	NASTα	0.277	0.0
700	roi1	Flow	fitmbf	NASTα	0.092	0.273
700	roi1	alpha	fitmbf	NASTα	0.223	0.007
700	roi1	va	fitmbf	NASTα	0.365	0.0
700	tac	Flow	fitmbf	NASTα	-0.017	0.738
700	tac	alpha	fitmbf	NASTα	0.149	0.004
700	tac	va	fitmbf	NASTα	0.326	0.0
800	roi1	Flow	fitmbf	NASTα	-0.033	0.736
800	roi1	alpha	fitmbf	NASTα	0.097	0.318
800	roi1	va	fitmbf	NASTα	0.225	0.019
800	tac	Flow	fitmbf	NASTα	-0.007	0.93
800	tac	alpha	fitmbf	NASTα	-0.095	0.223
800	tac	va	fitmbf	NASTα	0.012	0.875
900	roi1	Flow	fitmbf	NASTα	0.024	0.687
900	roi1	alpha	fitmbf	NASTα	0.382	0.0
900	roi1	va	fitmbf	NASTα	0.534	0.0
900	tac	Flow	fitmbf	NASTα	0.022	0.784
900	tac	alpha	fitmbf	NASTα	0.102	0.196
900	tac	va	fitmbf	NASTα	0.249	0.001
1000	roi1	Flow	fitmbf	NASTα	0.513	0.0
1000	roi1	alpha	fitmbf	NASTα	0.577	0.0
1000	roi1	va	fitmbf	NASTα	0.673	0.0
1000	tac	Flow	fitmbf	NASTα	-0.11	0.001
1000	tac	alpha	fitmbf	NASTα	0.001	0.981
1000	tac	va	fitmbf	NASTα	0.121	0.0

Figure 20. Correlation calculations from between the fitmbf and NASTα model. In the parameter column are all the parameters and on the corresponding row is the used region (TAC/ROI1), perfusion, Pearson value (r) and p_value.

4 Discussion

This thesis was combined to have a wide literacy overview, code creation and result evaluation. To be able to understand how PET-imaging data is acquired, the explanation in section one of radioactivity and its interaction with matter is explained. This is done to understand how the TAC data is gathered. Followed by an overview of the common diseases that cause the need for blood flow measuring and might be a reason for patient hospitalization has been explained. One of the leading reasons are CAD and myocardial ischemia. To be able to study these diseases, models can be used to understand the diseases while creating possible cures and solutions. For this reason, the compartmental models and other modeling methods are covered in the end of section one.

The materials and methods is reviewed in section two included multiple models, BASH code usage, parameter findings as well as python code debugging combined with new code creation, data evaluation and visualization, their comparison became an important part to be able to see how well they worked compared to each other. This was mainly done visually, using box-plots and functions, as the amount of data was significant. Also the Pearson correlation coefficient was calculated between NAIST with fit_h2o and fitmbf and for NASTα with fit_h2o and fitmbf. The methods for the study were mainly quantitative. And in the section three the results are reviewed.

As predicted the fit_h2o and fitmbf models gave parameters that fit with the ranges found in literature. The difference with these models where that fit_h2o was limited by perfusion at 500 [ml min-1 ml-1] (or 5 [ml/min/g]) where as the fitmbf went all the way to 1000 [ml min-1 ml-1] (or 10 [ml/min/g]). The fitmbf model eventually peaked at the same value of 500 [ml/min/g] when comparing the optimized parameters. The model of fit_h2o measures the blood flow tissue perfusion and fitmbf myocardial blood flow, so the values of these two models have differences

automatically.

The NAIST code worked when compared to the two models. Also the Pearsons r-value showed high correlation for most of the parameters in normal perfusion ranges. Same was with the NASTα model. It was slightly more robust when it comes to the high perfusion when comparing the correlation. Overall both models had high correlation values for normal perfusion ranges except for parameter vd. Both models had some low correlation for k2 parameters. This caused some problems in the perfusion values for NASTα as it is defined by k2. Some initial beginning guess optimization for the values for over 3 [ml/min/g] is needed. But over all for most of the perfusion the correlation here was also high. Both of the models worked well in perfusion values under 5 [ml/min/g] when using the simulated TAC data.

Mentioned earlier, real-life data is more complex, and NAIST and NASTα models had problems optimizing the values. Some of the results clustered together as hoped. But there was a clear problem in the parameter guessing of the NASTα model. It was not robust enough to handle the real data. Overall, certain parameters produced closely aligned results, suggesting potential for future refinement to enhance model robustness in these challenging datasets.

Some differences that are to be noted from the models. The NASTα model was built with similar perfusion and functions as in fitmbf. NAIST perfusion is similar to the fit_h2o model that measures the perfusable tissue perfusion.

To enhance the NASTα models' accuracy even more, having different and more robust methods for the parameter guessing could be beneficial. The method now is not robust for noisy data. In the case of tuning how to choose what parameter to use, using higher noise levels in the simulated data could be helpful. This would help the NASTα model better in the optimization of the k2 parameter, that the flow depends from. Now it has low correlation, and enhancing this would give better end results. Changing the clamping in the code could also prove to be beneficial. Now

the clamp might prevent the model from working in higher perfusions, but it should be taken in consideration if this is actually a need from the model.

More methods to evaluate the models could be integrated into them. In this thesis most of the evaluation happened using box plots and other functions as they were useful for tuning the models. For measuring the goodness of the fits AIC and R^2 were used. In the end a r-values were calculated for the correlation and means and standard deviations from the parameter values. Other methods could prove beneficial. Also p_values were calculated, but it is not the chosen evaluation method, even though it was left in the Figures.

The main phases of the thesis and the study question were met. NAIST code was fixed, made compatible with large amounts of data and included processing and evaluation methods. NASTα model was developed. To compare the models TPClib data was simulated. The verified fit_h2o and fitmbf models were used with this same simulated data. The robustness of all the models was tested simulating a really wide range of test data. And a small patient data was used in the end to test whether the new models would perform as well as the verified models. The models worked with the simulated data to perfusion of 5 [ml/min/g] but with the real patient data more tuning for the parameter guesses is still needed for the NAIST and NASTα model to perform well. With further refinement of the parameter estimation and selection produced, the models may have increased potential to extract more detailed information from the TAC's than is currently achievable with a single model.

5 Acknowledgment

When people reach achievements, behind those commonly is a net of people who have made such things possible. For first I want to thank all my supervisors, Jarmo Teuho, Seyed M. Hosseini and Jyrki Piilo. J. Teuho gave a interesting topic and the project over all covered a wide range of different areas in science, and usage of many different tools and methods. He made it possible for me to focus on the thesis with internships. Also, over the process they have always been available for advice regardless of a busy schedule, and I appreciate the effort he has put towards the supervising project. I want to thank Seyed M. Hosseini, another supervisor, who gave me some help in the writing and planning phases, as well as helped in parts where their expertise lined up. Next, I want to thank Jyrki Piilo who supervised from the physics and astronomy department, who also made time in their schedule and was always reachable. Overall, there are many people in the PET-centre of Turku that need to be thanked as well. Riku Klein, who was part of the planning process of the thesis. Minna Kangasperko who showed me around the centre. I want to thank all the people in PET-centre, everyone I have met are heart warming and nice people.

References

[1] B. Schumacher and M. Westmoreland, in book *Quantum Processes Systems, and Information* (Cambridge University Press, United Kingdom, 2010), pp. 1–12.

[2] P. Tandon, D. Prakash, S. C. Kheruka and N. N. Bhat, in book *Radiation Safety Guide for Nuclear Medicine Professionals* (Springer Nature Singapore, Singapore, 2022), pp. 21–35.

[3] N. N. Greenwood and A. Earnshaw, in book *Chemistry of the Elements* (Elsevier, U.K., 2012), pp. 20–29.

[4] B. H. Tonnessen and L. Pounds, Journal of Vascular Surgery **53**, 6S (2011).

[5] R. E. Carson, in book *Positron Emission Tomography: Basic Sciences*, edited by J. S. K. Dale L. Bailey and S. Surti (Springer London, London, 2005), pp. 13–39.

[6] S. Pommé, Metrologia **52**, S51 (2015).

[7] G. B. Saha, in book *Physics and Radiobiology of Nuclear Medicine* (Springer US, New York, NY, 2025), pp. 65–79.

[8] H. Zaidi and M.-L. Montandon, Scatter Compensation Techniques in PET, 2007.

[9] G. B. Saha, in book *Physics and Radiobiology of Nuclear Medicine* (Springer US, New York, NY, 2025), pp. 209–248.

[10] D. R. Schaart, Physics in Medicine and Biology **66**, 09TR01 (2021).

[11] F. H. Fahey, Journal of Nuclear Medicine Technology **30**, 39 (2002).

[12] A. K. Shukla and U. Kumar, Journal of medical physics **31**, 13 (2006).

[13] S. Surti, Journal of Nuclear Medicine **56**, 98 (2015).

[14] G. Wang, A. Rahmim and R. N. Gunn, IEEE Transactions on Radiation and Plasma Medical Sciences **4**, 663 (2020).

[15] E. E. Ter Voert, P. Veit-Haibach, S. Ahn, F. Wiesinger, M. M. Khalighi, C. S. Levin, A. H. Iagaru, G. Zaharchuk, M. Huellner and G. Delso, European journal of nuclear medicine and molecular imaging **44**, 1223 (2017).

[16] J. M. Hooker and R. E. Carson, Annual review of biomedical engineering **21**, 551 (2019).

[17] H. Iida, C. G. Rhodes, R. de Silva, L. I. Araujo, P. M. Bloomfield, A. A. Lammertsma and T. Jones, Journal of Nuclear Medicine **33**, 1669 (1992).

[18] O. Rainio and R. Klén, Annals of Nuclear Medicine **39**, 231 (2025).

[19] C. Rischpler, T. Higuchi and S. G. Nekolla, Current Cardiovascular Imaging Reports **8**, 9303 (2015).

[20] M. Krakauer, A. Ismail, U. Talleruphuus, A. C. Henriksen, M. N. Lonsdale, I. L. Rasmussen, S. Fuglsang, E. Prescott, P. Hovind and L. Marner, Journal of Nuclear Cardiology **30**, 2790 (2023).

[21] D. Daou, European Journal of Nuclear Medicine and Molecular Imaging **42**, 1899 (2015).

[22] M. Cubrilo-Turek, Ejifcc **14**, 67 (2003).

[23] P. Libby, R. Bonow, D. Mann, G. Tomaselli, D. Bhatt, S. Solomon and E. Braunwald, in book *Braunwald's Heart Disease - E-Book: A Textbook of Cardiovascular Medicine* (Elsevier Health Sciences, U.S.A, 2021), pp. 1062–1076.

[24] B. R. Pagliaro, F. Cannata, G. G. Stefanini and L. Bolognese, Heart failure reviews **25**, 53 (2020).

[25] I. Danad, P. G. Raijmakers, R. S. Driessen, J. A. Leipsic, R. Raju, C. Naoum, J. Knuuti, M. Mäki, R. S. Underwood, J. K. Min, K. Elmore, W. J. Stuijfzand, N. van Royen, I. I. Tulevski, A. G. Somsen, M. C. Huisman, A. van Lingen, M. W. Heymans, P. M. van de Ven, C. C. van Kuijk, A. A. Lammertsma, A. C. van Rossum and P. Knaapen, JAMA Cardiology **2**, 1100–1107 (2017).

[26] D. L. Li and M. W. Kronenberg, The American Journal of Medicine **134**, 968 (2021).

[27] M. Takafuji, K. Kitagawa, M. Ishida, Y. Ichikawa, S. Nakamura, S. Nakamori, T. Kurita, K. Dohi and H. Sakuma, Radiology: Cardiothoracic Imaging **3**, e210060 (2021).

[28] R. Hoek, P. A. van Diemen, P. G. Raijmakers, R. S. Driessen, Y. B. Somsen, R. W. de Winter, R. A. Jukema, J. W. Twisk, L. F. Robbers, P. van der Harst *et al.*, Journal of Nuclear Medicine **65**, 1113 (2024).

[29] J. Chahine and H. Alvey, *StatPearls [Internet]* (StatPearls Publishing, , 2023).

[30] B. R. Pagliaro, F. Cannata, G. G. Stefanini and L. Bolognese, Heart failure reviews **25**, 53 (2020).

[31] A. Lala and A. S. Desai, Heart failure clinics **10**, 353 (2014).

[32] J. Fan and T. Watanabe, Pathology international **72**, 151 (2022).

[33] A. N. DeVos, J. H. Spencer, S. E. Anderson and P. A. Iaizzo, in book *Handbook of Cardiac Anatomy, Physiology, and Devices*, edited by P. A. Iaizzo (Springer Nature Switzerland, Cham, 2024), pp. 177–201.

[34] C. Pizzi, B. Xhyheri, G. M. Costa, M. Faustino, M. E. Flacco, M. R. Gualano, G. Fragassi, F. Grigioni and L. Manzoli, Journal of the American Heart Association **5**, e004185 (2016).

[35] S. K. Kar and S. Tripathy, in book *Encyclopedia of Evolutionary Psychological Science*, edited by T. K. Shackelford and V. A. Weekes-Shackelford (Springer International Publishing, Cham, 2021), pp. 2408–2412.

[36] R. Sciagrà, M. Lubberink, F. Hyafil, A. Saraste, R. H. Slart, D. Agostini, C. Nappi, P. Georgoulias, J. Bucerius, C. Rischpler *et al.*, European journal of nuclear medicine and molecular imaging **48**, 1040 (2021).

[37] M. D. Brophey, I. M. Farukhi, R. Castanon, R. DeLaPena, L. Bradshaw and S. Banerjee, Journal of nuclear medicine technology **45**, 75 (2017).

[38] I. Danad, V. Uusitalo, T. Kero, A. Saraste, P. G. Raijmakers, A. A. Lammertsma, M. W. Heymans, S. A. Kajander, M. Pietilä, S. James *et al.*, Journal of the American College of Cardiology **64**, 1464 (2014).

[39] J. Teuho, J. Schultz, R. Klén, J. Knuuti, A. Saraste, N. Ono and S. Kanaya, Scientific Reports **12**, 2839 (2022).

[40] M. B. Møller, J. J. Linde, A. Fuchs, L. V. Køber, B. G. Nordestgaard and K. F. Kofoed, European Heart Journal-Cardiovascular Imaging **25**, 986 (2024).

[41] T. M. Bateman, G. V. Heller, R. Beanlands, D. A. Calnon, J. Case, R. deKemp, E. G. DePuey, M. Di Carli, E. C. Guler, V. L. Murthy, J. Rosenblatt, R. Sher, P. Slomka and T. D. Ruddy, Journal of Nuclear Medicine **62**, 1599 (2021).

[42] A. Gupta, A. Sharma and A. Goel, International Journal of Engineering Research **6**, 58 (2017).

[43] D. C. Montgomery, E. A. Peck and G. G. Vining, in book *Introduction to linear regression analysis* (John Wiley & Sons, USA, 2021), p. 12.

[44] R. E. Carson, in book *Positron Emission Tomography: Basic Sciences*, edited by D. L. Bailey, D. W. Townsend, P. E. Valk and M. N. Maisey (Springer London, London, 2005), pp. 127–159.

[45] P. K. Dunn, G. K. Smyth *et al.*, *Generalized linear models with examples in R* (Springer, U.S.A, 2018), Vol. 53, pp. 39–90.

[46] O. Hospodarskyy, V. Martsenyuk, N. Kukharska, A. Hospodarskyy and S. Sverstiuk, CITI **2024**, 2nd (2024).

[47] G. K. Smyth, Encyclopedia of environmetrics **3**, 1405 (2002).

[48] H. Iida, I. Kanno, A. Takahashi, S. Miura, M. Murakami, K. Takahashi, Y. Ono, F. Shishido, A. Inugami and N. Tomura, Circulation **78**, 104 (1988).

[49] V. Oikonen, Report tpcmod0005, Turku PET Centre Modelling, 2002.

[50] R. S. Driessen, P. G. Raijmakers, W. J. Stuijfzand and P. Knaapen, The international journal of cardiovascular imaging **33**, 1021 (2017).

[51] H. Ito, I. Kanno, H. Iida, J. Hatazawa, E. Shimosegawa, H. Tamura and T. Okudera, Annals of nuclear medicine **15**, 111 (2001).

[52] C. M. Wacker, F. Wiesmann, M. Bock, P. Jakob, J. J. Sandstede, A. Lehning, G. Ertl, L. R. Schad, A. Haase and W. R. Bauer, Magnetic Resonance in Medicine **47**, 1013 (2002).

[53] C. M. Wacker and W. R. Bauer, Herz **28**, 74 (2003).

[54] P. Kletting, T. Kull, S. N. Reske and G. Glatting, Physics in Medicine & Biology **54**, N501 (2009).

[55] H. Iida, C. G. Rhodes, R. de Silva, Y. Yamamoto, L. I. Araujo, A. Maseri and T. Jones, Journal of Nuclear Medicine **32**, 2169 (1991).

Use of AI in thesis

ChatGPT was used in fall 2025, to generate a base for oveleaf's flowchart code Flow chart was then edited by the author. Overleafs AI tool was used, for some parts of the english checking. All scientific content and analysis are work of the author. The Finnish version of the abstract was translated using google translator, and the text was from that modified. Office 365 Copilot was utilized to fix colloquial phrasing in some sentences. The few phrases that were selected to be changed were chosen by the author manually from the original text. Copilot was used to make the mean and standard deviation tables as well as the Pearson and p_value tables.

A Appendix The mathematical solution for further understanding the TPClib

In this TPClib code the β coefficient is included. So the equations are different from the ones mentioned in the section 4.2 TPClib. But the same solving method is used.

In the first Eq. A.1 the β coefficient is present.

$$a(T) = \frac{LV(T) - (1-\beta)C_i(T)}{\beta} \tag{A.1}$$

This Eq. A.1 is places to the Eq. 16 and the Eq. A.2 is acquired.

$$ROI(T) = \alpha C_i(T) + V_a(\frac{LV(T) - (1-\beta)C_i(T)}{\beta}) \tag{A.2}$$

From here the goal is to solve the $C_i(T)$ shown in Eq. A.6.

$$ROI(T) = \alpha C_i(T) + \frac{V_a LV(T)}{\beta} - \frac{V_a(1-\beta)C_i(T)}{\beta} \tag{A.3}$$

$$ROI(T) = C_i(T)(\alpha - \frac{V_a(1-\beta)C_i(T)}{\beta}) + \frac{V_a LV(T)}{\beta} \tag{A.4}$$

$$ROI(T) - \frac{V_a LV(T)}{\beta} = C_i(T)(\alpha - \frac{V_a(1-\beta)C_i(T)}{\beta}) \tag{A.5}$$

$$C_i(T) = \frac{ROI(T) - \frac{V_a}{\beta}LV(T)}{(\alpha - \frac{V_a(1-\beta)}{\beta})} \tag{A.6}$$

To get all the needed values we need also the integral of a(T), as can be seen from Eq. 20. The integral is in Eq. A.7.

$$\int_0^T a(T) = \frac{1}{\beta}\int_0^T LV(T) - \frac{(1-\beta)}{\beta}\int_0^T C_i(T) \tag{A.7}$$

With β the function for $\int C_i(T)$ is shown in Eq. A.8

$$\int_0^T C_i(T) = \frac{\int_0^T ROI(T) - \frac{V_a}{\beta}\int_0^T LV(T)}{(\alpha - \frac{V_a(1-\beta)}{\beta})} \tag{A.8}$$

Now when these equations are placed to the Eq. 15 we can solve the ROI(t):

$$C_i(T) = f(\frac{1}{\beta}\int_0^T LV(T)dt - \frac{(1-\beta)}{\beta}\int_0^T C_i(T)dt) - \frac{f}{p}(\frac{\int_0^T ROI(T)dt - \frac{V_a}{\beta}\int_0^T LV(T)dt}{(\alpha - \frac{V_a(1-\beta)}{\beta})}) \tag{A.9}$$

To make the equation more easily readable, lets mark the A as in Eq. A.10.

$$A = \alpha - \frac{V_a(1-\beta)}{\beta} \tag{A.10}$$

When the Eq. A.10 is placed to Eq. A.9 more simple Eq. A.11 is achieved.

$$C_i(T) = f(\frac{1}{\beta}\int_0^T LV(T)dt - \frac{(1-\beta)}{\beta}\int_0^T C_i(T)dt) - \frac{f}{p}(\frac{\int_0^T ROI(T)dt}{A} - \frac{\frac{V_a}{\beta}\int_0^T LV(T)dt}{A}) \tag{A.11}$$

Next different steps are shown in Eq. A.12- A.17 to get the final Eq. A.18 where the different variables from Eq. A.19 can be placed.

$$\begin{aligned}&\frac{ROI(T) - \frac{V_a}{\beta}LV(T)}{A} = \\ &f(\frac{1}{\beta}\int_0^T LV(T)dt - \frac{(1-\beta)}{\beta}(\frac{\int_0^T ROI(T) - \frac{V_a}{\beta}\int_0^T LV(T)}{A}) \\ &- \frac{f}{p}(\frac{\int_0^T ROI(T)dt}{A} - \frac{\frac{V_a}{\beta}\int_0^T LV(T)dt}{A})\end{aligned} \tag{A.12}$$

$$\begin{aligned}&\frac{ROI(T) - \frac{V_a}{\beta}LV(T)}{A} = \\ &\frac{f}{\beta}\int_0^T LV(T)dt - \frac{(f-\beta)}{\beta}\frac{\int_0^T ROI(T)}{A} + \frac{(f-\beta)}{\beta}\frac{(\frac{V_a}{\beta}\int_0^T LV(T)}{A}) \\ &- \frac{f}{p}\frac{\int_0^T ROI(T)dt}{A} + \frac{f}{p}\frac{\frac{V_a}{\beta}\int_0^T LV(T)dt}{A}\end{aligned} \tag{A.13}$$

$$\begin{aligned}&\frac{ROI(T) - \frac{V_a}{\beta}LV(T)}{A} = (\frac{f}{\beta} + \frac{(f-\beta)}{\beta}\frac{\frac{V_a}{\beta}}{A} + \frac{f}{p}\frac{\frac{V_a}{\beta}}{A})\int_0^T LV(T)dt \\ &- (\frac{f}{p}\frac{1}{A} - \frac{(f-\beta)}{\beta}\frac{1}{A})\int_0^T ROI(T)dt|| \cdot A\end{aligned} \tag{A.14}$$

$$\begin{aligned}&ROI(T) - \frac{V_a}{\beta}LV(T) = (\frac{f}{\beta}\cdot A + \frac{(f-\beta)}{\beta}\frac{V_a}{\beta} + \frac{f}{p}\frac{V_a}{\beta})\int_0^T LV(T)dt \\ &- (\frac{f}{p} - \frac{(f-\beta)}{\beta})\int_0^T ROI(T)dt|| + V_a LV(T)\end{aligned} \tag{A.15}$$

$$\begin{aligned}ROI(T) = &(\frac{f}{\beta}\cdot A + \frac{(f-\beta)}{\beta}\frac{V_a}{\beta} + \frac{f}{p}\frac{V_a}{\beta})\int_0^T LV(T)dt \\ &- (\frac{f}{p} + \frac{(f-\beta)}{\beta})\int_0^T ROI(T)dt + \frac{V_a}{\beta}LV(T)\end{aligned} \tag{A.16}$$

$$\begin{aligned}&ROI(T) = (\frac{f}{\beta}(\alpha - \frac{V_a(1-\beta)}{\beta} + (1-\beta)\frac{V_a}{\beta} + \frac{V_a}{p})\int_0^T LV(T)dt \\ &- (\frac{f}{p} + \frac{(f-\beta)}{\beta})\int_0^T ROI(T)dt + \frac{V_a}{\beta}LV(T)\end{aligned} \tag{A.17}$$

$$ROI(T) = \frac{f}{\beta}(\alpha + \frac{V_a}{p}) \int_0^T LV(T)dt - f(\frac{1}{p} + \frac{(1-\beta)}{\beta}) \int_0^T ROI(T)dt + \frac{V_a}{\beta} LV(T) \tag{A.18}$$

$$\begin{cases} V_{fit} & = \frac{V_a}{\beta} \\ K_1 & = \frac{f}{\beta}(\alpha + \frac{V_a}{p}) \\ k_2 & = f(\frac{1}{p} + \frac{(1-\beta)}{\beta}). \end{cases} \tag{A.19}$$

B Appendix Code used for the fit_h2o model

```
    #! /usr/bin/bash

export PATH=/home/path/of_simulation/bin:$PATH
# making a library to save the data
mkdir simulation_data-fit_h2o_noise_and_no_noise_FIXED_CV-"
$( date +"%d-%m-%Y")"

path_to_data="simulation_data-fit_h2o_noise_and_no_noise_FIXED_CV-$(
date +"%d-%m-%Y")"/""

####

# Create noise-free simulated TACs for blood and muscle with high
sampling rate

fit2dat -c=0,600,1 radiowater.fit "${path_to_data}radiowater.dat"
tactime -nogap "${path_to_data}radiowater.dat" 30 "${path_to_data}btac.tac"
# noise:

c=($(seq 0 2 10))
minSD=($(seq 0 0.042 0.42))
# simulating the noise:
for j in $(seq 0 1 10 ); do
 if [ $j -lt 10 ]; then n="_000$j" ;else n="_00$j" ;fi
 #the amount of noise simulated
    for i in $(seq 0 2 10); do
  echo  "i=$i"
  svar4tac -minsd=${minSD[i]}  -x=10 -separate
        "${path_to_data}btac.tac" ${i} "${path_to_data}btacCV${i}.tac"
  ##Value is the value of perfusion
        for value in 50 $(seq 100 100 1000); do
   echo "value=$value"
   ## Vb is the vascular volume
            for Vb in $(seq 10 2 14); do
    echo "Vb=$Vb"
    ## fA is the arterial fraction of vascular volume in percentages
                for fA in $(seq 0 5 30); do
                    echo "fA= $fA"
                    b2t_h2o -nosub -fpt
                    "${path_to_data}btacCV${i}$n.tac"
                    $value 0.91 1 $Vb $fA "${path_to_data}ttacCV${i}$n.tac"
                    tacadd -ovr "${path_to_data}temp.tac"
                    "${path_to_data}ttacCV${i}$n.tac"
```

```
tacadd "${path_to_data}temp.tac"
"${path_to_data}btacCV${i}$n.tac"
###
# Simulate a dynamic PET phantom image
###
# Do framing for the simulation
simframe -sec "${path_to_data}temp.tac" frames.dat
"${path_to_data}mbfsimCV${i}$n.tac"
# Savig the mbfsim.tac in folder.
# Simulate a 3D phantom image
simimyoc -fwhm=0 -diameter=50 -thickness=10
 -diamin=1 -dim=100 -pxlsize=1
 "${path_to_data}mbfsimCV${i}$n.tac"
 "${path_to_data}mbfsim1CV${i}$n.v"
simimyoc -fwhm=0 -diameter=50 -thickness=10
 -diamin=0.6 -dim=100 -pxlsize=1
 "${path_to_data}mbfsimCV${i}$n.tac"
 "${path_to_data}mbfsim2CV${i}$n.v"
simimyoc -3D -fwhm=10 -diameter=50
 -thickness=10 -diamin=0.6 -dim=100 -pxlsize=1
 "${path_to_data}mbfsimCV${i}$n.tac"
 "${path_to_data}mbfsim3CV${i}$n.v"
###
# Extract TACs automatically and rename the
generic "Mask"
###
# LV
img2dft "${path_to_data}mbfsim3CV${i}$n.v" lvcav.v
"${path_to_data}lvcav.dft"
tacren "${path_to_data}lvcav.dft" Mask lvcav
# Myocardium
img2dft "${path_to_data}mbfsim3CV${i}$n.v"
whole-muscle.v "${path_to_data}whole-muscle.dft"
tacren "${path_to_data}whole-muscle.dft" Mask whole
# ROI 1
img2dft "${path_to_data}mbfsim3CV${i}$n.v" roi1.v
"${path_to_data}roi1.dft"
tacren "${path_to_data}roi1.dft" Mask roi1
# ROI 2
img2dft "${path_to_data}mbfsim3CV${i}$n.v" roi2.v
"${path_to_data}roi2.dft"
tacren "${path_to_data}roi2.dft" Mask roi2
# ROI 3
img2dft "${path_to_data}mbfsim3CV${i}$n.v" roi3.v
"${path_to_data}roi3.dft"
```

```
                    tacren "${path_to_data}roi3.dft" Mask roi3

                    # Catenate all TAC into one file
                    tacadd "${path_to_data}catenated_${value}_${Vb}_${fA}
                    _CV${i}$n.dft" "${path_to_data}lvcav.dft"
                    "${path_to_data}whole-muscle.dft"
                    "${path_to_data}roi1.dft" "${path_to_data}roi2.dft"
                    "${path_to_data}roi3.dft"
     # Using the wanted modeling algorithm:
                    fit_h2o -ml -fpt -k2 -Delay=0
                    -fit="${path_to_data}fit_data"
                    "${path_to_data}lvcav.dft"
                    "${path_to_data}catenated_${value}_${Vb}_${fA}_CV${i}$
                    n.dft" 360
                    "${path_to_data}sim_results_${value}_${Vb}_${fA}_CV${i
                    }$n.res"
    done
   done
  done
 done
done
```

C Appendix Code used for the fitmbf model

```
    #! /usr/bin/bash

export PATH=/home/path/of_simulation/bin:$PATH
# making a library to save the data
mkdir simulation_data-fit_h2o_noise_and_no_noise_FIXED_CV-"
$( date +"%d-%m-%Y")"

path_to_data="simulation_data-fit_h2o_noise_and_no_noise_FIXED_CV-$(
date +"%d-%m-%Y")"/""

####

# Create noise-free simulated TACs for blood and muscle with high
sampling rate

fit2dat -c=0,600,1 radiowater.fit "${path_to_data}radiowater.dat"
tactime -nogap "${path_to_data}radiowater.dat" 30 "${path_to_data}btac.tac"
# noise:

c=($(seq 0 2 10))
minSD=($(seq 0 0.042 0.42))
# simulating the noise:
for j in $(seq 0 1 10 ); do
 if [ $j -lt 10 ]; then n="_000$j" ;else n="_00$j" ;fi
 #the amount of noise simulated
    for i in $(seq 0 2 10); do
  echo  "i=$i"
  svar4tac -minsd=${minSD[i]}  -x=10 -separate
        "${path_to_data}btac.tac" ${i} "${path_to_data}btacCV${i}.tac"
  ##Value is the value of perfusion
        for value in 50 $(seq 100 100 1000); do
   echo "value=$value"
   ## Vb is the vascular volume
            for Vb in $(seq 10 2 14); do
    echo "Vb=$Vb"
    ## fA is the arterial fraction of vascular volume in percentages
                for fA in $(seq 0 5 30); do
                    echo "fA= $fA"

     # Using the wanted modeling algorithm:
                   fitmbf -beta=0.95
                    "${path_to_data}catenated_${value}_${Vb}_${fA}_CV${i}$
                    n.dft" lvcav whole
```

```
                    "${path_to_data}mbfsim_results_${value}_${Vb}_${fA}_CV
                    ${i}$n.res"
    done
   done
  done
 done
done
```

D Appendix Pseudocode for NAIST model

```
def read_files(path):
    df=read in the file using path skipping the n first rows
    as they don't include usable data.
    Next tag each column to a correct information
    The file inclueds time data and five functions data points,
    where one is used as the function fed to the simulation
    return(time_start,time_end,aif,tac,roi1,roi2,roi3)

class model_single_component(nn.Module):
    def __init__(self,parameters):
        define the parameters using self
        self.parameter1
        self.parameter2
        etc.

    def convolution_in_segment(self,smaller_set_of_parameters):
        Here is  the function calculating the new points using the
        optimized parameters
        for value in range(lenght_of_time-1):
            The parameters in this section are taken form the
            correct place of the used parameter in question
            and fed to the function which will be fed to be
            the next point in the function.
        return(the_function_out)
    def forward(self, time,function_used_to_calculate_other_functions):
        (futcof=function_used_to_calculate_other_functions)
        Here parameters are clamped using torch
        pakage so that each parameter value
        wouldn't get values that are impossible
        for them in real sitsuations.
        c_out=self.convolution_in_segment(time,futcof,parameters)
        function_out=c_out+parameter1*futcof
        return(function_out)

def fit_single_component(time_change,futcof,wanted_function,parameters):
    Extracting the parameters from the parameters parameter.
    Calling the class object to find optimal
    parameters and adding them to
    device
    optimising the model parameters using Adam optimizer,
    and set out learning rate.

    Changing the lists to float tensors using
```

```
    torch and adding them to device.
    looping over from starting time to the times
    the iterations amount is set
     Calculating loss and optimizing the parameters
    Saving the parameters
    taking the optimized parameters from the model
    return(optimized parameters)

def convolution_calculation(time_seq,futcof,parameters):
    using the change of futcof, change in time and the
    optimiced parameters to calculate each new
    function point so the new calculated functions
    can be compared to the originals, and see how
    well the optimization has gone.

    for point in range of all points-1:
        The actula convoluton calculation function
        and saving the calculated points as numpy list.
    return(timepoints, new_function)

def get_function_from_aif(time_change,futcof,optimized_parameters):
    _, ca= convolution_calculation(time_change,futcof,parameters)
    calculated_function=ca+va*futcof
    return(calculated_function)

Next different metrics to measure how the functions fit
compared to the original functions:

def rsquared(original,simulated):
    r**2
    rsqured=metrics.r2_Score(originla,simulated)
    return rsqured

def mean_squere_error(original,simulated):
    mse=metrics.mean_squere_error(original,simulated)
    return mse

def sum_squere_error(original,simulated):
    sse=np.sum(original-simulated)**2)
    return sse

def AIC(n,sse,k):
    This calculated the AIC value using sse
    aic=(n*np.log(sse/n)+2*k)+((2*k*(k+1))/(n-k-1))
    return aic
```

```
next we have the visualisation function:

def plot_aif_tac(time, all original
and simulated functions, noise value, and values for aic calculation):
    all the functions are plotted in same image
    as well as the generated noise
    also the r squared values and AIC calculations
    for the certaine noise set is plotted in the
    image to compare how much they do change.
```

In the dynamic part, the functions are called and the optimized parameters are used in the convolutional function. All the simulated AIF's and ROI's from tpclib are run in order and all the parameters, are saved as well as the images where the original functions and the new simulated functions are plotted.

E Appendix pseudocode for changes to make NASTα model

```
class model_single_component(nn.Module):
    def __init__(self,parameters):
        define the parameters using self
        self.parameter1
        self.parameter2
        etc.

    def convolution_in_segment(self,smaller_set_of_parameters):
        Here is  the function calculating the new points using the
        optimized parameters
        for value in range(lenght_of_time-1):
            The parameters in this section are taken form the
            correct place of the used parameter in question
            and fed to the function which will be fed to be
            the next point in the function.
        return(the_function_out)
    def forward(self, time,function_used_to_calculate_other_functions):
        (futcof=function_used_to_calculate_other_functions)
        parameters are not clamped here anymore.
        c_out=self.convolution_in_segment(time,futcof,parameters)
        function_out=c_out+parameter1*futcof
        return(function_out)

def fit_single_component(time_change,futcof,wanted_function,parameters):
    Extracting the parameters from the parameters parameter.
    Calling the class object to find optimal
    parameters and adding them to
    device
    optimising the model parameters using Adam optimizer,
    and set out learning rate.

    Changing the lists to float tensors using
    torch and adding them to device.
    looping over from starting time to the times
    the iterations amount is set
    Calculating loss and optimizing the parameters
    Saving the parameters
    Clamping them for the next loop
    taking the optimized parameters from the model
    return(optimized parameters)
```

```
def get_function_from_aif(time_change,futcof,optimized_parameters):
    _, ca= convolution_calculation(time_change,futcof,parameters)
    calculated_function=ca*alpha+va*futcof
    return(calculated_function)
```

In the alpha model there is multiple loops that use the sum of the original tacs to define which parameter guesses are used in the simulating.

F Appendix Results from fit_h2o model

F.1 Box-plots

F.1.1 Appendix Results for boxplots of perfusion value 50 [ml min-1 ml-1] and 100 [ml min-1 ml-1] from fit_h2o model

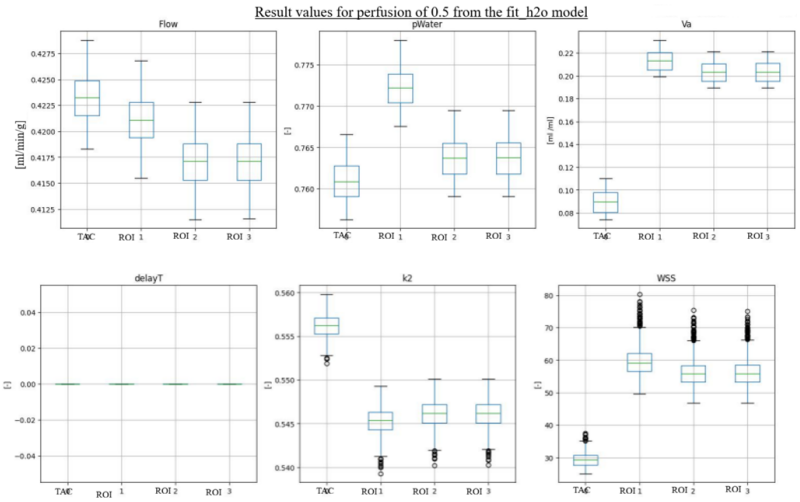

Figure F.1. In this figure are the box plots from all the parameters from the fit_h2o model for TAC and ROI's from perfusion value of 50 [ml min-1 ml-1]. The model performs well, us suspected, in low perfusions, having near to the simulated flow, having a Va value that is normal and pWater =vd, stays under 1 as should..The ranges were discussed in the results.

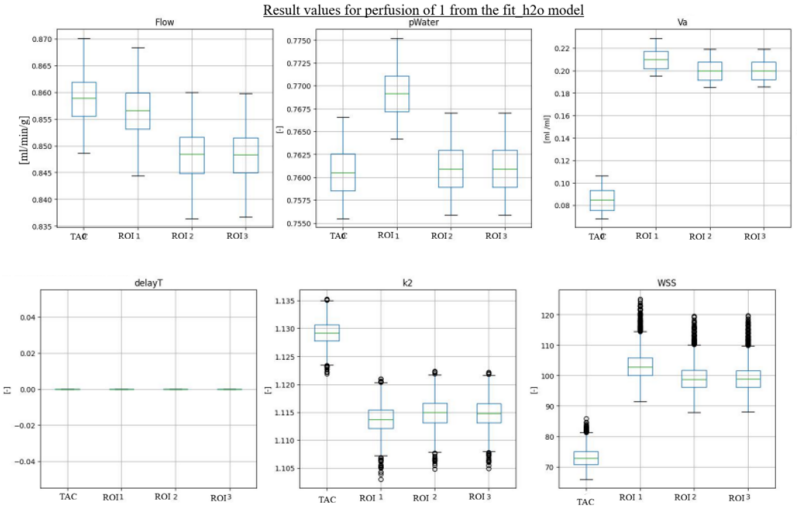

Figure F.2. In this figure are the box plots from all the parameters from the fit_h2o for TAC and ROI's from perfusion value of 100 [ml min-1 ml-1]. Here again values for flow are near to the values used in the b2t_h2o simulation data. Va is also staying in expected values and pWater =vd, stays under 1 as should.

F.1.2 Appendix Results for boxplots of perfusion value 300 [ml min-1 ml-1] and 400 [ml min-1 ml-1] from fit_h2o model

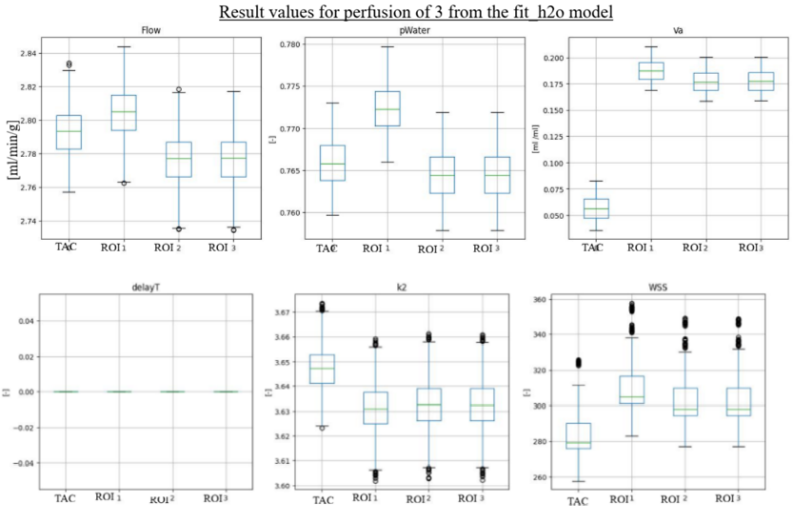

Figure F.3. In this figure are the box plots from all the parameters from the fit_h2o for TAC and ROI's from perfusion value of 300 [ml min-1 ml-1]. Here again values for flow are near to the values used in the b2t_h2o simulation data. Va is also staying in expected values, in slightly lower end, and pWater =vd, stays under 1 as should. WSS starting to get higher here.

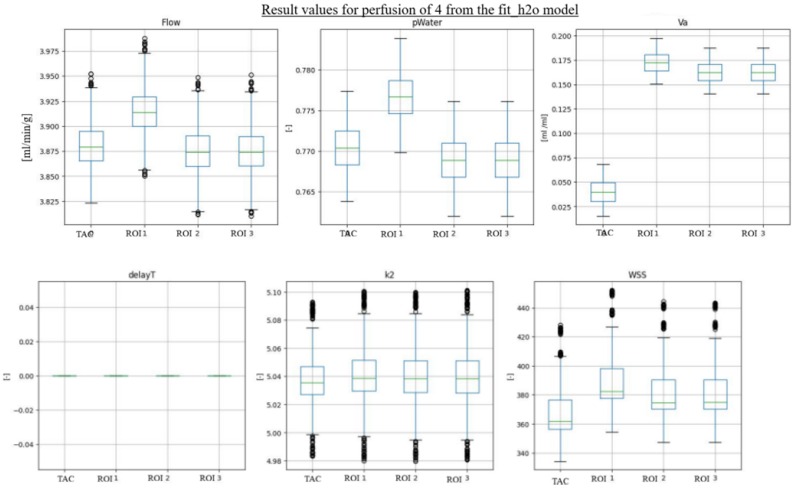

Figure F.4. In this figure are the box plots from all the parameters from the fit_h2o for TAC and ROI's from perfusion value of 400 [ml min-1 ml-1]. Here again values for flow are near to the values used in the b2t_h2o simulation data. Va is starting to be low, and pWater =vd, stays under 1 as should. WSS keeps on rising.

F.1.3 Appendix Results for boxplots of perfusion value 500 [ml min-1 ml-1] and 600 [ml min-1 ml-1] from fit_h2o model

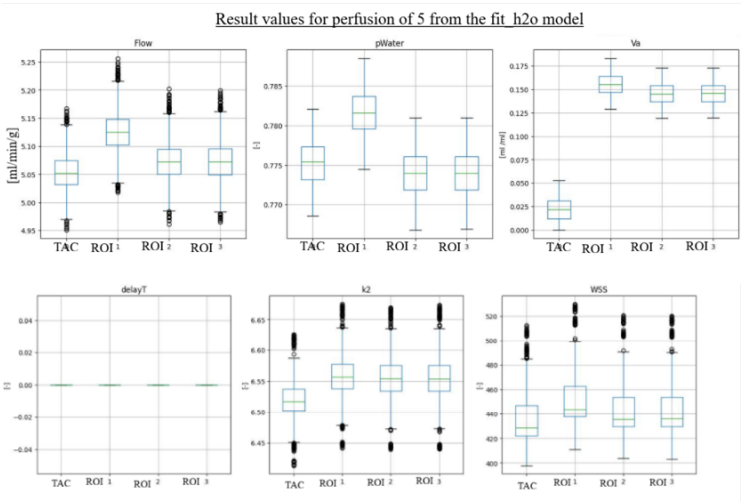

Figure F.5. In this figure are the box plots from all the parameters from the fit_h2o for TAC and ROI's from perfusion value of 500 [ml min-1 ml-1]. Here again values for flow are near to the values used in the b2t_h2o simulation data. Va is starting to be too low and pWater =vd, stays under 1 as should. WSS relativly similar compared to the earlier one.

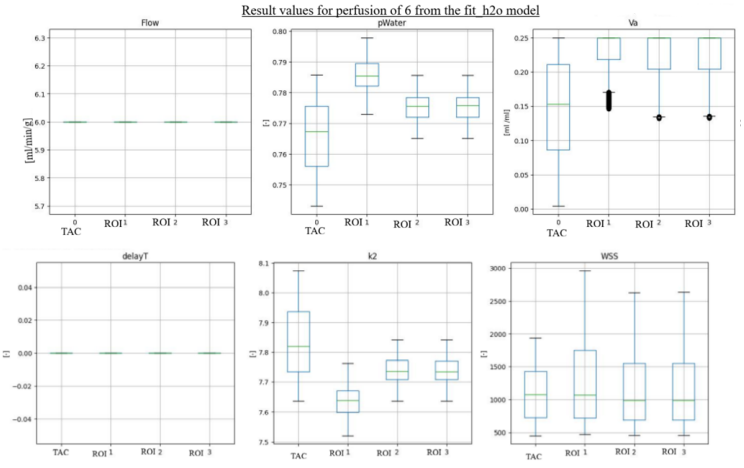

Figure F.6. In this figure are the box plots from all the parameters from the fit_h2o for TAC and ROI's from perfusion value of 600 [ml min-1 ml-1]. Here we can see that the flow has peaked, while in Va TAC is showing abnormal values. The ROIs are also peaked at 0.25. And here the WSS has spiked really high, indicating what we can also see, which is that the model doesn't work in these high perfusion.

F.2 Parameters as a function of perfusion.

F.2.1 Appendix Results for flow and k2 from fit_h2o model

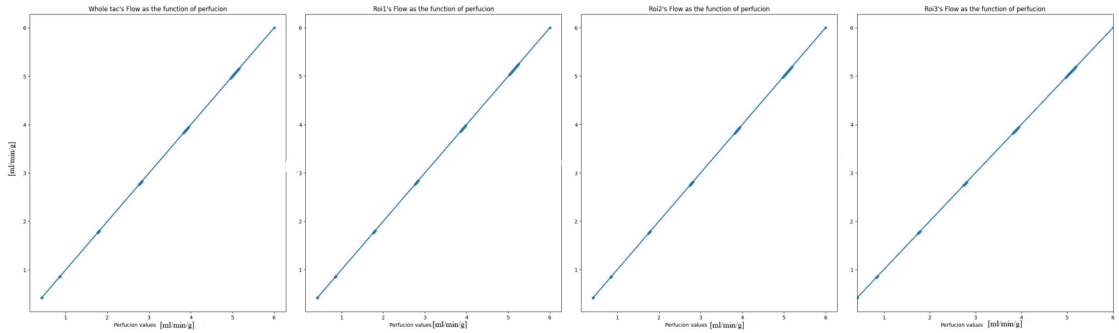

Figure F.7. In this figure the flow is plotted as a function of perfusion for the fit_h2o for TAC and ROI's. The model worked well with the perfusion prediction, till perfusion of 5, were we wan see a bigger cluster of points. These points are the result from the peak we saw in the last box plot.

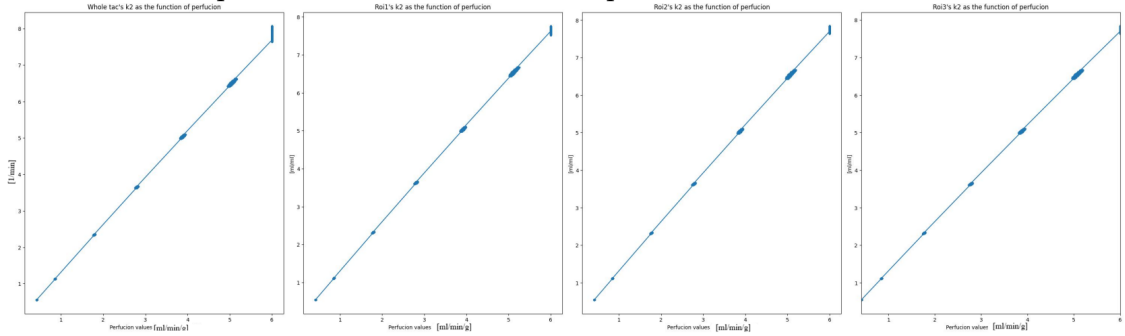

Figure F.8. In this figure the k2 is plotted as a function of perfusion for the fit_h2o for TAC and ROI's. As k2 is connected to perfusion it is showing similar pattern in the modelling. A difference is the peak of k2 values modeled in high perfusion, and it goes till 8, and most of the way the increase is linear.

F.2.2 Appendix Results for pWater and Va from fit_h2o model

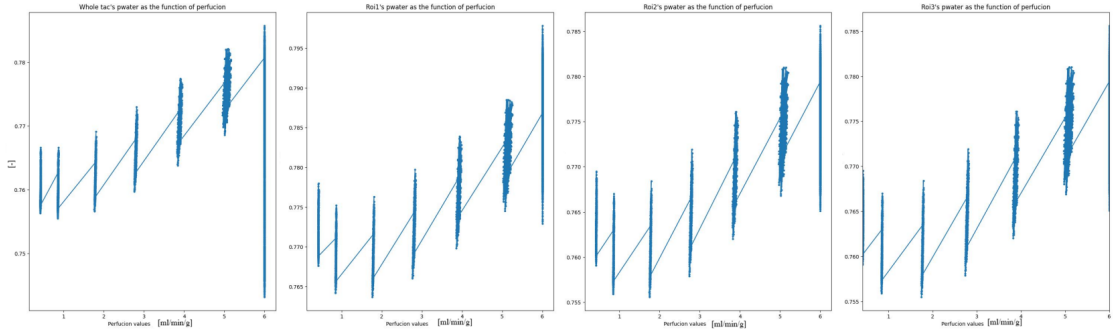

Figure F.9. In this figure the pWater (vd) is plotted as a function of perfusion for the fit_h2o for TAC and ROI's. Here the different values used to generate the original data and the noise are easier to see. The zigzag pattern has formed when differently generated perfusion were used.

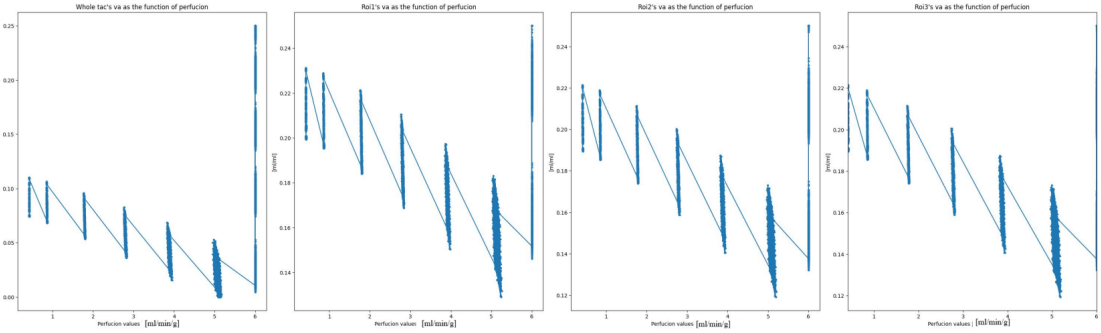

Figure F.10. In this figure the va is plotted as a function of perfusion for the fit_h2o for TAC and ROI's. For Va a optimal result would be to stay near the range of 0.24-0.20. On the other hand the point was to test different scenarios, so it might be that some of the values around 0.18 are still valid. Here again a larger cluster near the perfusion 5 can be seen, where the model had peaked. The zigzag pattern has formed when differently generated perfusion were used.

F.3 Results from fit_h2o model as mean ± standard deviation

Summary of results for fith2o model values as mean ± standard deviation.

	Flow	vd	va	k2
(50, 'roi1')	0.421 ± 0.002	0.772 ± 0.002	0.213 ± 0.009	0.545 ± 0.002
(50, 'whole')	0.423 ± 0.002	0.761 ± 0.002	0.090 ± 0.010	0.556 ± 0.001
(100, 'roi1')	0.857 ± 0.004	0.769 ± 0.002	0.210 ± 0.009	1.114 ± 0.003
(100, 'whole')	0.859 ± 0.004	0.761 ± 0.002	0.085 ± 0.010	1.129 ± 0.002
(200, 'roi1')	1.787 ± 0.009	0.769 ± 0.003	0.200 ± 0.009	2.322 ± 0.006
(200, 'whole')	1.786 ± 0.008	0.762 ± 0.003	0.072 ± 0.011	2.343 ± 0.005
(300, 'roi1')	2.805 ± 0.014	0.772 ± 0.003	0.188 ± 0.010	3.631 ± 0.011
(300, 'whole')	2.793 ± 0.014	0.766 ± 0.003	0.057 ± 0.011	3.647 ± 0.010
(400, 'roi1')	3.915 ± 0.023	0.777 ± 0.003	0.173 ± 0.010	5.040 ± 0.022
(400, 'whole')	3.881 ± 0.022	0.770 ± 0.003	0.040 ± 0.011	5.037 ± 0.020
(500, 'roi1')	5.126 ± 0.038	0.782 ± 0.003	0.156 ± 0.011	6.557 ± 0.042
(500, 'whole')	5.054 ± 0.035	0.775 ± 0.003	0.022 ± 0.012	6.518 ± 0.038
(600, 'roi1')	6.000 ± 0.000	0.786 ± 0.005	0.228 ± 0.033	7.636 ± 0.044
(600, 'whole')	6.000 ± 0.000	0.766 ± 0.011	0.145 ± 0.079	7.837 ± 0.114

Figure F.11. The mean values with standard deviation from each parameter for perfusion till 600 [ml min-1 ml-1]. Only TAC (whole in the fit_h2o model) and ROI1 are shown as the other ROIs had almost identical results with ROI1.

G Appendix Results from fitmbf model

G.1 Box-plots

G.1.1 Appendix Results for boxplots of perfusion value 50 [ml min-1 ml-1] and 100 [ml min-1 ml-1] from fitmbf model

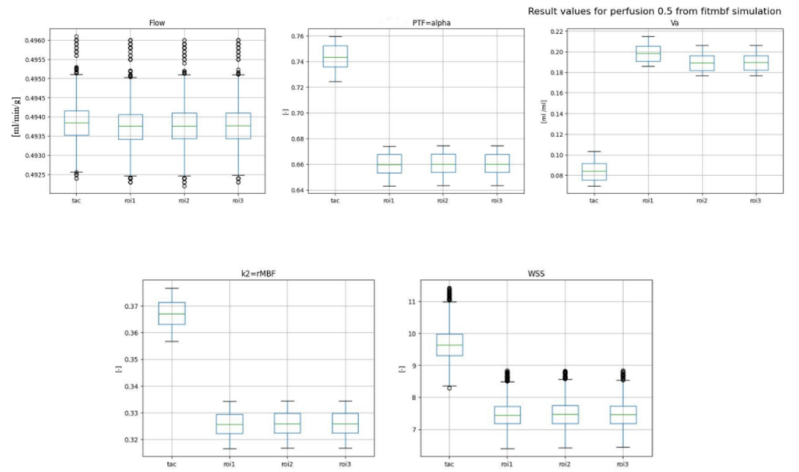

Figure G.1. In this figure are the box plots from all the parameters from the fitmb for TAC and ROI's from perfusion value of 50 [ml min-1 ml-1]. Here we can see the flow, perfusion, is near the simulated data, α is what is should be and Va is in range as well. WSS value in this is really small, meaning the function had a good fit to the simulated b2t_h2o TACs' and ROIs'.

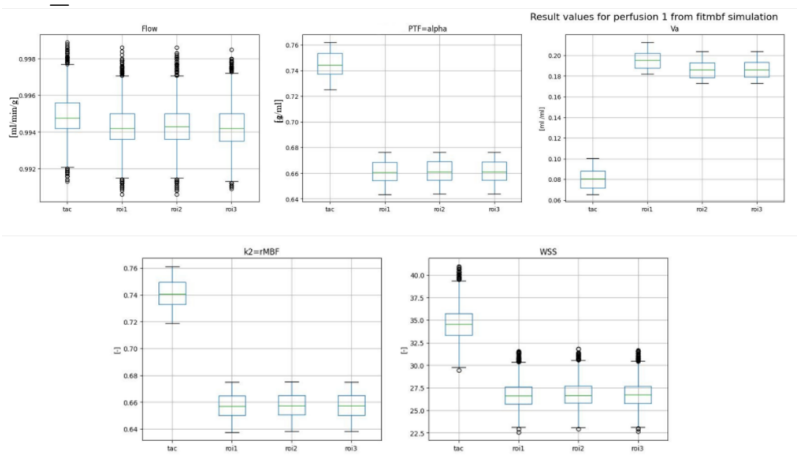

Figure G.2. In this figure are the box plots from all the parameters from the fitmbf for TAC and ROI's from perfusion value of 100 [ml min-1 ml-1]. Here we can see the flow, perfusion, is near the simulated data, α is what is should be and Va is in range as well. WSS value in this is really small, meaning the function had a good fit to the simulated b2t_h2o TACs' and ROIs'.

G.1.2 Appendix Results for boxplots of perfusion value 300 [ml min-1 ml-1] and 400 [ml min-1 ml-1] from fitmbf model

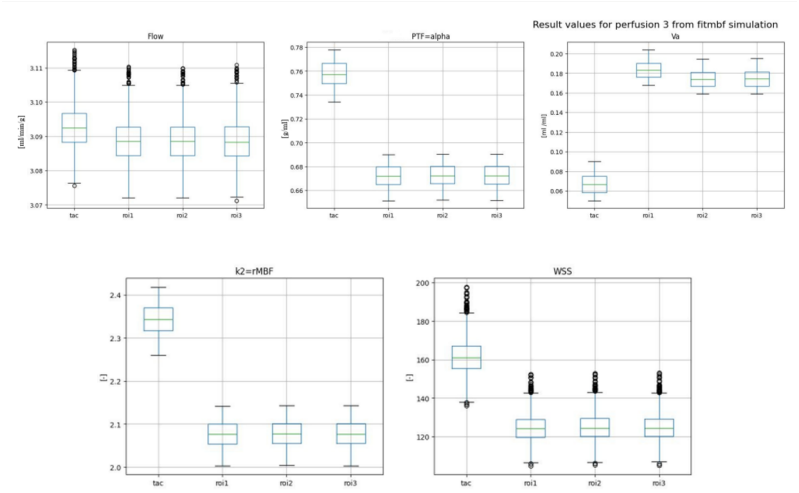

Figure G.3. In this figure are the box plots from all the parameters from the fitmbf for TAC and ROI's from perfusion value of 300 [ml min-1 ml-1]. Here we can see the flow, perfusion, is near the simulated data, α is what is should be and Va is in range as well. WSS value starts to get larger, meaning the function had a good fit to the simulated b2t_h2o TACs' and ROIs'.

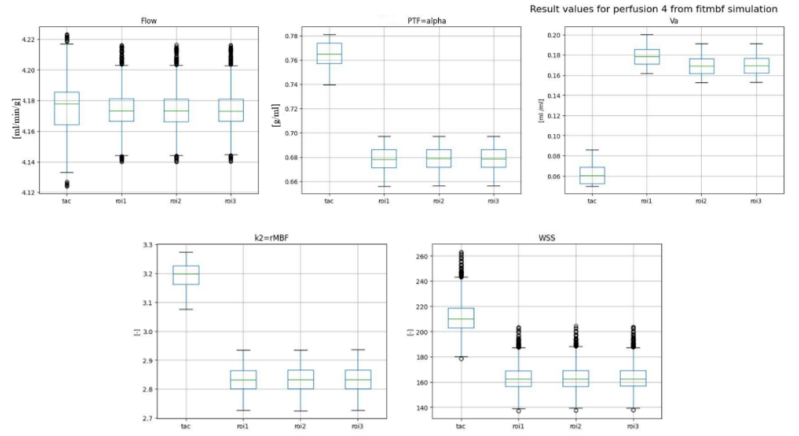

Figure G.4. In this figure are the box plots from all the parameters from the fitmbf for TAC and ROI's from perfusion value of 400 [ml min-1 ml-1]. Here we can see the flow, perfusion, is near the simulated data, α is what is should be and Va is in range as well. WSS value starts to get larger, meaning the function had a good fit to the simulated b2t_h2o TACs' and ROIs'.

G.1.3 Appendix Results for boxplots of perfusion value 500 [ml min-1 ml-1] from fitmbf model

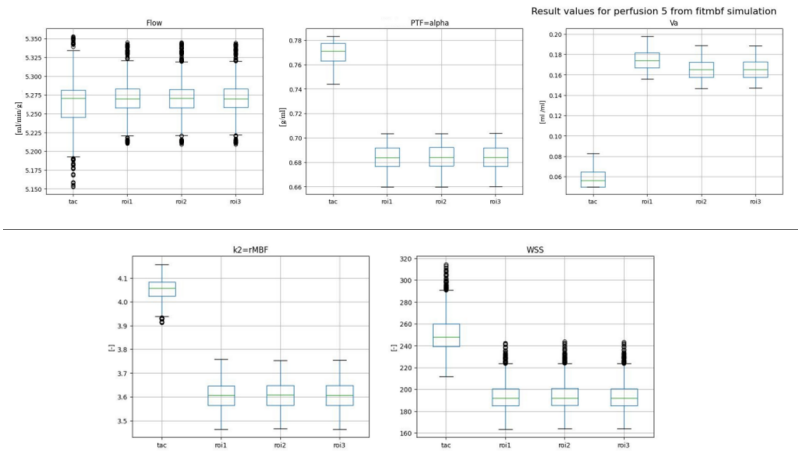

Figure G.5. In this figure are the box plots from all the parameters from the fitmbf for TAC and ROI's from perfusion value of 500 [ml min-1 ml-1]. Here we can see the flow, perfusion, is near the simulated data, α is what is should be and Va is in range as well. WSS value starts to get larger, meaning the function had a good fit to the simulated b2t_h2o TACs' and ROIs'.

G.2 Parameters as a function of perfusion.

G.2.1 Appendix Results for perfusion and ptf (α) from fitmbf model

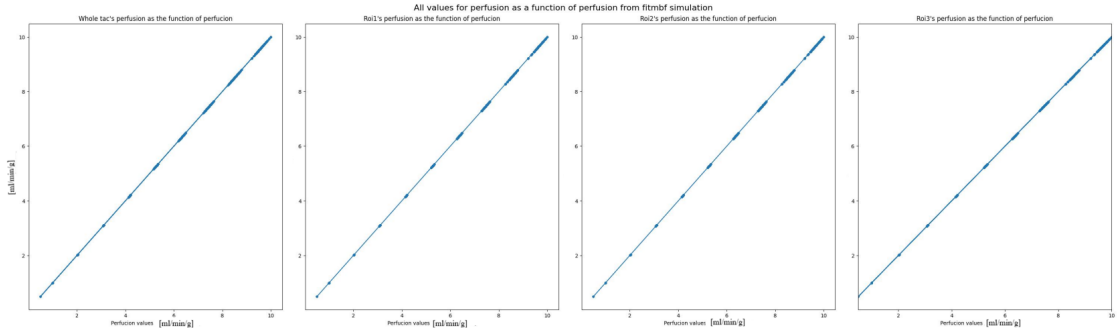

Figure G.6. In this figure the perfusion is plotted as a function of perfusion for the fitmbf for TAC and ROI's. Here we can see that the fitmbf model goes all the way till the 10. So this model doesn't have as strict peak as the others. The clusters of the used data can be seen starting to be sett in larger area in the line, while the perfusion gets higher

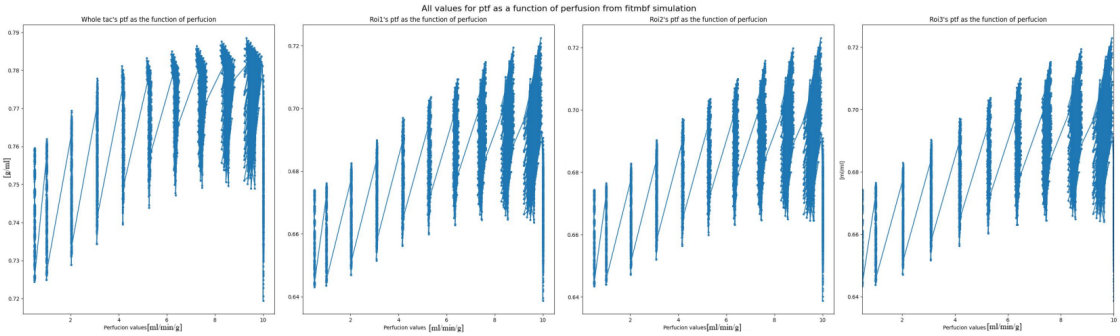

Figure G.7. In this figure the α (PTF) is plotted as a function of perfusion for the fitmbf for TAC and ROI's. Here we can see how in this model the α parameter has strict range from 0.72-0.79. The values in the higher perfusion over 0.76 start to get quit high over all, but the model have been quite consistent with the modeling.

G.3 Parameters as a function of perfusion.

G.3.1 Appendix Results for rMBF and Va from fitmbf model

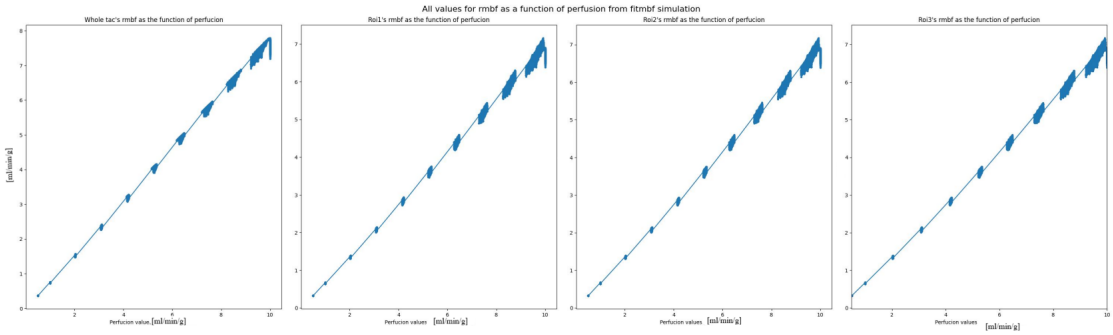

Figure G.8. In this figure the The mean blood flow in myocardial region (rMBF) is plotted as a function of perfusion for the fitmbf for TAC and ROI's. In this figure the cluster for the different data from same perfusions start to get more variations in the modeling after perfusion of 6.

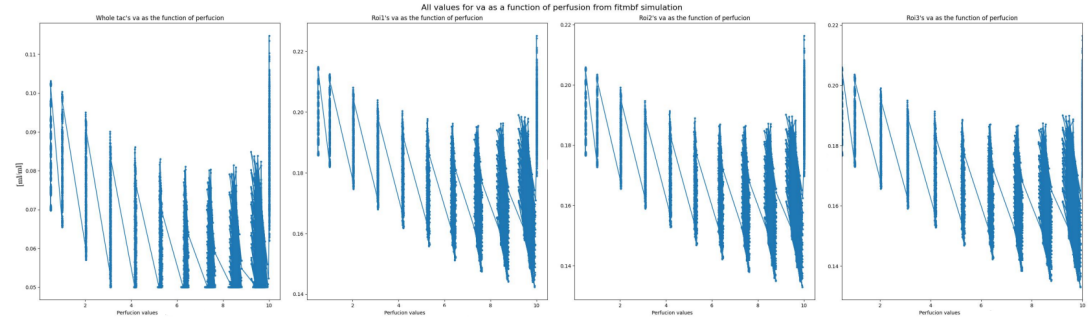

Figure G.9. In this figure the Va is plotted as a function of perfusion for the fitmbf for TAC and ROI's. Here the zigzag from the simulated data can be seen again. But again fitmbf stays in line with 0.22-0.14. Optimal value here would probably be something near constant, but the model performs surprisingly well with this wide range data.

G.4 Results from fitmbf model as mean ± standard deviation

Summary of results for fitmbf model values as mean ± standard deviation.

	Flow	alpha	va	rMBF	WSS
(50, 'roi1')	0.494 ± 0.001	0.660 ± 0.008	0.198 ± 0.008	0.326 ± 0.004	7.481 ± 0.433
(50, 'whole')	0.494 ± 0.001	0.743 ± 0.010	0.084 ± 0.009	0.367 ± 0.005	9.688 ± 0.555
(100, 'roi1')	0.994 ± 0.001	0.661 ± 0.009	0.195 ± 0.008	0.657 ± 0.009	26.781 ± 1.524
(100, 'whole')	0.995 ± 0.001	0.745 ± 0.010	0.080 ± 0.009	0.741 ± 0.010	34.673 ± 1.980
(200, 'roi1')	2.026 ± 0.004	0.666 ± 0.009	0.189 ± 0.008	1.349 ± 0.018	77.448 ± 4.576
(200, 'whole')	2.028 ± 0.004	0.750 ± 0.010	0.073 ± 0.010	1.522 ± 0.021	100.317 ± 5.929
(300, 'roi1')	3.089 ± 0.007	0.672 ± 0.009	0.183 ± 0.009	2.076 ± 0.029	125.132 ± 7.758
(300, 'whole')	3.093 ± 0.007	0.758 ± 0.010	0.067 ± 0.010	2.344 ± 0.033	162.064 ± 10.035
(400, 'roi1')	4.174 ± 0.014	0.678 ± 0.009	0.178 ± 0.009	2.832 ± 0.040	163.850 ± 10.720
(400, 'whole')	4.176 ± 0.016	0.765 ± 0.010	0.062 ± 0.009	3.193 ± 0.040	212.308 ± 13.979
(500, 'roi1')	5.271 ± 0.024	0.684 ± 0.009	0.174 ± 0.009	3.605 ± 0.054	193.965 ± 13.366
(500, 'whole')	5.264 ± 0.034	0.770 ± 0.009	0.058 ± 0.008	4.051 ± 0.043	251.643 ± 17.665
(600, 'roi1')	6.357 ± 0.028	0.687 ± 0.009	0.173 ± 0.009	4.368 ± 0.064	216.397 ± 15.254
(600, 'whole')	6.335 ± 0.048	0.774 ± 0.008	0.056 ± 0.007	4.900 ± 0.047	282.768 ± 21.053
(700, 'roi1')	7.357 ± 0.036	0.686 ± 0.009	0.176 ± 0.009	5.043 ± 0.072	239.147 ± 25.385
(700, 'whole')	7.346 ± 0.036	0.779 ± 0.007	0.053 ± 0.006	5.722 ± 0.052	307.826 ± 19.306
(800, 'roi1')	8.034 ± 0.352	0.691 ± 0.011	0.171 ± 0.012	5.551 ± 0.201	264.084 ± 26.342
(800, 'whole')	8.291 ± 0.227	0.781 ± 0.005	0.052 ± 0.005	6.478 ± 0.193	322.278 ± 16.035
(900, 'roi1')	8.813 ± 0.269	0.695 ± 0.012	0.167 ± 0.012	6.127 ± 0.156	261.247 ± 27.492
(900, 'whole')	8.800 ± 0.295	0.776 ± 0.006	0.055 ± 0.006	6.833 ± 0.234	314.315 ± 20.223
(1000, 'roi1')	9.876 ± 0.165	0.678 ± 0.016	0.186 ± 0.017	6.694 ± 0.114	271.741 ± 23.920
(1000, 'whole')	9.849 ± 0.172	0.760 ± 0.016	0.075 ± 0.017	7.479 ± 0.084	329.865 ± 13.494

Figure G.10. The mean values with standard deviation from each parameter for perfusion till 1000 [ml min-1 ml-1]. Only TAC (whole in the fitmbf model) and ROI1 are shown as the other ROIs had almost identical results with ROI1.

H Appendix Results from NAIST model

H.1 Box-plots

H.1.1 Appendix Results for boxplots of perfusion value 50 [ml min-1 ml-1] and 100 [ml min-1 ml-1] from NAIST model

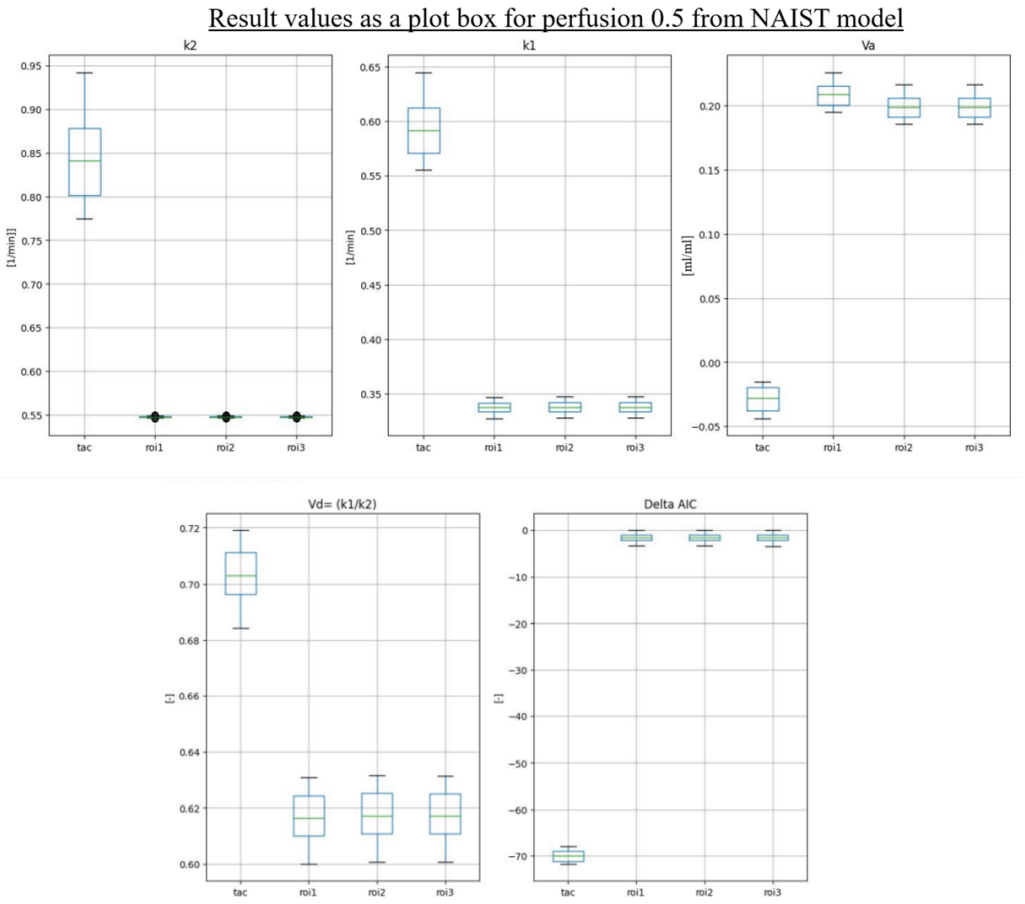

Figure H.1. In this figure are the box plots from all the parameters from the NAIST for TAC and ROI's from perfusion value of 50 [ml min-1 ml-1]. Here we can see that the ROIs perform quite well. TAC has problems with this small perfusion. It breaks in almost everything, k2 is high, K1 is high and Va is negative (not possible). Also the ΔAIC value for the model is noticeable higher.

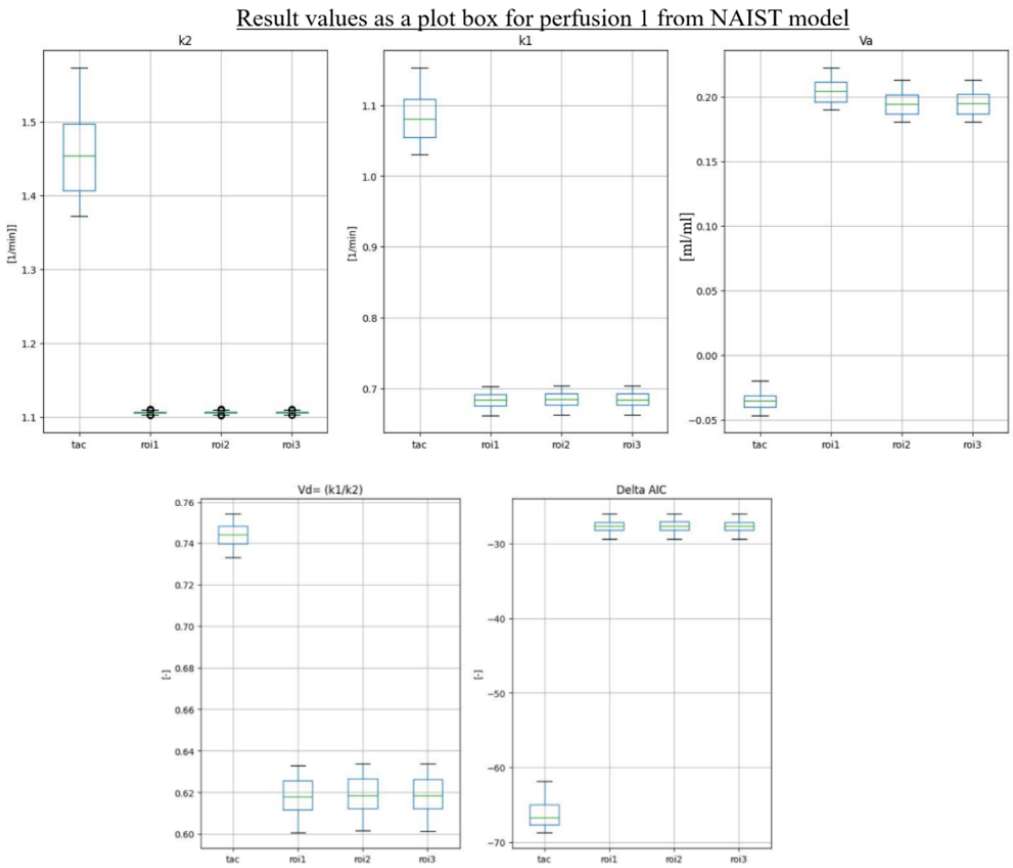

Figure H.2. In this figure are the box plots from all the parameters from the NAIST for TAC and ROI's from perfusion value of 100 [ml min-1 ml-1]. Here again we can see that the ROIs perform quite well. TAC has problems with this small perfusion. It breaks in almost everything, as k2 is high, K1 is high and Va is negative (not possible). Also the ΔAIC value for the model is noticeable higher.

H.1.2 Appendix Results for boxplots of perfusion value 300 [ml min-1 ml-1] and 400 [ml min-1 ml-1] from NAIST model

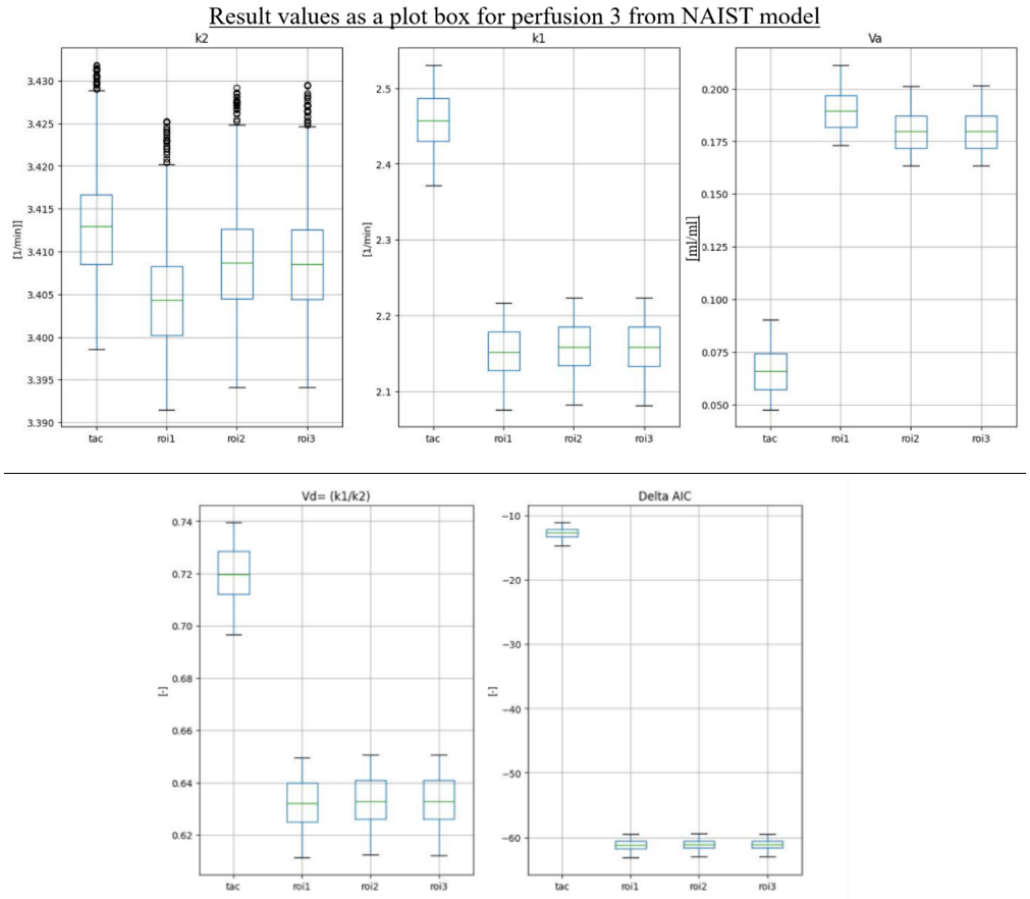

Figure H.3. In this figure are the box plots from all the parameters from the NAIST for TAC and ROI's from perfusion value of 300 [ml min-1 ml-1]. But here the model starts to perform better, as it did in the 200 perfusions that is shown in results.

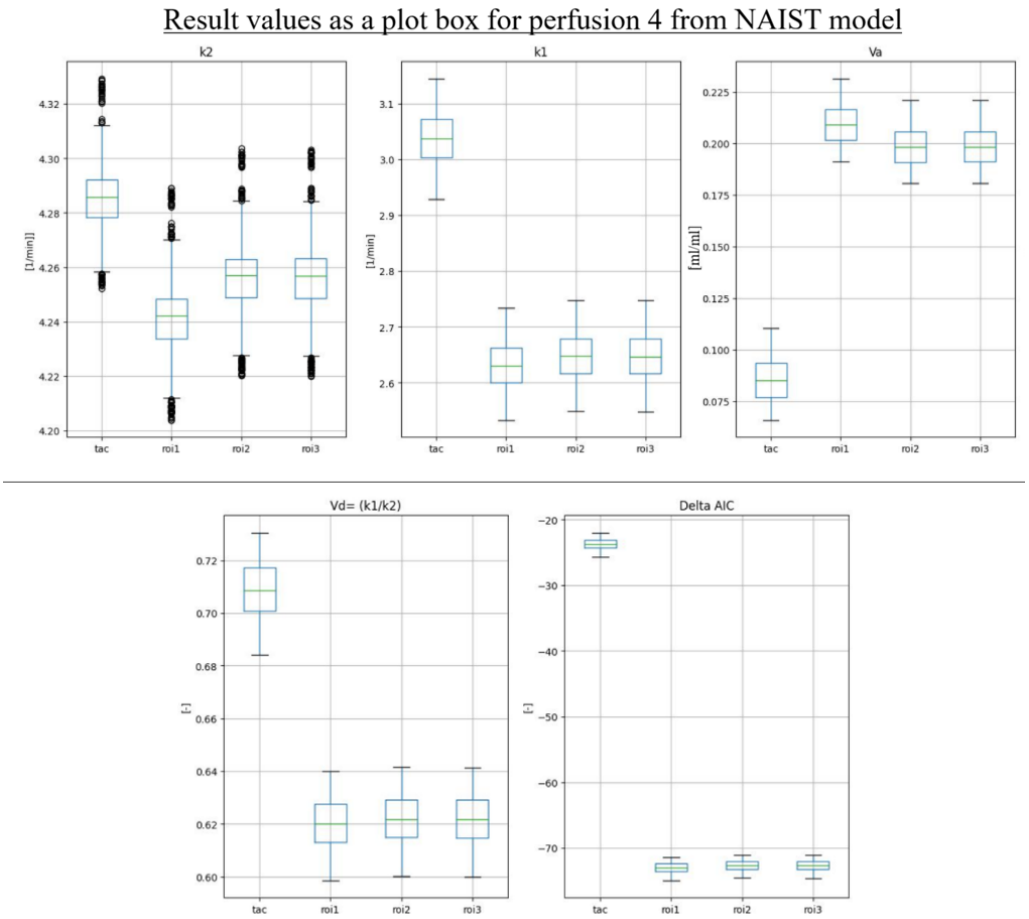

Figure H.4. In this figure are the box plots from all the parameters from the NAIST for TAC and ROI's from perfusion value of 400 [ml min-1 ml-1]. Here the values are around what they should. ΔAIC is small.

H.1.3 Appendix Results for boxplots of perfusion value 500 [ml min-1 ml-1] and 600 [ml min-1 ml-1] from NAIST model

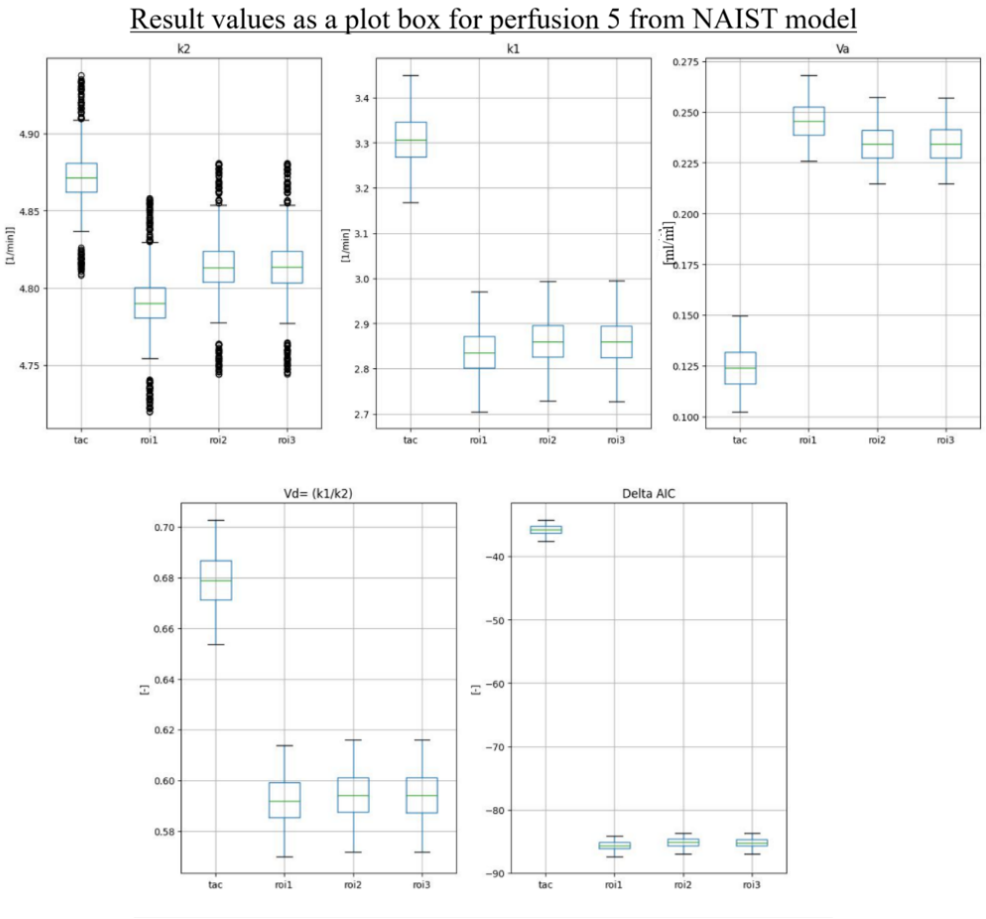

Figure H.5. In this figure are the box plots from all the parameters from the NAIST for TAC and ROI's from perfusion value of 500 [ml min-1 ml-1]. Here the Va starts to get higher, but nothing too out of ordinary yet.

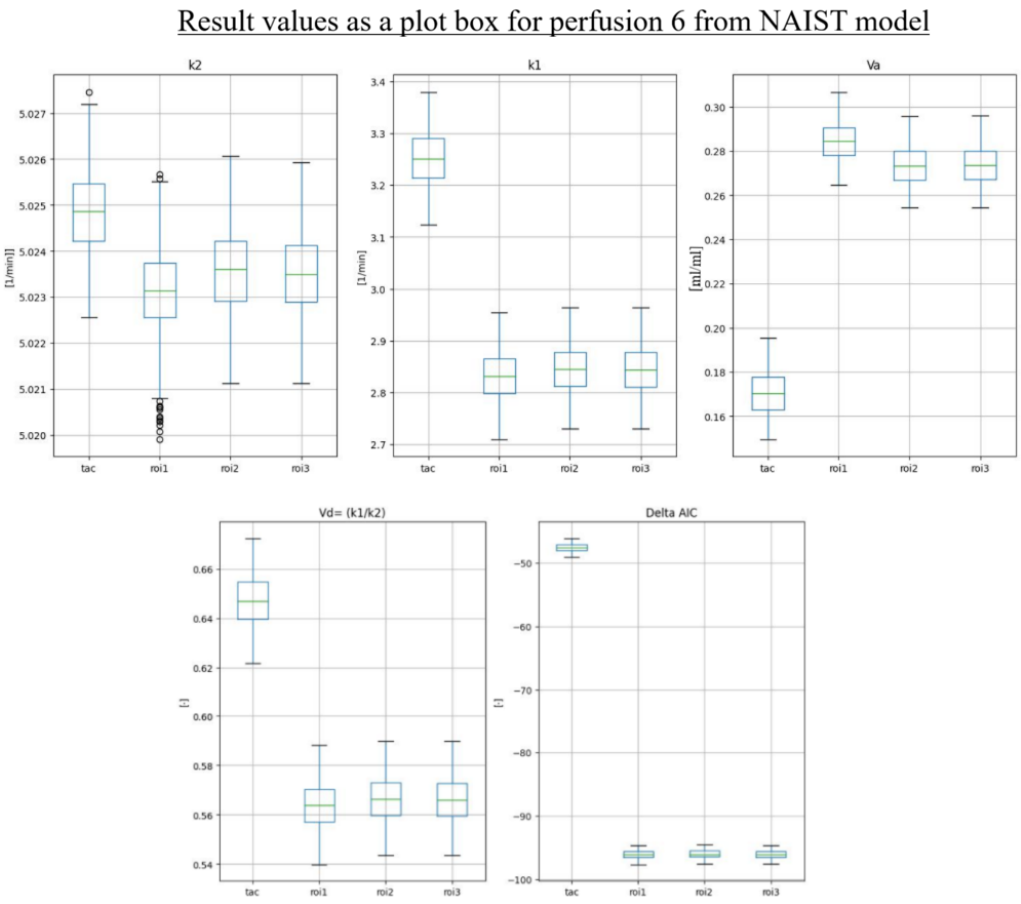

Figure H.6. In this figure are the box plots from all the parameters from the NAIST for TAC and ROI's from perfusion value of 600 [ml min-1 ml-1]. But here Va is clearly too high. Also the $|\Delta AIC|$ is decreasing meaning the fit is not as good as it was.

H.1.4 Appendix Results for boxplots of perfusion value 700 [ml min-1 ml-1] and 800 [ml min-1 ml-1] from NAIST model

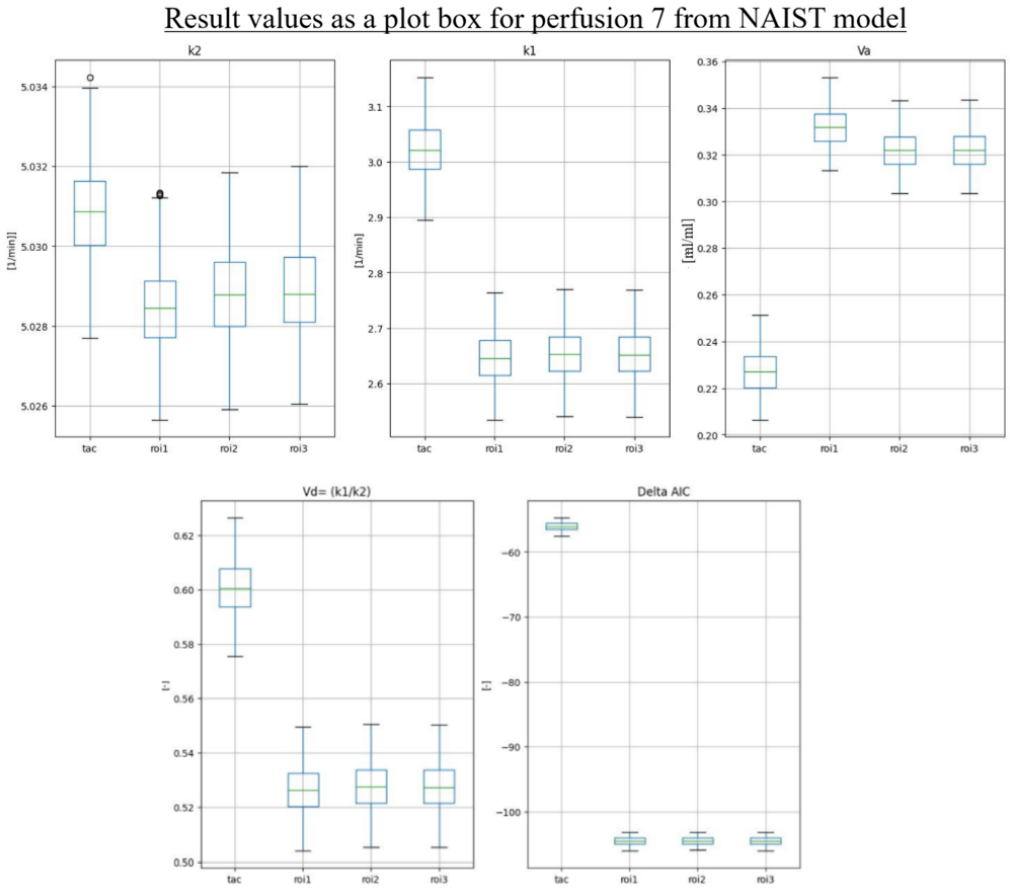

Figure H.7. In this figure is the box plots from all the parameters from the NAIST for TAC and ROI's from perfusion value of 700 [ml min-1 ml-1]. Regardless of the low $|\Delta AIC|$ the model has fully peaked now. K1 should be higher and the Va is too high.

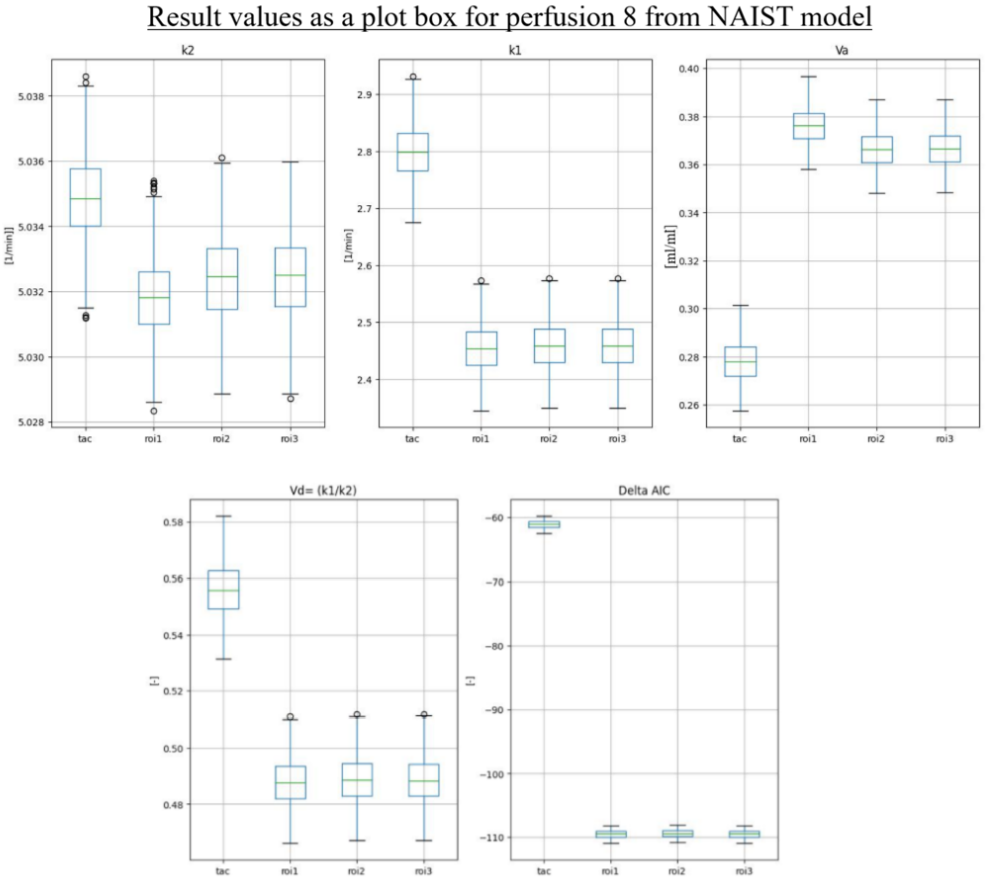

Figure H.8. In this figure is the box plots from all the parameters from the NAIST for TAC and ROI's from perfusion value of 800 [ml min-1 ml-1]. Here we can further see the model starting to mall function, as the Va keeps going up the K1 decreases.

H.1.5 Appendix Results for boxplots of perfusion value 900 [ml min-1 ml-1] and 1000 [ml min-1 ml-1] from NAIST model

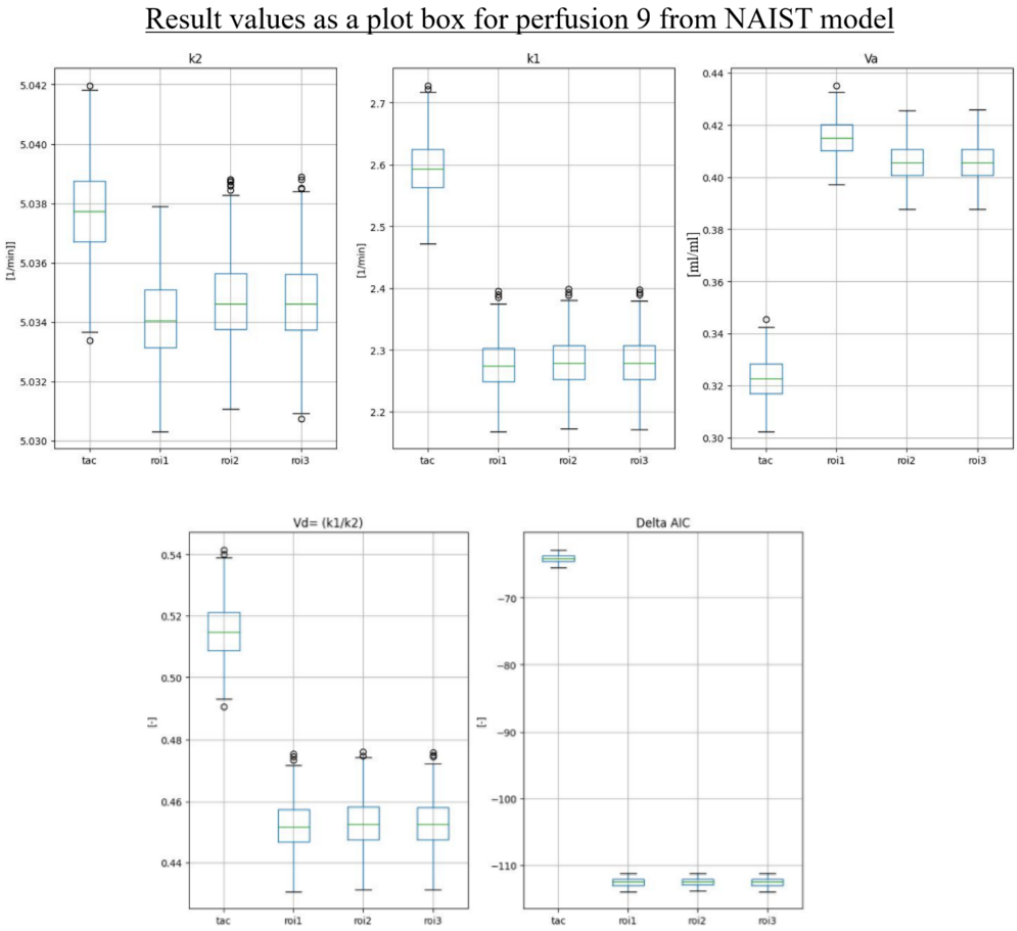

Figure H.9. In this figure is the box plots from all the parameters from the NAIST for TAC and ROI's from perfusion value of 900 [ml min-1 ml-1]. These values Are just out of the scope. The k2 hasn't risen sense 5 while Va is in 0.44. This model could benefit from having tighter range the model is allowed to predict the values.

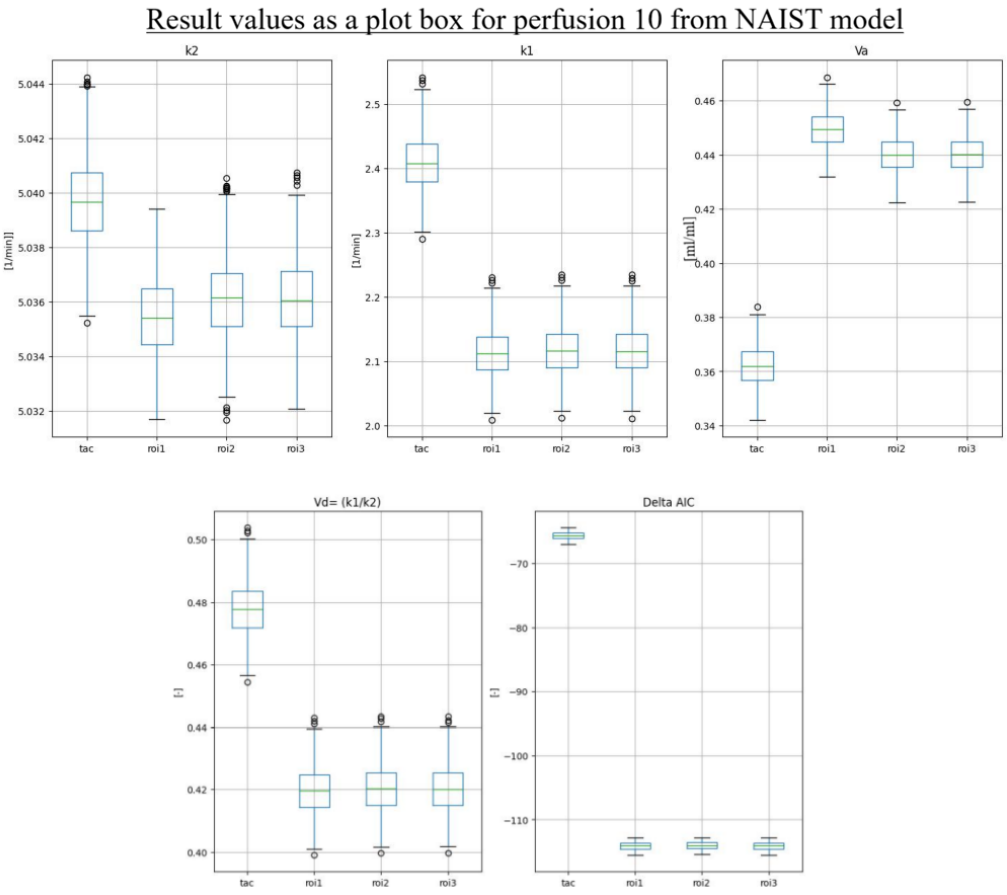

Figure H.10. In this figure is the box plots from all the parameters from the NAIST for TAC and ROI's from perfusion value of 1000 [ml min-1 ml-1]. Regardless of the bad parameters, the function fitted still well. Which has no use, when the parameters are this much of. But it is normal that the model has some limits. This one as is is limited till perfusion of 5.

H.2 Parameters as a function of perfusion.

H.2.1 Appendix Results for k1 and k2 from NAIST model

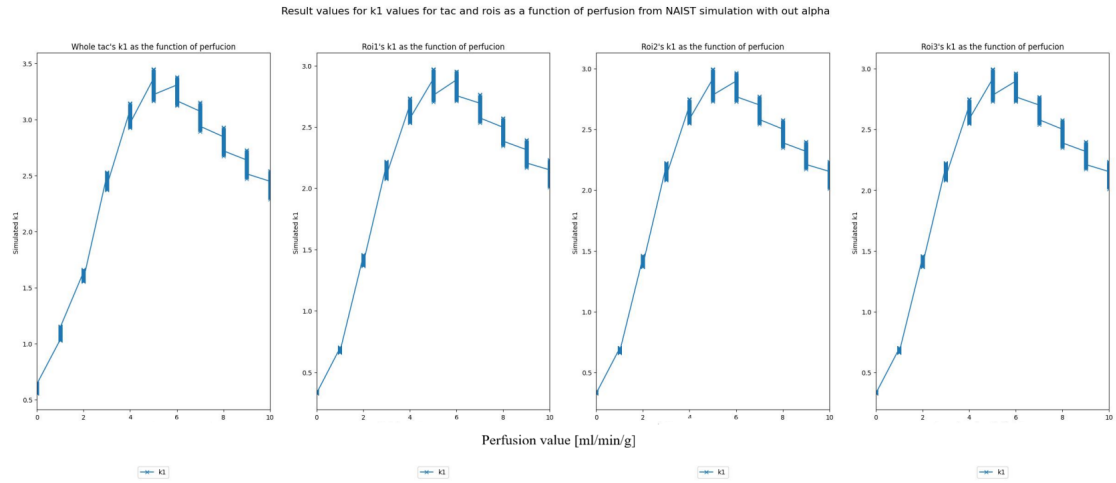

Figure H.11. In this figure the k1 is plotted as a function of perfusion for the NAIST for TAC and ROI's. From these figures the peak of perfusion 5, is even more clearer.

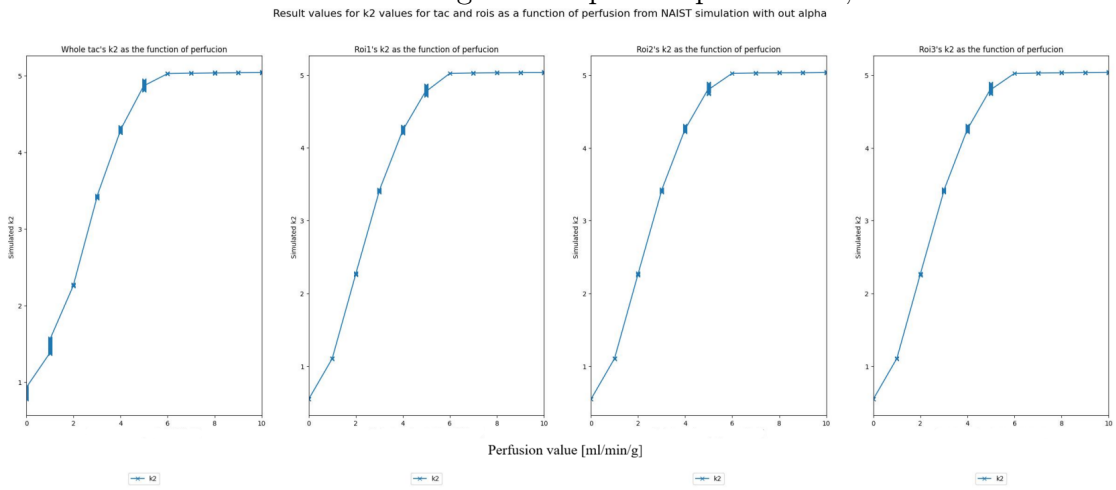

Figure H.12. In this figure the k2 is plotted as a function of perfusion for the NAIST for TAC and ROI's. The value of k2 was limited till 5, which can be seen here.

H.2.2 Appendix Results for va and vd from NAIST model

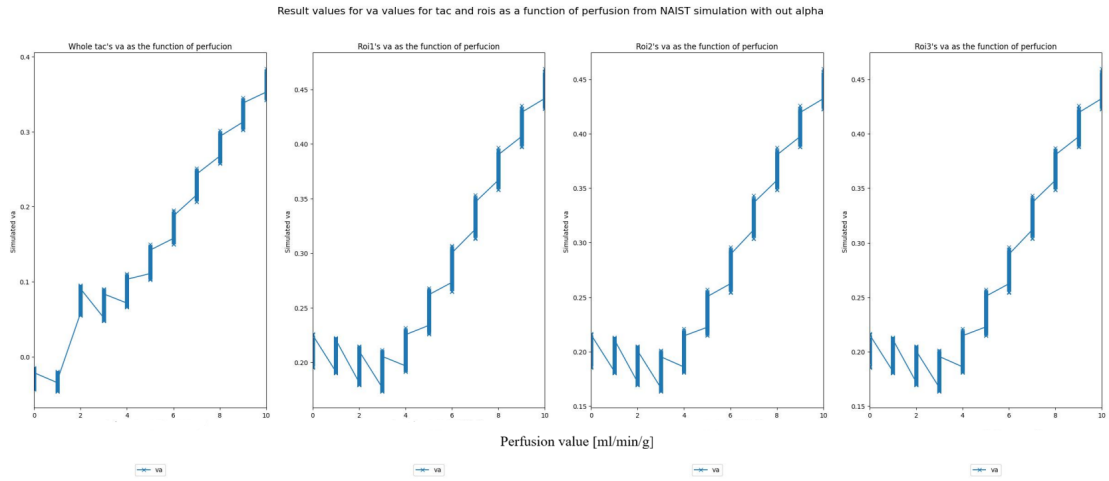

Figure H.13. In this figure the va is plotted as a function of perfusion for the NAIST no α for TAC and ROI's. The parameter Va worked well tile perfusion of 4 or 5. After that the values are just too high.

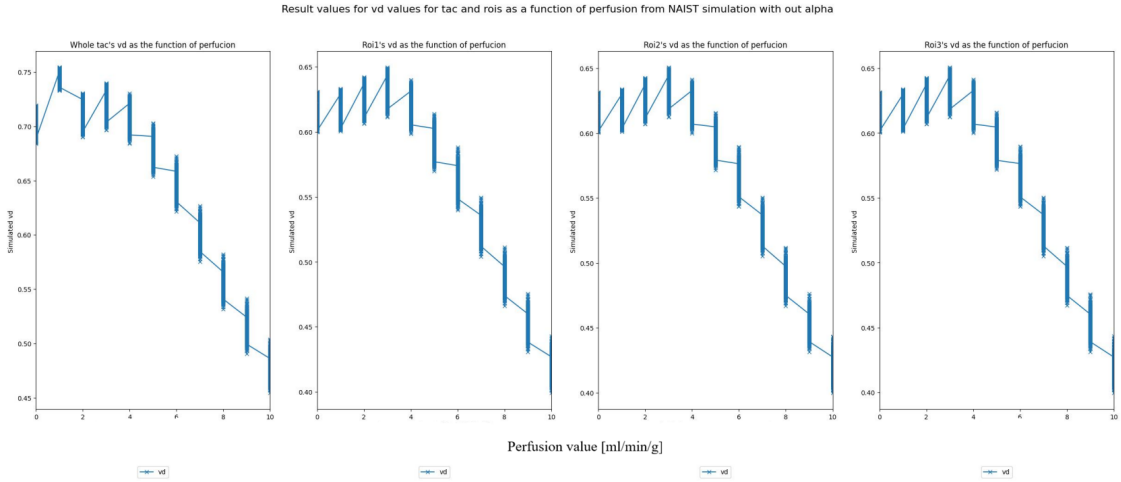

Figure H.14. In this figure the vd is plotted as a function of perfusion for the NAIST no α for TAC and ROI's. Here again the decline can be seen already after perfusion of 4 [ml/min/g]. Before the values are ≈ 0.72.

H.3 Results from NAIST model as mean ± standard deviation

Summary of results for NAIST model values repsented with mean ± standard deviation.

	perfusio	k1	k2	va	vd
(50, 'roi1')	0.3376 ± 0.0067	0.3376 ± 0.0047	0.5477 ± 0.0007	0.2084 ± 0.0087	0.6164 ± 0.0085
(50, 'tac')	0.5921 ± 0.02	0.5921 ± 0.0242	0.8427 ± 0.0453	-0.0288 ± 0.0088	0.7031 ± 0.009
(100, 'roi1')	0.6833 ± 0.0136	0.6833 ± 0.0096	1.1058 ± 0.0015	0.2041 ± 0.0088	0.6179 ± 0.0085
(100, 'tac')	1.0816 ± 0.0295	1.0816 ± 0.0322	1.4541 ± 0.053	-0.0359 ± 0.0053	0.744 ± 0.0051
(200, 'roi1')	1.416 ± 0.0289	1.416 ± 0.0203	2.2637 ± 0.0038	0.1946 ± 0.0089	0.6255 ± 0.0086
(200, 'tac')	1.6114 ± 0.0376	1.6114 ± 0.0231	2.2637 ± 0.0038	0.0724 ± 0.0102	0.7119 ± 0.0098
(300, 'roi1')	2.1521 ± 0.0443	2.1521 ± 0.0309	3.4047 ± 0.0067	0.1897 ± 0.009	0.6321 ± 0.0088
(300, 'tac')	2.4569 ± 0.057	2.4569 ± 0.0344	3.413 ± 0.0066	0.0661 ± 0.0102	0.7199 ± 0.0099
(400, 'roi1')	2.6308 ± 0.0535	2.6308 ± 0.0388	4.242 ± 0.0131	0.2093 ± 0.0088	0.6202 ± 0.0087
(400, 'tac')	3.0368 ± 0.0683	3.0368 ± 0.0424	4.2859 ± 0.0119	0.0853 ± 0.0099	0.7086 ± 0.0098
(500, 'roi1')	2.8354 ± 0.0573	2.8354 ± 0.045	4.7898 ± 0.0211	0.2457 ± 0.0085	0.5919 ± 0.0084
(500, 'tac')	3.306 ± 0.0739	3.306 ± 0.0494	4.8712 ± 0.0194	0.1242 ± 0.0095	0.6787 ± 0.0095
(600, 'roi1')	2.8313 ± 0.053	2.8313 ± 0.0425	5.0231 ± 0.0008	0.2845 ± 0.008	0.5637 ± 0.0084
(600, 'tac')	3.2508 ± 0.0677	3.2508 ± 0.0467	5.0248 ± 0.0008	0.1704 ± 0.009	0.6469 ± 0.0093
(700, 'roi1')	2.6459 ± 0.0455	2.6459 ± 0.0394	5.0284 ± 0.001	0.3319 ± 0.0073	0.5262 ± 0.0078
(700, 'tac')	3.0215 ± 0.0591	3.0215 ± 0.0443	5.0309 ± 0.0011	0.2271 ± 0.0083	0.6006 ± 0.0088
(800, 'roi1')	2.4537 ± 0.0399	2.4537 ± 0.0374	5.0318 ± 0.0011	0.3761 ± 0.0068	0.4876 ± 0.0074
(800, 'tac')	2.7986 ± 0.052	2.7986 ± 0.0424	5.0349 ± 0.0012	0.278 ± 0.0077	0.5558 ± 0.0084
(900, 'roi1')	2.4537 ± 0.0399	2.4537 ± 0.0374	5.0318 ± 0.0011	0.3761 ± 0.0068	0.4876 ± 0.0074
(900, 'tac')	2.7986 ± 0.052	2.7986 ± 0.0424	5.0349 ± 0.0012	0.278 ± 0.0077	0.5558 ± 0.0084
(1000, 'roi1')	2.1938 ± 0.0902	2.1938 ± 0.0884	5.0348 ± 0.0015	0.4324 ± 0.0182	0.4357 ± 0.0176
(1000, 'tac')	2.5007 ± 0.1184	2.5007 ± 0.101	5.0387 ± 0.0017	0.3424 ± 0.0208	0.4963 ± 0.0201

Figure H.15. The mean values with standard deviation from each parameter for perfusion till 1000 [ml min-1 ml-1]. Only TAC and ROI1 are shown as the other ROIs had almost identical results with ROI1.

I Appendix Results from NASTα model

I.1 Box-plots

I.1.1 Appendix Results for boxplots of perfusion value 50 [ml min-1 ml-1] and 100 [ml min-1 ml-1] from NASTα model

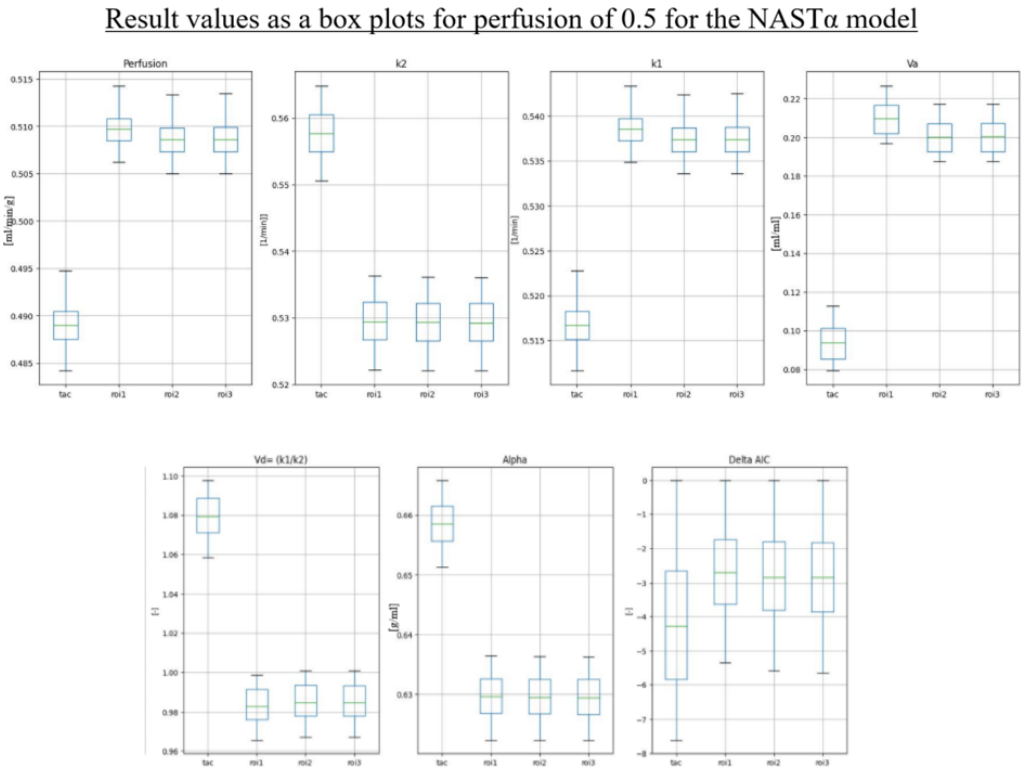

Figure I.1. In this figure is the box plots from all the parameters from the NASTα for TAC and ROI's from perfusion value of 50 [ml min-1 ml-1]. Here we can see the model works for all the TAC and ROIs quite well. The only value that is off is the α value that is lower than commonly recorded.

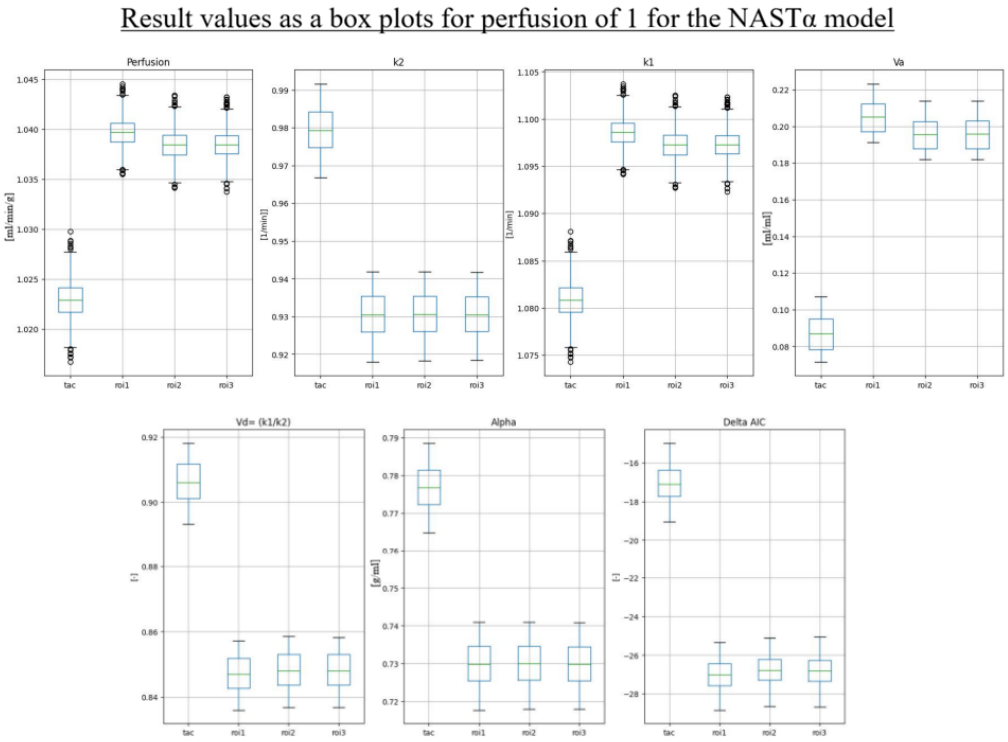

Figure I.2. In this figure is the box plots from all the parameters from the NASTα for TAC and ROI's from perfusion value of 100 [ml min-1 ml-1]. Here againt he values are good and the α fits more the recorded values. As seen the function fit from ΔAIC is low.

I.1.2 Appendix Results for boxplots of perfusion value 300 [ml min-1 ml-1] and 400 [ml min-1 ml-1] from NASTα model

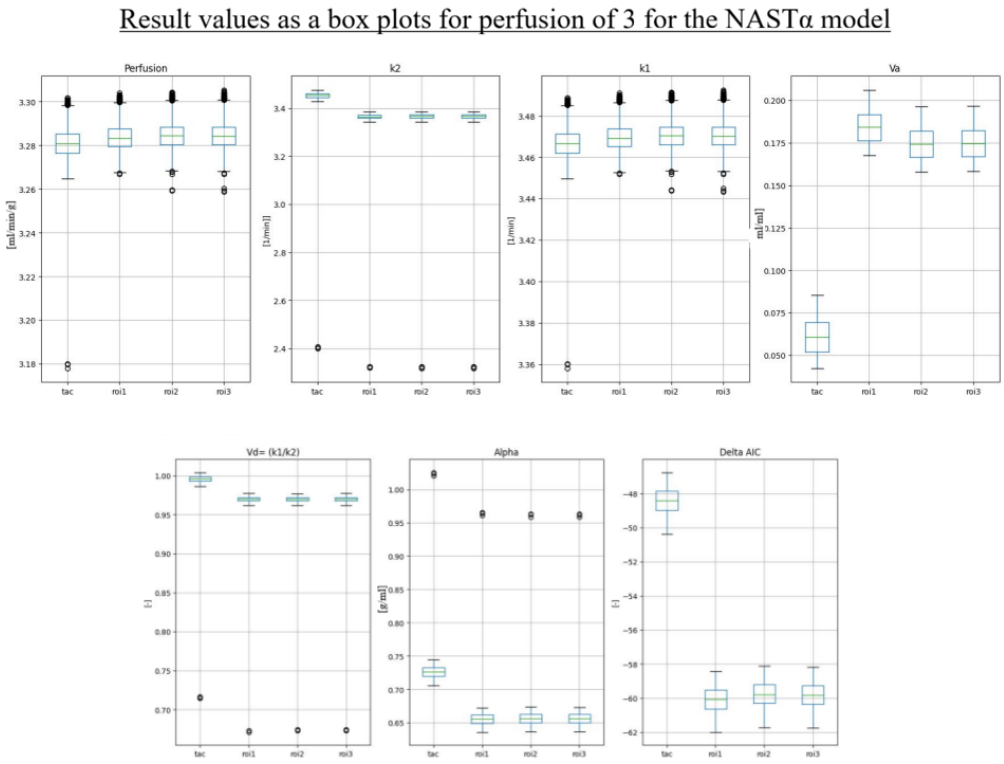

Figure I.3. In this figure is the box plots from all the parameters from the NASTα for TAC and ROI's from perfusion value of 300 [ml min-1 ml-1]. Here most of the parameters have been optimized well. The outliers in the plots are results from using wrong guesses for the parameters in the beginning. Regardless the values that have used the correct set have worked. Vd is near one, but it is still under. As seen the function fit from ΔAIC is low.

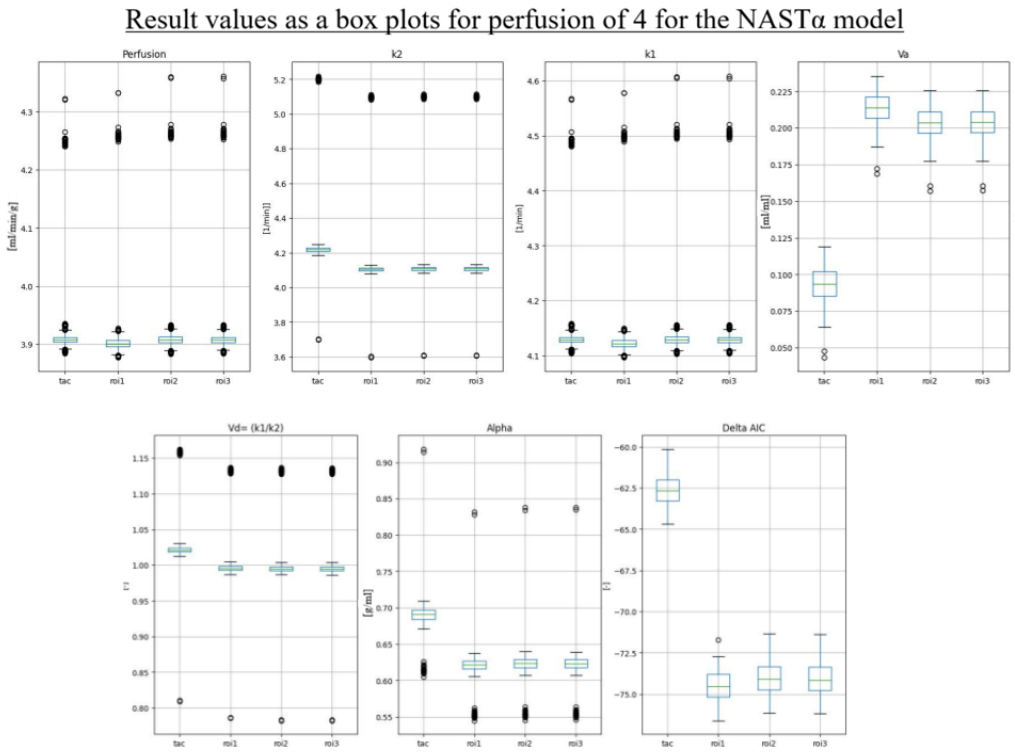

Figure I.4. In this figure is the box plots from all the parameters from the NASTα for TAC and ROI's from perfusion value of 400 [ml min-1 ml-1]. Here also some outliers can be seen. These are again result from using the wrong parameter guesses in the beginning. Over all the other parameter results look good, except the Vd for the TAC, that goes bit over 1, excluding the outliers. In future the starting parameters for perfusion 400 [ml min-1 ml-1] should be more tuned. As seen the function fit from ΔAIC is low.

I.1.3 Appendix Results for boxplots of perfusion value 500 [ml min-1 ml-1] and 600 [ml min-1 ml-1] from NASTα model

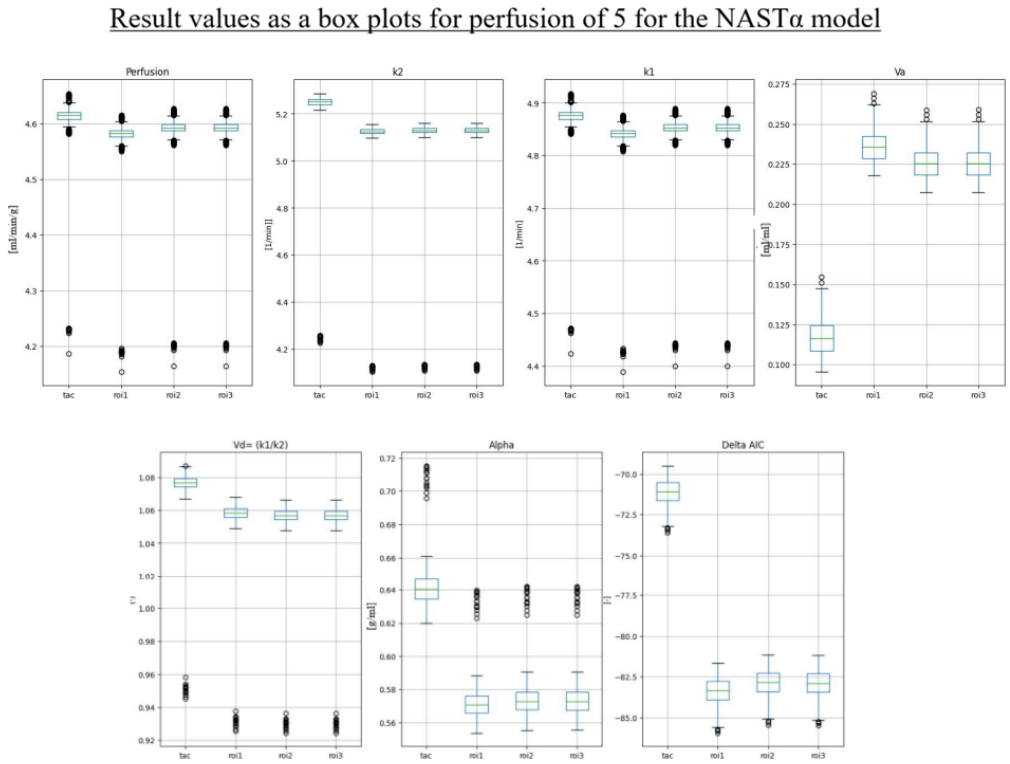

Figure I.5. In this figure is the box plots from all the parameters from the NASTα for TAC and ROI's from perfusion value of 500 [ml min-1 ml-1]. Here some problems with the parameters start to be seen. But this could be due to the clamp used that might limit other parameters from getting higher values. Over all this model seems to break in this perfusion. As seen the function fit from ΔAIC is low.

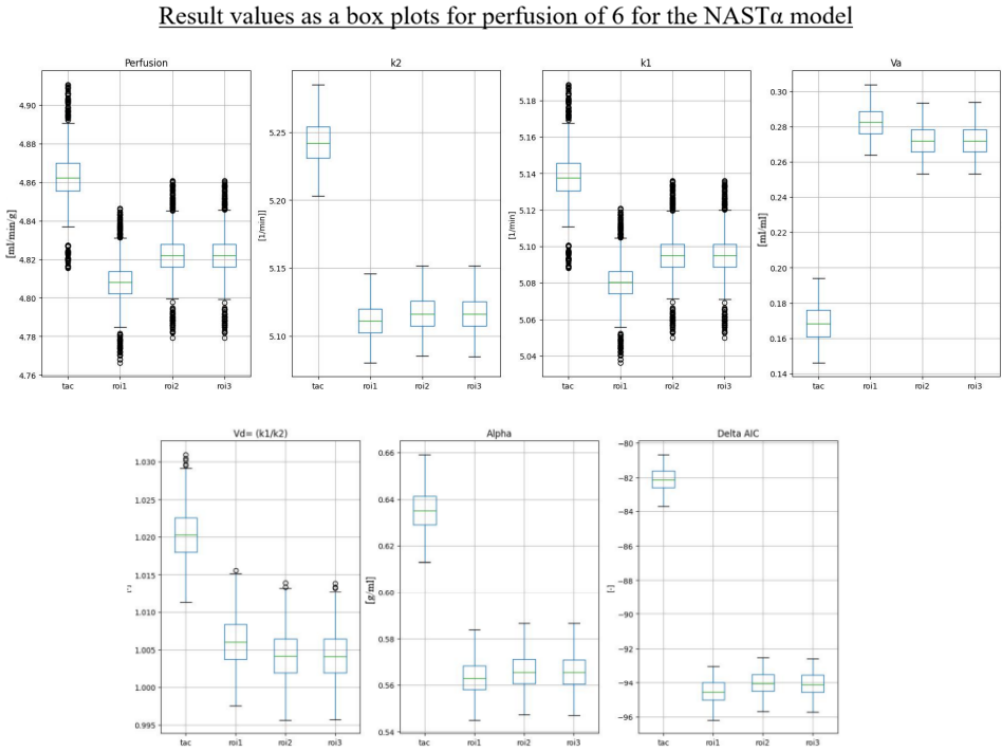

Figure I.6. In this figure is the box plots from all the parameters from the NASTα for TAC and ROI's from perfusion value of 600 [ml min-1 ml-1]. From here on the parameters start to be more off. Values for α are too low, Va starts to get higher values. Interesting thing is that the Vd is near 1. So even the values are bit off, tuning the beginning guesses more could actually result in better results. As seen the function fit from ΔAIC is low.

I.1.4 Appendix Results for boxplots of perfusion value 700 [ml min-1 ml-1] and 800 [ml min-1 ml-1] from NASTα model

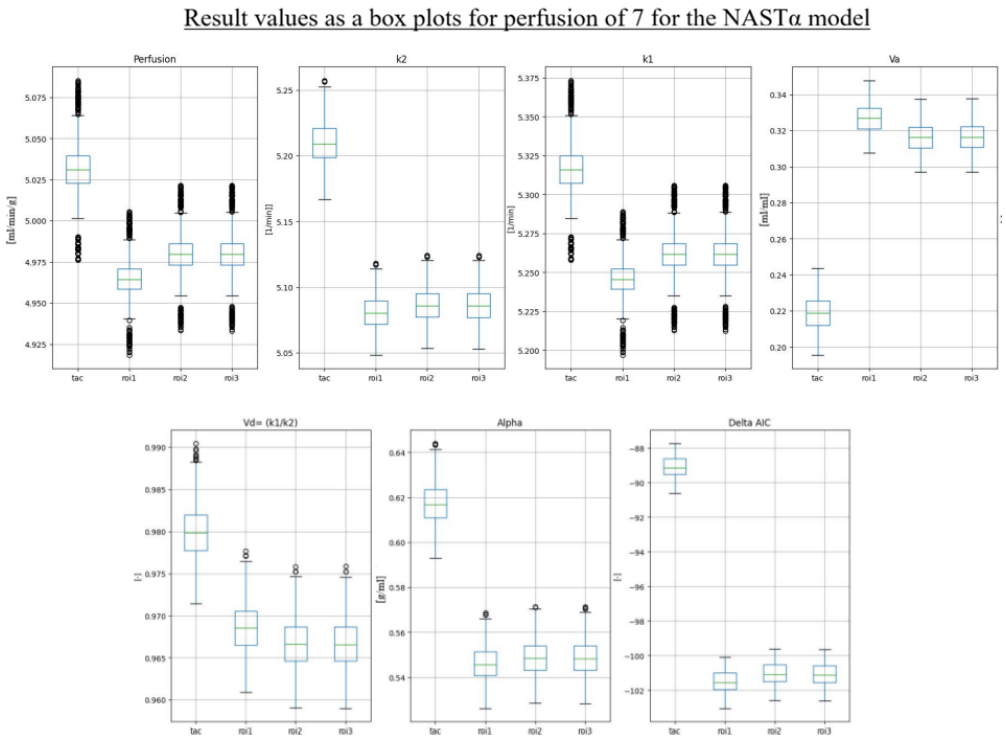

Figure I.7. In this figure is the box plots from all the parameters from the NASTα for TAC and ROI's from perfusion value of 70 0[ml min-1 ml-1]. Here the values are already in the limits. For Va the values are too high and for α the values are too low. The Vd is under one, so this could actually benefit from testing different beginning guesses, as they are slightly off. As seen the function fit from ΔAIC is low.

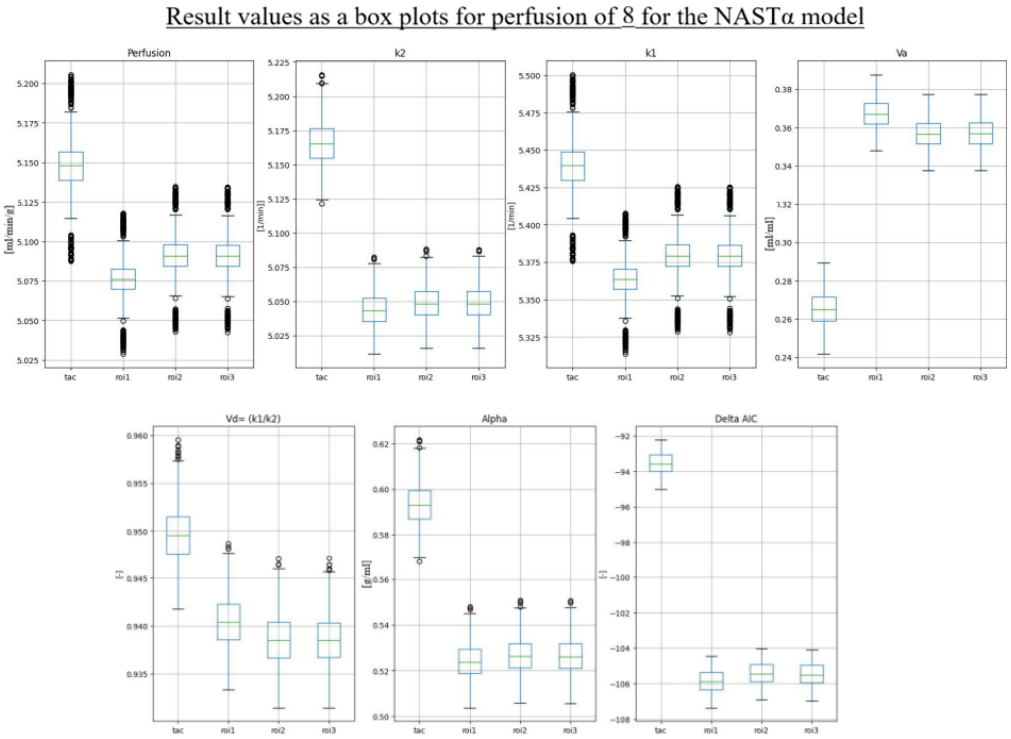

Figure I.8. In this figure is the box plots from all the parameters from the NASTα for TAC and ROI's from perfusion value of 800 [ml min-1 ml-1]. As mentioned earlier the values are now off, but again the Vd is under one. As the values are not too much of the model could benefit from tuning the beginning guesses to find optimal values for this high perfusion set from 500-1000 [ml min-1 ml-1]. As seen the function fit from ΔAIC is low.

I.1.5 Appendix Results for boxplots of perfusion value 900 [ml min-1 ml-1] and 1000 [ml min-1 ml-1] from NASTα model

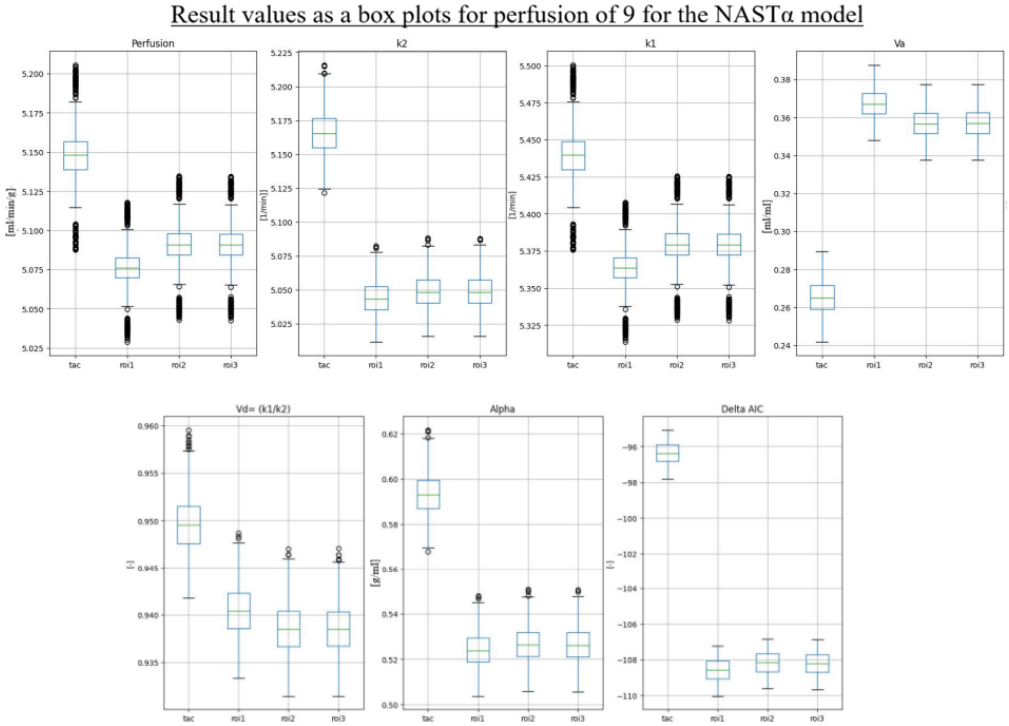

Figure I.9. In this figure is the box plots from all the parameters from the NASTα for TAC and ROI's from perfusion value of 900 [ml min-1 ml-1]. Even that the 800 [ml min-1 ml-1] and 900 [ml min-1 ml-1] are identical this is not a mistake but the model did perform this way for these two. As seen the function fit from ΔAIC is low.

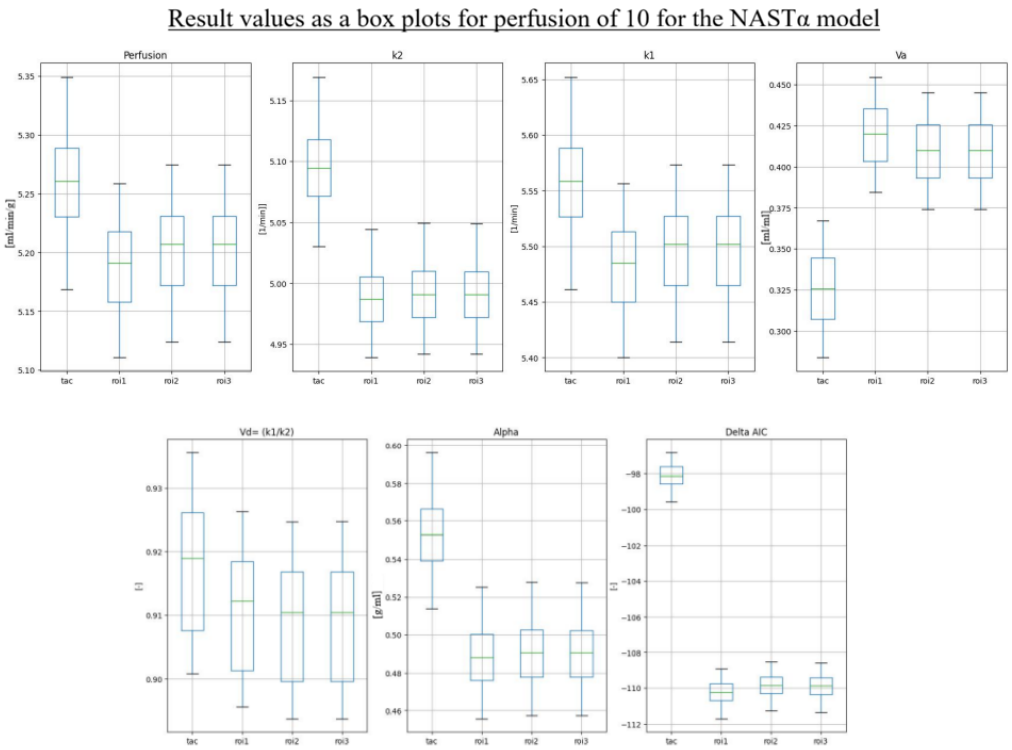

Figure I.10. In this figure is the box plots from all the parameters from the NASTα for TAC and ROI's from perfusion value of 1000 [ml min-1 ml-1]. The value for Va keeps increasing and for α decreasing. These values are too high and low for now. Here also Vd is under 1. As seen the function fit from ΔAIC is low.

I.2 Parameters as a function of perfusion.

I.2.1 Appendix Results for k2 and perfusion from NASTα model

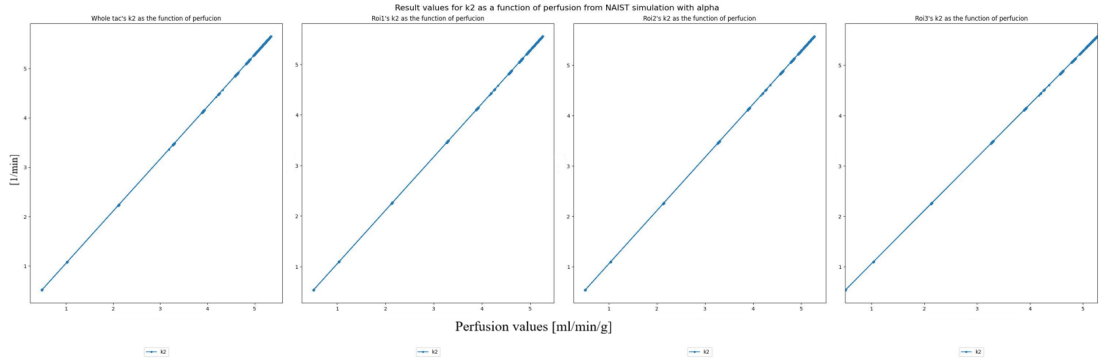

Figure I.11. In this figure the k2 is plotted as a function of perfusion for the NASTα for TAC and ROI's. The value increases linearly.

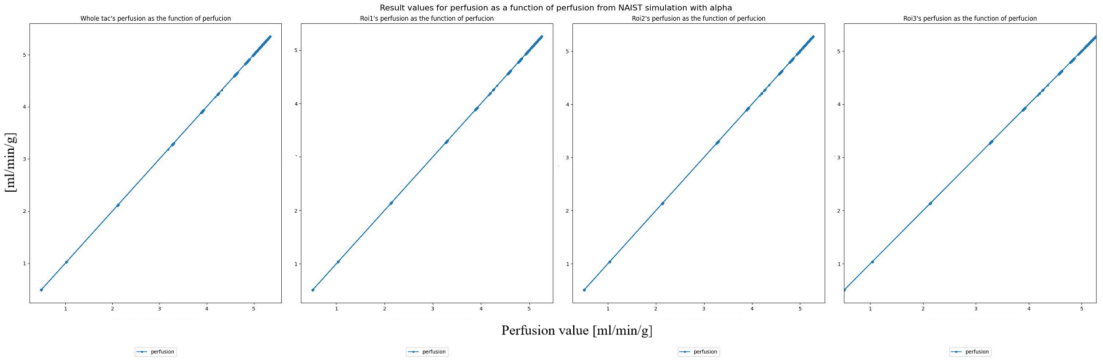

Figure I.12. In this figure the perfusion is plotted as a function of perfusion for the NASTα for TAC and ROI's. Here also the perfusion increases linearly.

I.2.2 Appendix Results for Va and vd from NASTα model

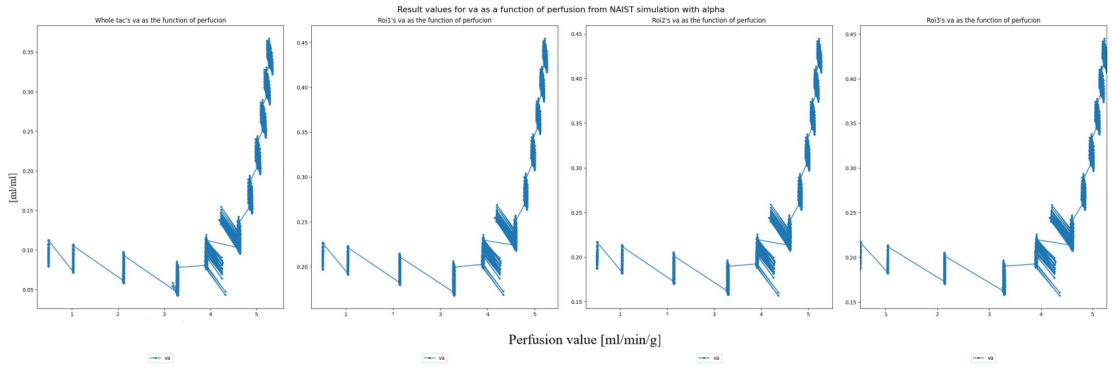

Figure I.13. In this figure the Va is plotted as a function of perfusion for the NASTα for TAC and ROI's. Here we can see the models parameter guessing failing between the 4 and 5. All the points should cluster like in perfusion 2 and 3 in a same perfusion line, but they are based out to this wider range.

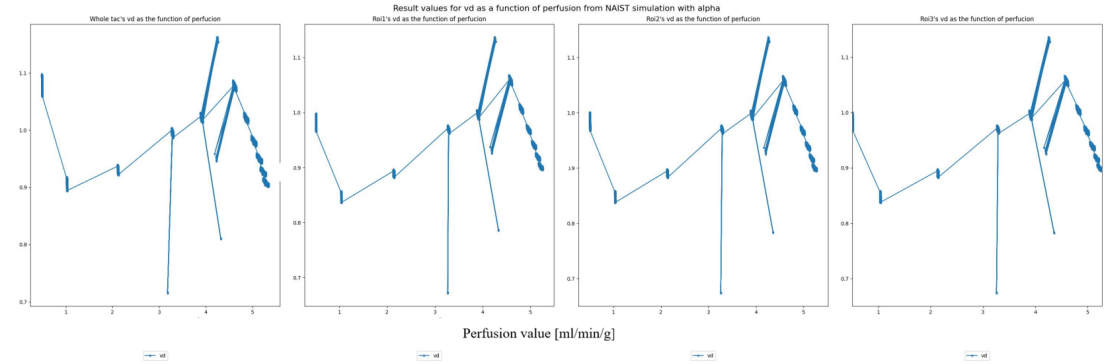

Figure I.14. In this figure the vd is plotted as a function of perfusion for the NASTα for TAC and ROI's. Here the outliers are easier to see. The clear lines away from the clusters are straight indicators from the model failing. Either clusters or clear zigzag should be forming.

I.3 Results from NASTα model as mean ± standard deviation

Summary of results for NASTα model values repsented with mean ± standard deviation.

	perfusio	k1	k2	va	vd	alpha
(50, 'roi1')	0.5097 ± 0.0015	0.5294 ± 0.0034	0.5385 ± 0.0016	0.2097 ± 0.0084	0.983 ± 0.0089	0.6296 ± 0.0034
(50, 'tac')	0.489 ± 0.0019	0.5576 ± 0.0033	0.5167 ± 0.002	0.0936 ± 0.0094	1.0792 ± 0.0101	0.6585 ± 0.0034
(100, 'roi1')	1.0397 ± 0.0015	0.9304 ± 0.0055	1.0986 ± 0.0016	0.205 ± 0.0086	0.8469 ± 0.0055	0.7298 ± 0.0054
(100, 'tac')	1.0229 ± 0.0018	0.9793 ± 0.0057	1.0809 ± 0.0019	0.0869 ± 0.0097	0.906 ± 0.0062	0.7767 ± 0.0054
(200, 'roi1')	2.1386 ± 0.0035	2.0098 ± 0.008	2.2597 ± 0.0037	0.1949 ± 0.0089	0.8894 ± 0.0035	0.7031 ± 0.0071
(200, 'tac')	2.1158 ± 0.0038	2.0809 ± 0.0084	2.2357 ± 0.004	0.0753 ± 0.0099	0.9308 ± 0.0044	0.7637 ± 0.007
(300, 'roi1')	3.2837 ± 0.0074	3.3621 ± 0.0515	3.4697 ± 0.0079	0.1844 ± 0.0091	0.969 ± 0.0148	0.6562 ± 0.0169
(300, 'tac')	3.2809 ± 0.009	3.4499 ± 0.0521	3.4667 ± 0.0095	0.061 ± 0.0103	0.9951 ± 0.0141	0.7269 ± 0.0166
(400, 'roi1')	3.9082 ± 0.0503	4.1211 ± 0.1321	4.1296 ± 0.0532	0.214 ± 0.0086	0.9978 ± 0.0202	0.6211 ± 0.0138
(400, 'tac')	3.9145 ± 0.0482	4.2335 ± 0.1312	4.1362 ± 0.0509	0.0938 ± 0.0101	1.0233 ± 0.0202	0.6897 ± 0.0154
(500, 'roi1')	4.5775 ± 0.0453	5.1124 ± 0.1131	4.8368 ± 0.0479	0.2358 ± 0.0085	1.0569 ± 0.0146	0.5714 ± 0.0095
(500, 'tac')	4.6101 ± 0.0449	5.2381 ± 0.1132	4.8712 ± 0.0474	0.1166 ± 0.0099	1.0752 ± 0.0145	0.6411 ± 0.0107
(600, 'roi1')	4.8076 ± 0.012	5.1109 ± 0.0114	5.0799 ± 0.0127	0.2825 ± 0.0077	1.0061 ± 0.0031	0.5632 ± 0.0068
(600, 'tac')	4.8624 ± 0.0149	5.2423 ± 0.0145	5.1378 ± 0.0158	0.1685 ± 0.0091	1.0204 ± 0.0032	0.6349 ± 0.008
(700, 'roi1')	4.9642 ± 0.0133	5.0806 ± 0.0115	5.2453 ± 0.0141	0.3268 ± 0.0072	0.9686 ± 0.0028	0.546 ± 0.007
(700, 'tac')	5.0309 ± 0.0173	5.2095 ± 0.0149	5.3159 ± 0.0183	0.2188 ± 0.0086	0.98 ± 0.003	0.6171 ± 0.0083
(800, 'roi1')	5.0758 ± 0.0139	5.0438 ± 0.0113	5.3633 ± 0.0147	0.3672 ± 0.0068	0.9404 ± 0.0026	0.524 ± 0.007
(800, 'tac')	5.1479 ± 0.0188	5.1656 ± 0.0149	5.4394 ± 0.0199	0.2652 ± 0.0081	0.9497 ± 0.0029	0.5931 ± 0.0085
(900, 'roi1')	5.0758 ± 0.0139	5.0438 ± 0.0113	5.3633 ± 0.0147	0.3672 ± 0.0068	0.9404 ± 0.0026	0.524 ± 0.007
(900, 'tac')	5.1479 ± 0.0188	5.1656 ± 0.0149	5.4394 ± 0.0199	0.2652 ± 0.0081	0.9497 ± 0.0029	0.5931 ± 0.0085
(1000, 'roi1')	5.1872 ± 0.0331	4.9872 ± 0.0212	5.481 ± 0.035	0.4195 ± 0.0172	0.91 ± 0.0089	0.4882 ± 0.0139
(1000, 'tac')	5.2591 ± 0.035	5.0949 ± 0.0274	5.557 ± 0.037	0.3258 ± 0.0201	0.9169 ± 0.0096	0.5529 ± 0.0161

Figure I.15. The mean values with standard deviation from each parameter for perfusion till 1000 [ml min-1 ml-1]. Only TAC and ROI1 are shown as the other ROIs had almost identical results with ROI1.

J Appendix All models mean ± standard deviation

Summary of results for all model values repsented with mean ± standard deviation.

	Perfusion	Parameter	NAIST	NASTα	fith2o	fitmbf
0	50	Flow	0.465 ± 0.013	0.499 ± 0.002	0.422 ± 0.002	0.494 ± 0.001
1	50	alpha		0.644 ± 0.003		0.701 ± 0.009
2	50	k1	0.465 ± 0.014	0.543 ± 0.003		
3	50	k2	0.695 ± 0.023	0.528 ± 0.002	0.551 ± 0.001	
4	50	va	0.090 ± 0.009	0.152 ± 0.009	0.151 ± 0.010	0.141 ± 0.009
5	50	vd	0.660 ± 0.009	1.031 ± 0.010	0.767 ± 0.002	
6	100	Flow	0.882 ± 0.022	1.031 ± 0.002	0.858 ± 0.004	0.995 ± 0.001
7	100	alpha		0.753 ± 0.005		0.703 ± 0.009
8	100	k1	0.882 ± 0.021	0.955 ± 0.006		
9	100	k2	1.280 ± 0.027	1.090 ± 0.002	1.121 ± 0.002	
10	100	va	0.084 ± 0.007	0.146 ± 0.009	0.147 ± 0.010	0.138 ± 0.009
11	100	vd	0.681 ± 0.007	0.876 ± 0.006	0.765 ± 0.002	
12	200	Flow	1.514 ± 0.033	2.127 ± 0.004	1.786 ± 0.009	2.027 ± 0.004
13	200	alpha		0.733 ± 0.007		0.708 ± 0.009
14	200	k1	1.514 ± 0.022	2.045 ± 0.008		
15	200	k2	2.264 ± 0.004	2.248 ± 0.004	2.333 ± 0.005	
16	200	va	0.133 ± 0.010	0.135 ± 0.009	0.136 ± 0.010	0.131 ± 0.009
17	200	vd	0.669 ± 0.009	0.910 ± 0.004	0.766 ± 0.003	
18	300	Flow	2.304 ± 0.051	3.282 ± 0.008	2.799 ± 0.014	3.091 ± 0.007
19	300	alpha		0.692 ± 0.017		0.715 ± 0.009
20	300	k1	2.304 ± 0.033	3.406 ± 0.052		
21	300	k2	3.409 ± 0.007	3.468 ± 0.009	3.639 ± 0.010	
22	300	va	0.128 ± 0.010	0.123 ± 0.010	0.122 ± 0.010	0.125 ± 0.009
23	300	vd	0.676 ± 0.009	0.982 ± 0.014	0.769 ± 0.003	
24	400	Flow	2.834 ± 0.061	3.911 ± 0.049	3.898 ± 0.022	4.175 ± 0.015
25	400	alpha		0.655 ± 0.015		0.722 ± 0.009
26	400	k1	2.834 ± 0.041	4.177 ± 0.132		
27	400	k2	4.264 ± 0.013	4.133 ± 0.052	5.038 ± 0.021	
28	400	va	0.147 ± 0.009	0.154 ± 0.009	0.106 ± 0.011	0.120 ± 0.009
29	400	vd	0.664 ± 0.009	1.011 ± 0.020	0.774 ± 0.003	
30	500	Flow	3.071 ± 0.066	4.594 ± 0.045	5.090 ± 0.037	5.267 ± 0.029
31	500	alpha		0.606 ± 0.010		0.727 ± 0.009
32	500	k1	3.071 ± 0.047	5.175 ± 0.113		
33	500	k2	4.831 ± 0.020	4.854 ± 0.048	6.537 ± 0.040	
34	500	va	0.185 ± 0.009	0.176 ± 0.009	0.089 ± 0.011	0.116 ± 0.009
35	500	vd	0.635 ± 0.009	1.066 ± 0.015	0.779 ± 0.003	
36	600	Flow	3.041 ± 0.060	4.835 ± 0.013	6.000 ± 0.000	6.346 ± 0.038
37	600	alpha		0.599 ± 0.007		0.730 ± 0.009
38	600	k1	3.041 ± 0.045	5.177 ± 0.013		
39	600	k2	5.024 ± 0.001	5.109 ± 0.014	7.737 ± 0.079	
40	600	va	0.227 ± 0.009	0.225 ± 0.008	0.187 ± 0.056	0.114 ± 0.008
41	600	vd	0.605 ± 0.009	1.013 ± 0.003	0.776 ± 0.008	
42	700	Flow	2.834 ± 0.052	4.998 ± 0.015		7.351 ± 0.036
43	700	alpha		0.582 ± 0.008		0.732 ± 0.008
44	700	k1	2.834 ± 0.042	5.145 ± 0.013		
45	700	k2	5.030 ± 0.001	5.281 ± 0.016		
46	700	va	0.279 ± 0.008	0.273 ± 0.008		0.114 ± 0.008
47	700	vd	0.563 ± 0.008	0.974 ± 0.003		
48	800	Flow	2.626 ± 0.046	5.112 ± 0.016		8.163 ± 0.289
49	800	alpha		0.559 ± 0.008		0.736 ± 0.008
50	800	k1	2.626 ± 0.040	5.105 ± 0.013		
51	800	k2	5.033 ± 0.001	5.401 ± 0.017		
52	800	va	0.327 ± 0.007	0.316 ± 0.007		0.111 ± 0.008
53	800	vd	0.522 ± 0.008	0.945 ± 0.003		
54	900	Flow	2.626 ± 0.046	5.112 ± 0.016		8.806 ± 0.282
55	900	alpha		0.559 ± 0.008		0.736 ± 0.009
56	900	k1	2.626 ± 0.040	5.105 ± 0.013		
57	900	k2	5.033 ± 0.001	5.401 ± 0.017		
58	900	va	0.327 ± 0.007	0.316 ± 0.007		0.111 ± 0.009
59	900	vd	0.522 ± 0.008	0.945 ± 0.003		
60	1000	Flow	2.347 ± 0.104	5.223 ± 0.034		9.862 ± 0.169
61	1000	alpha		0.521 ± 0.015		0.719 ± 0.016
62	1000	k1	2.347 ± 0.095	5.041 ± 0.024		
63	1000	k2	5.037 ± 0.002	5.519 ± 0.036		
64	1000	va	0.387 ± 0.020	0.373 ± 0.019		0.130 ± 0.017
65	1000	vd	0.466 ± 0.019	0.913 ± 0.009		

Figure J.1. The mean values with standard deviation from each parameter from all the models

K Appendix Flow chart for the study with patient data

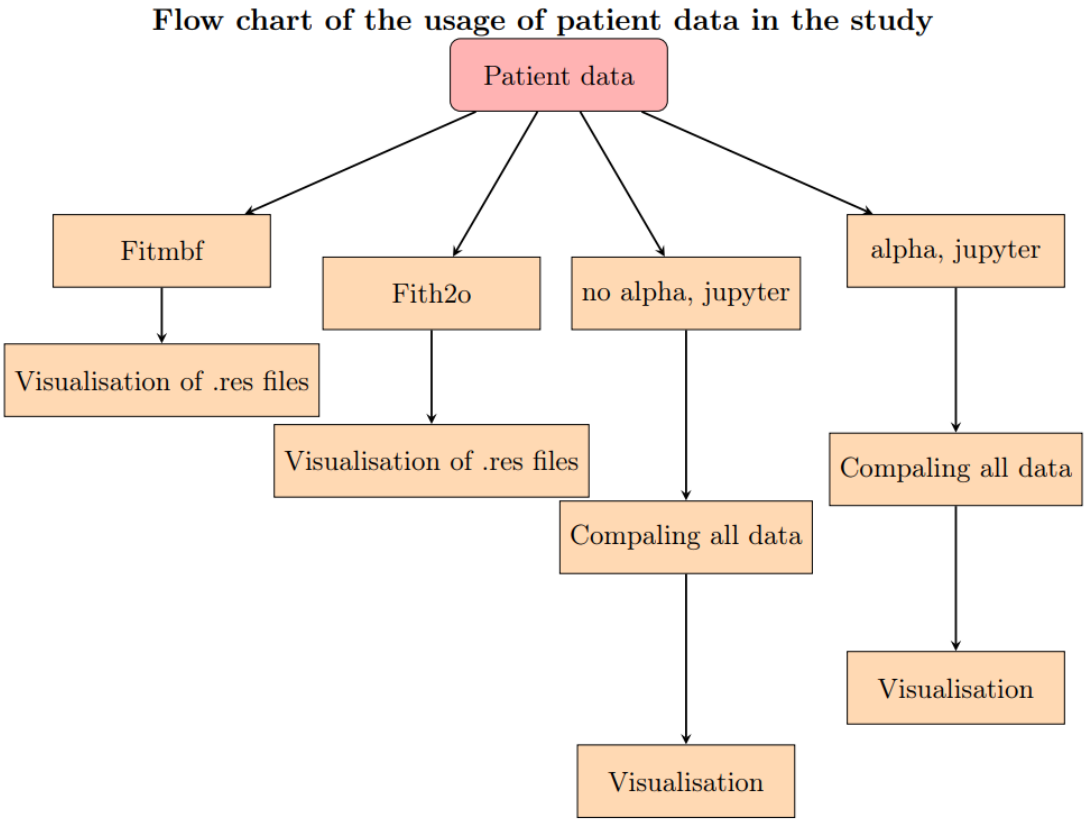

Figure K.1. Flow chart for patient data run. Patient data is used for all the models and from this all the box-plots and functions are done. Each model had either weighted sum of squares or R^2 and Akaike Information Criterion (AIC) used as a measure of goodness of fit. To analyze the results more, scatted plots were made. For the thesis only the scatter plot is shown.